Single Molecule Force Spectroscopy Investigations of Amyloid-β Aggregation

by
Francis Hane

A thesis
presented to the University of Waterloo
in fulfillment of the
thesis requirement for the degree of
Doctor of Philosophy
in
Biology

Waterloo, Ontario, Canada, 2013

AUTHOR'S DECLARATION

I hereby declare that I am the sole author of this thesis, except where noted. This is a true copy of the thesis, including any required final revisions, as accepted by my examiners.

I understand that my thesis may be made electronically available to the public.

Abstract

Alzheimer's Disease is a neurodegenerative disease affecting over five million people in the United States alone, with almost half a million new cases every year. As the population ages, these figures will only increase unless an effective treatment can be found. Amyloid-β is the protein implicated in, and believed to be causal to Alzheimer's Disease. Amyloid-β has been known to misfold into β-sheets and aggregate into neurotoxic oligomers or relatively inert amyloid fibrils. A variety of aggravating factors have been implicated including an excess of metal ions, various genetic anomalies, and the intracellular depositions of neurofibrillatory tangles (NFT).

This PhD thesis advances the understanding of Alzheimer's disease by demonstrating how the presence of copper ions influences the unbinding force of two amyloid-β peptides affecting the initial aggregation pathway by increasing the force between two amyloid-β peptides. The results provide evidence to the hypothesis that the addition of metals increases the amyloid oligomer content in the brain beyond that which the brain can naturally clear.

Current Alzheimer's pharmacological research is focused on developing amyloid aggregation inhibitors that would slow down the accumulation of amyloid oligomers and thereby slow the onset of Alzheimer's symptoms. A high throughput method of testing potential aggregation inhibitors that is far more efficient than current testing methods is demonstrated. An aggregation inhibitor was tested that functions by inhibiting the initial self-dimerization of amyloid-β preventing further aggregation. The results show that this inhibitor, named SG1, greatly reduces the experimental yield (a parameter calculated during force spectroscopy experiments) of the force experiments demonstrating a drastically lower amyloid-amyloid

affinity. The natural conclusion to these results is that if amyloid-β cannot dimerize, it cannot continue to aggregate.

Using dynamic force spectroscopy, the height and width of the energy barrier of amyloid-β dimerization is calculated using a variety of different models. These different models are compared and their relative advantages and disadvantages discussed.

ACKNOWLEDGMENTS

I would not have been able to complete this degree without the support of numerous people and I wish to acknowledge their support. First of all, my wife Melesa and my children Mya and Calvin, who have graciously sacrificed in order for me to complete this degree. Secondly, I wish to thank my supervisor, Prof. Zoya Leonenko for taking a chance on me and giving me freedom in my research and giving me the flexibility of completing my research on my own schedule. Also, I would like to thank Prof. Leonenko for her guidance and her relentless efforts at teaching me how to discuss results and teaching me the value of attention to detail and clear scientific communication. I also wish to acknowledge Prof. James Forrest. Prof. Forrest directed me to Prof. Leonenko when I first enquired about doing biophysical research. In addition, having Prof. Forrest present at committee meetings was like being subjected to medieval torture: it was painful, but I'm a better scientist because of it. I would like to thank Prof. Arvi Rauk for his insightful comments and collaboration by contributing molecular dynamic simulations to my project. I would like to thank Prof. Scott Taylor for the synthesis of APS. I am thankful to my committee members Profs. Bernard Glick, Brendan McConkey, Elizabeth Meiering, for their encouragement in digging deeper into my project. I owe a debt of gratitude to Dr. Simon Attwood for his direction in force spectroscopy analysis and Dr. Bo-Hyun Kim who shared with me the technical details on single molecule force spectroscopy and surface modification. Lastly, I am indebted to my fellow graduate students that I have had the privilege of working with: Brad Moores, Liz Drolle, Brenda Lee, Robbie Hendersen, Erin Faught and Vince Choi. Thank you for your enduring friendship and for answering my various questions on subjects that you are far more knowledgeable on than I.

DEDICATION

This thesis is dedicated to Mya and Calvin Hane. Work hard, have a good attitude, and be people of unimpeachable character. Never miss an opportunity to do the right thing. May you never forget to question the world around you.

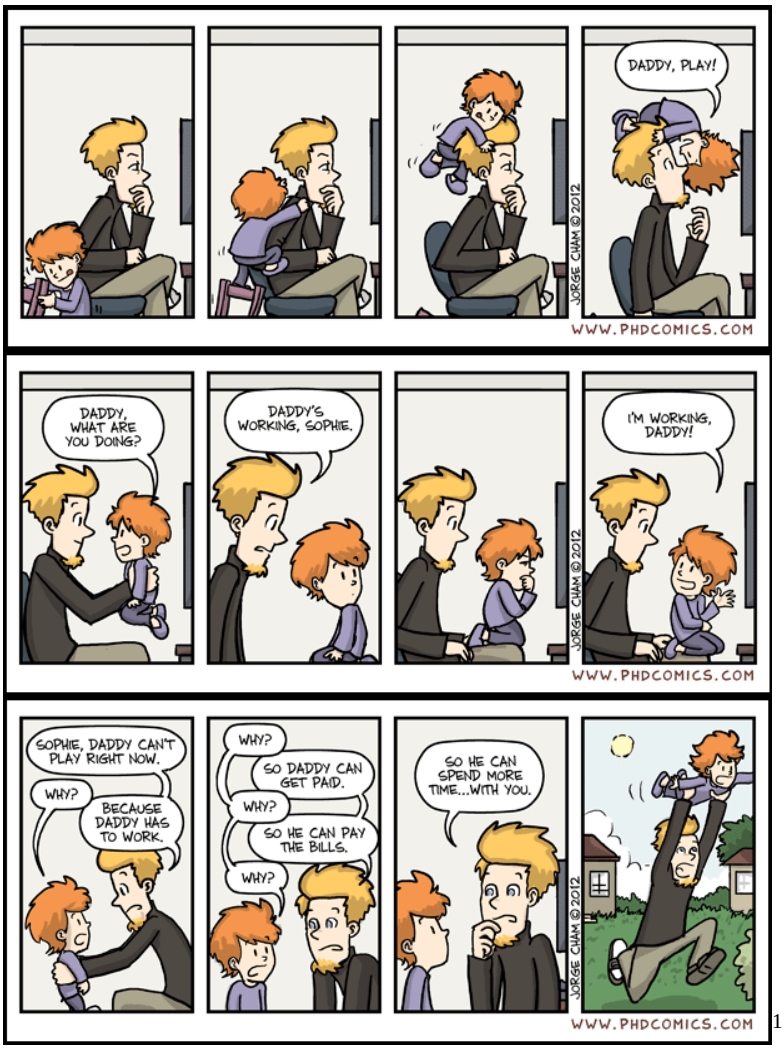

[1]

[1] I wish I could submit a PhD thesis with a chapter consisting solely of my favorite PhD comics. PhD Comics copyright Jorge Cham. Reprinted with permission.

TABLE OF CONTENTS

List of Figures

Chapter 1
Introduction

This thesis contains the results of four years of investigation studying the single molecule interactions of amyloid-β, the protein implicated in Alzheimer's disease. During the course of this research, approximately 50,000 force curves were collected and analyzed. Because of the dilute solutions used during these experiments, approximately 10-15% of these approaches provide reliable information and are subject to further analysis yielding important kinetic and statistical mechanical information on the single molecule interactions between two amyloid-β peptides.

The first chapter of this thesis consists of a literature review covering the most pertinent and current advances in the relevant fields of study. Alzheimer's disease, the amyloid-β peptide, and atomic force spectroscopy are all given brief reviews to serve as a primer for the discussion of the results of the research. The number of journal articles being published in peer-reviewed periodicals, especially in the field of Alzheimer's research, appears to be growing exponentially: a search of "amyloid-beta" on PubMed returns over 20,000 results with 90% of these reports having been published within the past ten years. Given the voluminous amount of research data available, only the results of the most highly cited and relevant publications are referenced in this thesis. Extensive reviews are noted in selected sections in chapter one should the reader wish to explore the subject matter in further depth.

Chapter 2 describes the objectives of this research and hypothesis' as identified at the outset of the investigations contained within the PhD thesis proposal.

Chapter 3 contains the results of an atomic force spectroscopy (AFS) and atomic force microscopy (AFM) study of the effect of copper on single molecule interactions between amyloid-β.

Chapter 4 contains the results of a study of how potential amyloid aggregation inhibitors affect the unbinding force between two molecules. The results demonstrate how atomic force spectroscopy can be used as an initial high throughput drug discovery tool to probe and ligand-receptor interactions or competitive binding.

Chapter 5 reports the results of the statistical mechanical and kinetic information involved in the dimerization of two amyloid-β peptides using competing dynamic force spectroscopy (DFS) models and comparing these models to one another.

Appendix A contains all atomic force spectroscopy protocols.

Appendix B contains list of other publications written by the author of this thesis but were not part of the PhD research plan.

Certain sections of thesis have been adapted from the author's PhD thesis proposal, a literature review conducted during course work, from the author's master's thesis (Hane, 2009) or from articles published in academic journals with the author of this thesis being the lead author of those articles.

1.1. Alzheimer's Disease

Alzheimer's Disease (AD) is a neurodegenerative disorder which results in progressive cognitive impairment, including dementia, personality changes, judgment, language skills and memory loss, eventually resulting in the death of the individual. AD is a member of the protein misfolding diseases family. The twenty-seven protein misfolding diseases identified all have an implicated protein which misfolds and aggregates causing a specific pathology (Sipe et al.,

2010) (Stefani, 2012). AD is associated with the amyloid-β (Aβ) peptide. Other diseases in the protein misfolding disease family include Parkinson's (α-synuclein), Huntington's (Huntingtin), and Cruetzfeld-Jacobs (PrPc).

The pathology which would later be identified as Alzheimer's disease was first identified by Alois Alzheimer in 1907 (Alzheimer, 1907). A significant period of time elapsed between the time that Dr. Alzheimer identified the disease until any significant progress was made in the study of Alzheimer's disease: it was not until the mid- to late 1980's that the amyloid-β peptide was shown to be correlated with AD symptoms (Masters, Simms, Weinman, Multlraup, McDonaid, & Beyreuther, 1985) (Tanzi, McClatchey, Lampereti, Villa-Komaroff, Gusella, & Neve, 1988) and the amyloid hypothesis was proposed (Selkoe, 1991).

Pathologically, Alzheimer's disease is identified post-mortem by the presence of extracellular amyloid plaques and intracellular neurofibrillary tangles (NFT). Research by Selkoe and others has shown that amyloid-β is the primary constituent in these amyloid plaques, and hyper-phosphorolated tau protein the primary constituent in NFT's (Selkoe, 1991). In addition, advancements have been made in elucidating the factors that influence the symptoms of Alzheimer's, the molecular pathways of amyloid-β aggregation, and possible therapeutic approaches to slow the onset of AD.

By the turn of the last century, research results started to show that neuronal synapses were most affected by amyloid neurotoxicity by impairing potentiation as a result of the interaction between amyloid oligomers and the neuronal synapse (Walsh, et al., 2004) (Walsh & Selkoe, 2004). Concurrently, various groups reported that the misfolding of amyloid proteins was not an abnormal occurrence: rather, it is an intrinsic property to the backbone of any polypeptide chain (Dobson & Karplus, 1999). In addition, research showed that cytotoxicity is a

generic effect of all amyloid oligomers (Bucciantini M. , et al., 2002) and is associated with the initial misfold of oligomers setting off the amyloid cascade (Kayed, 2003) (Stefani, 2012).

Post mortem examinations of patients with Alzheimer's symptoms have shown a reduction in the physical size of the temporal and frontal lobes, hippocampus and amygdala- the regions involved in memory and learning process. This cerebral atrophy is the direct result of neuronal apoptosis and synaptic atrophy appearing concurrently with the presence of amyloid plaques and tau tangles (Mattson M. , 2004). In addition, inflammatory cytokines formed by degenerating neurons and activated microglia around the amyloid plaques may contribute to the symptoms associated with Alzheimer's disease (Mattson M. , 2004).

Despite extensive research into Alzheimer's and amyloid-β, no clear mechanism of action has been uniformly accepted, and little progress has been made in developing pharmaceuticals that eliminate, prevent, or even significantly slow the devastation caused by AD (Neugroschl & Sano, 2010).

1.1.1. Alzheimer's Epidemiology

Currently, Alzheimer's disease affects nearly 12 million individuals across the world. By 2050, epidemiologists have estimated that this number will triple to nearly 36 million individuals (Citron, 2004). In the United States, 5.4 million Americans have been diagnosed with AD including 5.2 million citizens over the age of 65 and 200,000 with early onset AD under the age of 65 (Alzheimer's Association, 2011) (Hebert, Scherr, Bienas, Bennett, & Evans, 2003). Late onset AD is defined as AD occurring in persons over 65 years of age. Likewise, early onset AD is defined as AD symptoms occurring prior to the age of 65. In Canada alone, the Canadian Study of Health and Aging Working Group has estimated that more than 300,000 individuals over the age of 65 suffer from dementia and of those 64% have been diagnosed with AD. By

2031, 750,000 individuals will suffer from various dementias, with the majority being the result of Alzheimer's disease (Canadian Study of HeaIth and And Working Group, 1994).

AD affects women to a greater extent than men; however, given the longer mean lifespan of women, when age specific incidence of AD are studied, there is no significant gender difference (Seshadri, Wolf, Au, & McNulty, 1997) (Hebert, Scherr, McCann, & Beckett, 2001).

Nearly all protein misfolding diseases are age dependent. As modern medicine has found cures for previously lethal diseases, such as pneumonia and infectious diseases, an increasing number of people are living sufficiently long lives to present with Alzheimer's symptoms (Krishnan, et al., 2012). Furthermore, because of the age dependent manner in which protein misfolding diseases manifest, the toxic amyloid misfold in implicated proteins has not been selected against by evolutionary pressures (Krishnan, et al., 2012).

AD disproportionally affects North Americans of African and Hispanic descent to a greater extent than those of European ancestry: people of African descent are twice as likely to be diagnosed with AD (Potter, Plassman, Burke, Kabeto, & Langa, 2009) and Hispanics one and one half times more likely (Gurland, Wilder, Lantigua, Stern, & Chen, 1999) to be diagnosed compared to whites.

Low levels of education, traumatic brain injury, high-fat and high-calorie diets and lack of physical exercise have all been correlated to higher rates of AD (Mayeux R. , 2003) (Mattson M. , 2003) (Cotman & Berchtold, 2002).

The National Center for Health Statistics reported that Alzheimer's was listed as the underlying cause of death for 82,476 people in the United States making it the fifth leading cause of death (Minino, Xu, & Kochanek, 2010). In 2008, the mortality rate for Alzheimer's disease the United States was 27.1 deaths per 100,000 people (Alzheimer's Association, 2011).

After an AD diagnosis for a person over the age of 65 years, the average AD patient survives between 4 and 8 years; however, survival of up to 20 years has been reported (Brookmeyer, Corrada, Curriero, & Kawas, 2002) (Alzheimer's Association, 2011).

The economic costs of AD is far greater than the direct costs associated with pharmaceutical treatment. For each individual suffering from AD, there is a person responsible for their care. In 80% of cases, these caregivers are unpaid family members diverting vital labour resources from the economy providing 17 billion hours of unpaid care (Alzheimer's Association, 2011). Currently, the total cost associated with AD in the US is $183 billion dollars annually.

Aggregate payments for health care, long-term care and hospice care for people diagnosed with Alzheimer's disease and other dementias are projected to increase from $183 billion in 2011 to $1.1 trillion in 2050 (in 2011 dollars) (Alzheimer's Association, 2011). The data indicate that the incidence of AD, along with associated direct and indirect costs will continue to climb as the population ages. Investment in Alzheimer's research is a wise venture which may mitigate the future costs of a population with a high incidence of AD. Neugroschl and Sano (Neugroschl & Sano, 2010) have estimated that there would be 2 million fewer cases of AD over a period of 50 years if the onset of AD could be delayed by two years resulting in a decreased need for nursing care and lost productivity of family caregivers.

1.1.2. Alzheimer's Etiology

Classically, the presence of amyloid plaques in the brain, which showed apple green birefringence when stained with Congo Red, was the definitive post mortem diagnosis for AD. In the past these plaques were believed to be causal to AD. However, research within the past ten years has shown that this actual case is far more nuanced. Many people display post-mortem

cerebral amyloid plaques without ever presenting with any Alzheimer's symptoms. Prominent researchers such as Selkoe have analogized that amyloid plaque are like "jails" which neutralize toxic oligomers. Once the "jails" are full, there are too many oligomers for the "police" (neuroclearance mechanisms) to deal with and the oligomers can wreck their havoc on the brain. Attempting to prevent amyloid plaques would release the "bad guys" causing more damage (Selkoe, Amyloid hypothesis - beta oligomers and plaques). Conversely, some people diagnosed with Alzheimer's disease do not have any amyloid plaques post-mortem. This inconsistent phenomenon can be caused by either a false diagnosis or poor specificity of the classical Alzheimer's signs post-mortem.

Amyloid fibrils were the first amyloid species identified that make up amyloid plaques. Amyloid fibrils are long, thin insoluble fibers made up of the amyloid-β peptide arranged in a cross β sheet structure. Interestingly enough, spider webs have a similar tertiary structure.

Recent research has shown that fibrils are relatively inert compared to their oligomeric counterparts. Whether oligomers are precursors to fibrils or form along a separate pathway is a subject of current research and academic debate (Yamaguchi et al. 2010).

The exact mechanism by which amyloid-β produces neurodegenerative symptoms remains unclear, although several mechanisms have been suggested to explain why amyloidosis results in specific pathologies. Research by Lal and colleagues indicates that oligomeric amyloid-β forms ion channels in lipid membranes resulting in higher levels of intracellular calcium (Lin, Bhatia, & Lal, 2001). Perturbations in membrane fluidity have been suggested by Murphy (Kremer, Pallitto, Sklansky, & Murphy, 2000) and Gattz (Muller, Eckert, Scheuer,, Cairns, & Gattz, 1998). Free radical production has been identified by Koppal (Butterfield, Varadarajan, & Koppal, 1999) and changes in lipid metabolism have been demonstrated by

Koudinova (Koudinov, Berezov, & Koudinova, 1998). Other mechanisms which have been researched are: induction of cell apoptosis (Loo, Copani, Pike, Whittemore, Walencewicz, & Cotman, 1993), the formation of ion channels in cell membrane altering ion homeostasis (Arispe, Pollard, & Rojas, 1993), and the production of toxic levels of hydrogen peroxide (Behi, Davis, Lesley, & Schubert, 1994).

Clinical diagnosis for AD, based on accepted mental and cognitive testing, is considered to be reliable for the diagnoses of AD. 90% of patients diagnosed with AD are found to have AD on autopsy (Knopman, S, J, Chui, & Corey-Bloom, 2001). Recent advances have shown promise in making an AD diagnosis using cerebrospinal fluid or blood for patients who have not yet presented with AD symptoms (DeMeyer, Shapiro, Vanderstichele, Vanmechelen, & Engelborghs, 2010).

1.1.3. Alzheimer's Genetics

A number of factors have been implicated in Alzheimer's disease including genetic mutations. Amyloid-β is cleaved from the amyloid precursor protein (APP) located on chromosome 21. APP is cleaved by the α-, β-, and γ-secretases to from 3 amyloid products of which amyloid- β is one, cleaved by the γ-secretase, also referred to as BACE1.

Autosomal dominant mutations in APP, presenilin 1 (PSEN1) or presenilin 2 (PSEN2) results in the individual developing familial (early onset) AD (Bertram & Tanzi, 2005) and occur in 10% of all AD cases. Point mutations in the APP gene result in a higher concentration of the more highly neurotoxic amyloid-β (1-42) compared to amyloid-β (1-40) (Suzuki, et al., 1994).

Mutations in PSEN1 or PSEN2 occur in 50% of all early onset AD cases. Mutant PSEN1 increases the production of Aβ42 and accelerates the deposition of AB. Knocking out PSEN1 genes in mice neurons resulted in γ-secretase activity being abolished (Scheuner, et al., 1996).

All three of these genes (APP, PSEN1, PSEN2) are located on different chromosomes, yet all share a common biochemical pathway- all three lead to an abnormal production of amyloid-β. Individuals with Down's syndrome (trisomy 21) will develop Alzheimer's disease because they have two copies of chromosome 21, doubling their potential production of amyloid-β (Masters, Simms, Weinman, Multlraup, McDonaid, & Beyreuther, 1985) (Mattson M. , 2004).

Nearly 30 genes and a variety of environmental risk factors have been implicated in late onset AD, but no other gene has been shown to influence late onset AD as much as the apoE4 allele which codes the ApoE protein (Bertram & Tanzi, 2005) which is involved in cholesterol metabolism (Mahley, 1988). Inheriting one apoE4 allele increases the risk of late onset AD because of higher amyloid deposition in the cerebral cortex (Schmechel, 1993) as a result of a failure of amyloid clearance mechanisms (Mawuenyega, et al., 2010). Inheriting alleles from both parents compounds the probability of late onset AD (Alzheimer's Association, 2011) however carrying both alleles of apoE4 is no guarantee that an individual will suffer from AD.

Apolipoprotein E2 has been shown to act as a protective factor against AD. In AD patients, the apoE2 allele is under represented while the apoE4 allele is overrepresented compared to the general population (Harper & Lansbury, 1999).

Certain genetic mutations have also been demonstrated to increase the aggregation of amyloid-β. Sandberg and colleagues demonstrated that amyloid-β with the arctic E22G mutation forms protofibrils at a greater rate than does wildtype amyloid-β (Sandberg, et al., 2010).

Other mutations have shown to have a neuroprotective effect. The A673T mutation in the APP gene, commonly found in people of Icelandic decent, has been shown to protect against cognitive decline in elderly people who do not suffer yet from any cognitive decline by reducing the aggregation of amyloid-β by approximately 40% (Jonsson, et al., 2012).

1.1.4. The Amyloid Cascade Hypothesis

The notion that amyloid-β is the causative agent in the etiology of Alzheimer's disease has been a controversial one (Hardy, 2006). However, few researchers have managed to present alternative hypothesis that explain the majority of pathological and biophysical phenomenon which are manifest in the progression of Alzheimer's disease. Like all scientific hypotheses, the amyloid cascade hypothesis has not been without some modifications over time even though the basic precepts of the hypothesis remain intact.

The identification of amyloid-β as the major constituent in amyloid plaques was first identified in the mid 1980's (Allsop, Landon, & Kidd, 1983). Within a few years, Hardy and Higgins proposed their amyloid cascade hypothesis in their highly cited review (Hardy & Higgins, 1992). Hardy, Selkoe and colleagues were the first to propose that amyloid-β is the causative agent of Alzheimer's disease and that all other phenomenon such as neurofibrillatory tangles, tau phosphorylation, vascular damage, neuronal death, dementia, and finally death, follow, in that order, from the over- production of amyloid-β (Hardy & Allsop, 1991) (Selkoe, 1991). The deposition of amyloid often begins in the mediotemporal lobe, then spreads further to the neocortex (Bonda, Lee, Blair, Zhu, Perry, & Smith, 2011).

A number of revisions to the amyloid cascade hypothesis have been accepted by the research community without compromising the underlying premise that amyloid-β is the causative agent of Alzheimer's disease. Firstly, it is now widely accepted that small molecular weight aggregates are the most neurotoxic amyloid species rather than amyloid fibrils or amyloid plaques (Klug, Losic, Subasinghe, Aguilar, Martin, & Small, 2003) (Kayed R. H., 2003) leading some authors to refer to an "oligomer cascade hypothesis". Secondly, in late onset AD, the incorrect cleaving of APP into the more pathogenic Aβ42 form as opposed to the more stable

Aβ40 (Bush & Tanzi, 2008) has been linked to AD symptoms rather than the overproduction of amyloid-β. In addition, the insufficient clearance of amyloid-β from the brain has been associated with late onset AD in cases where known genetic factors are absent (Mawuenyega, et al., 2010). The amyloid cascade hypothesis assumes a linear progression of the disease, however, considerable evidence is mounting that different amyloid species with varying degrees of toxicities may lie along different reaction pathways. Factors such as metals catalyze the aggregation process along differing pathways.

One of the recurring criticisms of the amyloid cascade hypothesis is that it fails to explain the unequal distribution of amyloid deposition in the brain; many people have been observed to have neuronal amyloid plaques during post mortem autopsy without demonstrating any Alzheimer's symptoms while they were alive (Bush & Tanzi, 2008). Lastly, the amyloid cascade hypothesis is unable to explain why Alzheimer's is an age related disease or why there are considerable vascular pathologies related to AD (Roy & Rauk, 2005).

1.2. Amyloid-β

Amyloid-β was first identified by Glemer and Wong in 1984 as the principal component of amyloid deposits (Glenner & Wong, 1984). This seminal work led to the proposal of the amyloid cascade hypothesis which posits that the presence of these amyloid plaques, leading to a post-mortem diagnosis of AD, or more likely their oligomers, disrupts the neuronal cell membrane leading to neurodegeneration. Amyloid-β has a peptide length of 39-43, with the majority of amyloid found in senile plaques having a peptide length of 42 (Masters, Simms, Weinman, Multlraup, McDonaid, & Beyreuther, 1985).

The amyloid-β peptide is an ill-defined peptide, the secondary structure of which is largely dependent on the environment. In aqueous solution, amyloid-β occurs predominantly in a

random coil conformation. When associated with a membrane, amyloid-β consists of a hydrophilic, extracellular region located at residues 1-28, and a hydrophobic, transmembrane alpha-helical coil at residues 29-42 (Barrow & Zagorski, 1992).

The gene encoding the amyloid precursor protein (APP) is found on chromosome 21 and is expressed in a variety of glial, endothelial, epithelial and spleen cells. The function of APP is unclear at this point, but research has suggested that APP may have a role as an autocrine factor to stimulate the proliferation of fibroblasts (Saitoh, et al., 1989) and as a modulator of cell adhesion. In addition, APP is implicated in the regulation of intracellular calcium (Mattson, Cheng, Culwell, Esch, Lieberburg, & Rydel, 1993), metal ion homeostatsis (Hesse, Beher, Masters, & Multhaup, 1994), and cell growth (Saitoh, et al., 1989). Recently, Sanders and colleagues demonstrated that APP may have a cholesterol binding site with E693 and N698 accepting and donating a hydrogen bonds to bind cholesterol providing evidence that APP may have a role in cholesterol regulation and metabolism (Barrett, et al., 2012).

Once amyloid-β is cleaved from APP by the secretase enzymes, amyloid-β is a soluble monomeric peptide in an aqueous environment and is cleared from the brain in healthy persons. In pathological cases, amyloid-β misfolds, aggregates and becomes neurotoxic (Selkoe, 2000) with intermediate oligomers likely the most neurotoxic species (Kayed R. H., 2003). Amyloid-β has been shown to form a variety of quaternary structures including amyloid fibrils (Petkova, et al., 2002), and a broad class of possibly intermediate structures termed amyloid oligomers which include a variety of structures such as pre-fibrillar oligomers (PFO) (Glabe, 2008) and annular protofibrils (APF) (Kayed R. , et al., 2009) among others.

1.2.1. Fibril Structure

The amyloid fibril appears to be a ubiquitous structure intrinsic to the protein backbone structure accessible to virtually any polypeptide sequence (Chiti & Dobson, 2006). Fortunately amyloid fibrils have only been shown to be associated with a limited number of diseases including Alzheimer's, Parkinson's, the prion disease and about twenty seven other diseases of various severity. Despite a similar end structure[2], there seems to be no commonality among primary protein structure linking these proteins. The classical biophysical definition of an amyloid fibril is a protein structure which exhibits red-green birefringence when exposed to circularly polarized light. Identification of amyloid fibrils is also made by determining binding to Congo red or Thioflavin T. Today, various methods including x-ray diffraction, NMR, atomic force microscopy, and electron microscopy have shown that fibrils formed by different properties share similar properties, including a structure made up of unbranched protofilaments (Nelson 2006). Mature amyloid fibrils are observed to be approximately 100Å in diameter and composed of 20–35Å wide protofilaments.

While amyloid-β has a poorly defined monomeric structure due to its insolubility and difficulty in crystallization, recent advances have allowed researchers to solve the structure of amyloid fibrils (Luhrs, et al., 2005). There is general agreement amongst researchers (Nelson & Eisenberg, 2006) that amyloid β peptides have a β sheet secondary structure which stack in a parallel or anti-parallel fashion to form β sheets running perpendicular to the fibril axis (Kirchner, Abraham, & Selkoe, 1986).

Figure 1 shows a 3D cartoon of a parallel structure of a single amyloid protofilament. A mature amyloid fibril is formed when these single protofilaments wrap around one another to form a multifilament fibril as shown in figure 2.

[2] The term "native structure" and "functional structure" are purposely not used in this context.

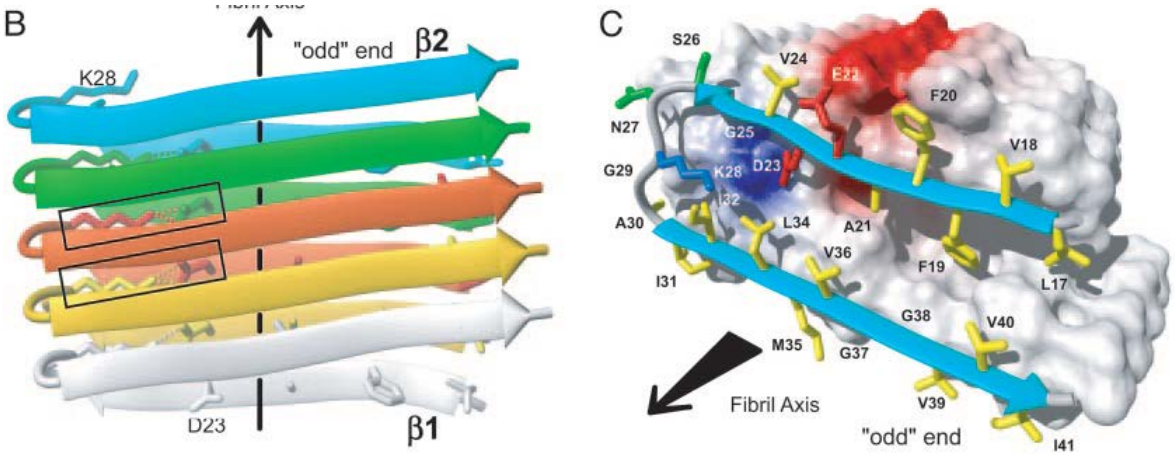

Figure 1 - Model of β sheet amyloid structure. Figure reprinted with permission from (Luhrs, et al., 2005). Copyright 2005, National Academy of Sciences, USA.

This model has been characterized as each monomer having an unstructured N-terminal (1-16) region with two hydrophobic regions (16-23 and 28-35) connected by a loop region 24-27 (Mithu, Sarkar, Bhowmik, Chandrakesan, Maiti, & Madhu, 2011). The regions which fold back on themselves have been demonstrated to move by a few amino acid sequences. An interior salt bridge forms between Asp23 and Lys28 which is detectable by NMR and MD simulations. This salt bridge is imperative for the self-dimerization of amyloid-β and an important element of fibril structure (Buchete, Tycko, & Hummer, 2005) (Ma & Nossinov, 2002). Short amino acid sequences of 14-28 have been shown to form fibrils aiding in the synthesis and purification of fibril forming peptides (Gorevic, Castaiio, Sarnia, & Fmgione, 1987). Intermolecular interactions amongst the side chains are formed between the odd-numbered residues of the first strand of the *n*th molecule and the even-numbered residues of the second strand of the (*n* -1)th molecule (Luhrs, et al., 2005) (Balbach, et al., 2002). These anti parallel sheets are held together by hydrogen bonds. All fibrils have been shown to form a left handed helix (Bauer, et al., 1995) (Goldsbury, et al., 1997) (Ionescu-Zanetti, et al., 1999) (Harper, Liber, & Lansbury, 1997).

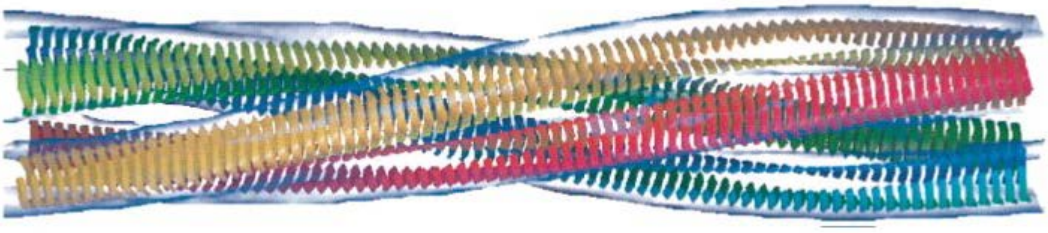

Figure 2 - Model of amyloid fibril. Figure reprinted with permission from (Jimenez, Nettleton, Bouchard, Robinson, Dobson, & Saibil, 2002). Copyright 2005, National Academy of Sciences, USA.

In the past, amyloid fibrils were believed to be structures of beta sheets arranged in an antiparallel conformation. As a result of NMR spectra reported within the last 10 years, opinion has shifted and a prevailing consensus has slowly emerged that the majority of amyloid-β fibrils are in fact stacked in a parallel conformation in most naturally occurring fibrils (Antzutkin, Balbach, Leapman, Rizzo, Reed, & Tycko, 2000) (Balbach, et al., 2002), though solid state NMR has shown anti-parallel β-sheet stacking under certain conditions *in vitro* (Buchete, Tycko, & Hummer, 2005).

Fibrils formed by amyloid-β (1-40) and amyloid-β (1-42) appear to have a similar structure on a molecular level (Mithu, Sarkar, Bhowmik, Chandrakesan, Maiti, & Madhu, 2011). Differing reports have shown a few differences between amyloid-β (1-40) and amyloid-β (1-42). Firstly, amyloid-β (1-42) has a intramolecular β-sheet at the C-terminus whereas amyloid-β (1-40) does not (Masuda, Uemura, & Irie, 2008). Secondly, the loop region at 24-27 is different from the two forms of amyloid-β although these differences are under dispute (Petkova, Yau, & Tycko, 2006) (Paravastu, Leapman, & Tycko, 2008) (Chimon, Shaibat, & Ishii, 2007). Despite these differences the two peptides contain many common structural features including the unstructured N-terminus, side chain interactions, and a salt-bridge formed between Asp23 and Lys28 (Mithu, Sarkar, Bhowmik, Chandrakesan, Maiti, & Madhu, 2011). Fibrillar structure has

been shown to differ when the fibrils are grown in different solutions (Petkova, Leapman, Guo, Yau, Mattson, & Tycko, 2005). The conformation of the less structured N-terminus of the monomer can alter the fibril structure even though the structural beta-sheet structures remain intact (Mithu, Sarkar, Bhowmik, Chandrakesan, Maiti, & Madhu, 2011).

X-ray diffraction studies have demonstrated beta-sheets with polypeptide chains running roughly perpendicular to the fibril axis and hydrogen bonds formed between chains running parallel to the fibril axis (Makin, Atkins, Sikorski, Johanssen, & Serpell, 2005). This is referred to as a cross-beta pattern (Antzutkin, Balbach, Leapman, Rizzo, Reed, & Tycko, 2000). Molecular dynamics simulations show that strong hydrophobic interactions between non-polar residues of the beta-strand result in a well packed fibril core which improves the stability of the amyloid fibrils (Buchete, Tycko, & Hummer, 2005). A parallel beta-sheet structure forms a linear chain with internuclear distance of approximately 4.8Å. In an antiparallel β-sheet structure, a planar zigzag pattern would emerge with internuclear distances exceeding 4.8Å.

Most of the evidence for antiparallel beta sheets is from experiments conducted using infrared absorbance spectra which shows a strong amide I band at 1630 cm^{-1} and a weak band at 1690 cm^{-1}. This has been interpreted as being characteristic of anti-parallel sheets (Antzutkin, Balbach, Leapman, Rizzo, Reed, & Tycko, 2000). Stacking of amyloid-β can be anti-parallel, made up of parallel dimers or parallel stacks of anti-parallel dimers (Antzutkin, Balbach, Leapman, Rizzo, Reed, & Tycko, 2000). Tycko and colleagues compared fibrils formed from antiparallel beta sheets and fibrils formed from parallel beta sheets and found that antiparallel sheets nucleate and are metastable with respect to parallel structure conversion. Both are equally neurotoxic (Qiang, Yau, Luo, Mattson, & Tycko, 2012).

Parallel and antiparallel beta sheets have been found in a variety of different proteins suggesting that parallel beta sheets may be a universal feature of amyloid structures whenever the polypeptide contains greater than one beta strand forming segment (such as the 16-23 and 28-35 segments of amyloid-β (Qiang, Yau, Luo, Mattson, & Tycko, 2012). The alignment of hydrophobic residues of amyloid-β (1-40) in parallel structures maximizes hydrophobic interactions within the beta sheet (Antzutkin, Balbach, Leapman, Rizzo, Reed, & Tycko, 2000). Usually only peptides with one hydrophobic segment form antiparallel beta sheets allowing all hydrophobic segments to interact within a planar antiparallel beta sheet which is favoured by electrostatic interactions between terminal groups (Qiang, Yau, Luo, Mattson, & Tycko, 2012).

Tycko and colleagues modified an amyloid-β (1-40) peptide chain with a D23N amino acid substitution and, contrary to expectations, demonstrated the existence of anti-parallel beta sheets. This discovery required a revision to existing understanding of fibril structure. Previous assumptions (Antzutkin, Balbach, Leapman, Rizzo, Reed, & Tycko, 2000) assumed a two dimensional plane for fibril formation. If fibril development occurs in three dimensions, though beta strand segments altered by loops or bends in a multilayered structure, both parallel and antiparallel structures can create alignments which are favourable to hydrophobic segment interactions between layers (Qiang, Yau, Luo, Mattson, & Tycko, 2012). From this understanding, it is possible that multilayered cross beta motifs could form sequences as long as the sequences contain more than two hydrophobic beta strands. Substituting a charged D23 residue for the neutral N23 residue destabilizes the electrostatic interactions. In some parallel amyloid-β (1-40) fibrils, D23 and K28 are paired stabilizing the structure (Qiang, Yau, Luo, Mattson, & Tycko, 2012).

Antiparallel fibrils are thermodynamically metastable. Antiparallel structures eventually evolve towards parallel structures when grown together with parallel fibrils. If the rate of spontaneous nucleation of antiparallel structure is greater than the rate of spontaneous nucleation of parallel structures, antiparallel conformations will dominate leading to a greater proportion of relatively short antiparallel fibrils. These fibrils will eventually shrink and disappear as monomers become more stable parallel fibrils. Parallel structures are more stable than antiparallel structures because they have more ordered residues, longer beta strand segments and possible better packing of hydrophobic side chains (Qiang, Yau, Luo, Mattson, & Tycko, 2012).

1.2.2. Oligomer Structure

Amyloid oligomers are often thought of as fibrils which have not fully matured; however, recent structural data has demonstrated that this view is overly simplistic. In fact, the term "oligomer" is a very broad term and denotes a non-native, aggregated peptide structure which is not an amyloid fibril. Some oligomeric species may eventually end as an amyloid fibril, while others travel on an off-pathway reaction coordinate. The biochemical definition of an amyloid oligomer has been identified as an amyloid species reactive to the A11 antibody and OC- whereas fibrillar species are OC+ and A11- (Kayed, 2003).

A variety of laboratories have demonstrated a diverse set of precursor or off-pathway structures to the amyloid fibril and referred to these unique species as aggregates (Kayed, 2003), micelles (Soreghan, Kosmoski, & and Glabe, 1994) , protofibrils (Harper, Liber, & Lansbury, 1997) (Walsh, et al., 1999), prefibrillar aggregates (Bucciantini M. , et al., 2002), toxic amyloid-β fibrillar oligomers (TABFO's) (Stroud, Liu, Teng, & Eisenberg, 2012), ADDL's (Lambert, et al., 1998), prefibrillar oligomers (PFO's) (Glabe, 2008), globulomers (Yu, et al., 2009) and annular protofibrils (APF's) (Kayed R. , et al., 2009). It is unclear which of these structures lie

on-pathway to the amyloid fibril, and whether any of them are overlapping species observed at different points along the aggregation pathway. Some of these structures lie on the reaction pathway to fibrils, and others lie off pathway (Necula, Kayed, Milton, & Glabe, 2007).

Oligomers and protofibrils show some common structural similarity with mature amyloid fibrils. The two beta strand sections (~16-23 and 28-28) are connected by a short loop region. However in oligomers and protofibrils, the first strand is shorter than the first strand in mature fibrils and a shift takes place during maturation to elongate this strand into mature fibrils (Scheidt H. , Morgado, Rothemund, Huster, & Fandrich, 2011) (Scheidt, Morgado, & Huster, 2012). Furthermore, Glu22 and Ile31 are closer in protofibrils than in mature fibrils (Scheidt, Morgado, & Huster, 2012). Huster and coworkers speculated that this structural rearrangement of intramolecular hydrogen bonds to intermolecular hydrogen bonds occurs in the last transition from protofibrils to mature amyloid fibrils. Beta-sheets appear antiparallel in oligomers and protofibrils, and parallel in mature fibrils as observed when using solid state NMR (Scheidt, Morgado, & Huster, 2012). X-ray diffraction studies of multimeric protein assemblies have shown peptides consisting of 2 densely packed beta-sheets with individual strands oriented with strands from one sheet anti parallel with the strands from the sheet immediately adjacent (Liu, Sawaya, Cheng, Zheng, Nowick, & Eisenberg, 2011). Often, beta-sheets appear antiparallel in oligomers and protofibrils and parallel in mature fibrils as observed by solid state NMR (Scheidt, Morgado, & Huster, 2012).

While there have been an increasing number of reports published within the last five years of oligomeric structures, (Scheidt H. , Morgado, Rothemund, Huster, & Fandrich, 2011) (Moores, Drolle, Attwood, Simons, & Leonenko, 2011), a definitive x-ray diffraction or 3D NMR structure of an amyloid-β oligomer has yet to be resolved (Barz & Urbanc, 2012).

Protofibrils are believed to be the immediate precursors to mature amyloid fibrils and are longer and more linear than oligomers, but they lack the high order and periodicity of mature fibrils and are thinner and shorter than mature fibrils (Walsh, et al., 1999) (Fandrich, 2012).

Molecular dynamics (MD) simulations conducted by Yu and colleagues show that the initial step in oligomerization is the formation of an amyloid dimer, the smallest neurotoxic oligomer. Once dimers are formed, they serve as building blocks for an annular ring of monomers forming an amyloid oligomer (Yu & Zheng, 2011) possibly leading to the species described as annular protofibrils (APF's) as described by Glabe and coworkers (Kayed R. , et al., 2009). These species may be identical to the ones identified by Bowers and colleagues as especially toxic tetramers, hexamers which can stack to form toxic dodecameric ion channels disrupting cellular homeostasis (Bernstein, et al., 2009). It is likely that these species were identical to those initially identified by Lal and colleagues as the cytotoxic commonality, linking the amyloid misfolding diseases by inducing ion channels (Quist, et al., 2005).

These annular aggregates (APF's) consist of a water filled channel or ion pore which may contribute to ion dyshomeostatis within the neuron (Connelly, et al., 2012). The hexomeric annular oligomer, as predicted and directly observed by Lal and colleagues, (Connelly, et al., 2012), is believed to insert into the membrane to act as calcium channel as demonstrated by Lin, Quist and Arispe (Lin, Bhatia, & Lal, 2001) (Quist, et al., 2005) (Arispe, Pollard, & Rojas, 1993). Its hexomeric structure was shown using MD simulations and correlates well with the observations of Bernstein and colleagues demonstrating the importance of dodecamers, a multiple unit of the hexomer in protein misfolding pathogenesis (Bernstein, et al., 2009). The membrane disrupting activities of these annular oligomers has been reviewed by Fandrich (Fandrich, 2012).

Molecular dynamics by Mu and colleagues predicted the structure of amyloid oligomers in a lipid membrane environment. Mu showed that the oligomers have a hydrophobic core and hydrophilic surface. As a result, Mu speculated that oligomerization is driven by hydrophobic effects with electrostatic effects contributing to stabilize the structure (Zhao, Chiu, Benoit, Chew, & Mu, 2011).

While the bilevel dodecamer appears to be consistent from experimental data, Zheng and colleague predicted a single level, 12-mer structure using molecular dynamics simulations (Yu & Zheng, 2011) as shown in figure 3.

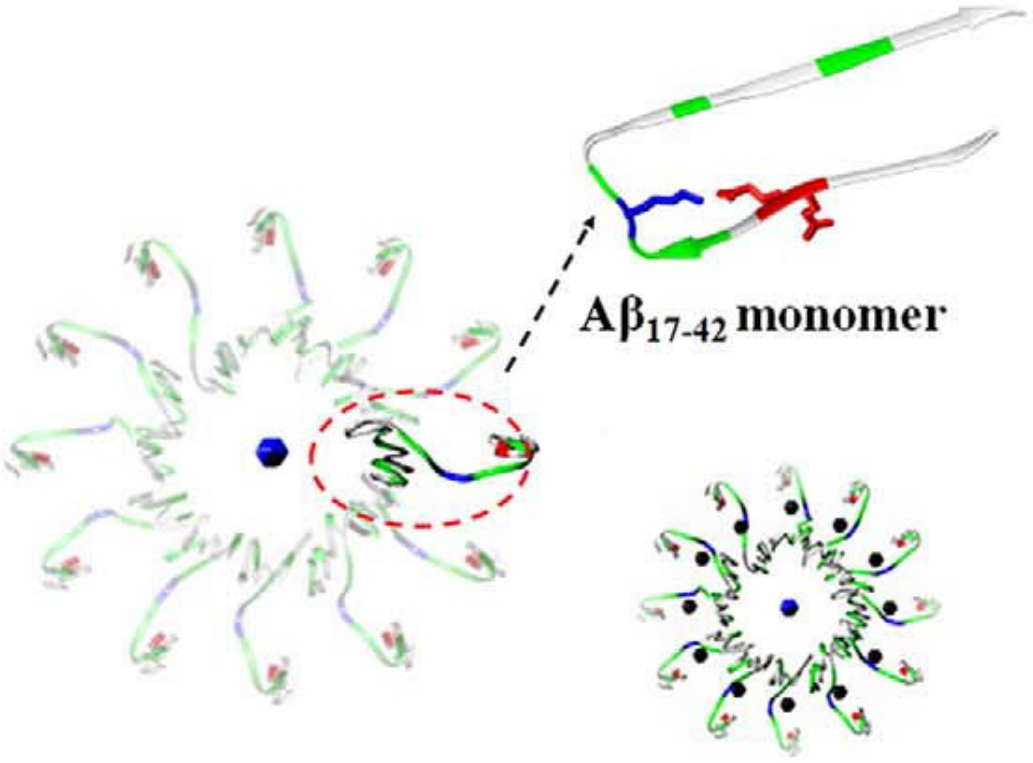

Figure 3 - MD simulation of amyloid oligomer formation. Figure adapted with permission from (Yu & Zheng, 2011).

Eisenberg and coworkers prepared a novel species of amyloid oligomer named a toxic amyloid-β fibrillar oligomer (TABFO). TABFO's share a mature cross-β structure where side chains penetrate adjacent β-sheets holding the sheets together (Stroud, Liu, Teng, & Eisenberg, 2012). However TABFO's are not short protofilaments. As a result of this structural similarity, TABFO's are OC+, similar to amyloid fibrils, yet they cannot seed new populations of amyloid fibrils. The mean mass of TABFO's is equivalent to 19 ± 4 amyloid-β monomers.

Various reports have demonstrated oligomer diameters in excess of 50 nm (Broersen, Rousseau, & Schymkowitz, 2010) (Fandrich, 2012). Whether these species are an ordered oligomer or an amorphous globulomer is unclear.

Similar, but not identical oligomeric structures are formed by Aβ40 and Aβ42. The addition of Ile41 and Ala42 at the C-terminus of Aβ42 contribute considerably to the folding of the peptide chain. These residues are hydrophobic and therefore contribute to the hydrophobic propensity of beta-sheet formation as well as reduce electrostatic contacts allowing a more diverse set of interactions with more distant residues within the protein (Côté, Laghaei, Derreumaux, & Mousseau, 2012).

Amyloid-β Neurotoxicity

Amyloid-β toxicity was first identified in the 1980's with the discovery that amyloid-β is the prime constituent in amyloid plaques (Allsop, Landon, & Kidd, 1983) (Glenner & Wong, 1984) (Hardy & Allsop, 1991) (Masters, Simms, Weinman, Multlraup, McDonaid, & Beyreuther, 1985). However, the mechanisms of action of amyloid-β were not elucidated until the last two decades.

Seven general methods of amyloid toxicity have been identified in the literature. (The chemistry of these mechanisms is explained later in this chapter):

1) Amyloid causes an inflammatory reaction with the cell membrane (Verdier & Penke, 2004).

2) Neuronal oxidative stress is caused by reactive oxidative species (ROS) (Mutisya, Bowling, & Beal, 1994).

3) The binding of amyloid-β to metals such as copper, zinc and iron results in oxidative stress (Sayre, Perry, & Smith, 1999).

4) Competitive binding of membrane receptors (Wang, Walsh, Rowan, Selkoe, & Anwyl, 2004).

5) Formation of ion channels alters cell homeostasis (Kayed, 2003) (Lin, Bhatia, & Lal, 2001).

6) The increased permeability of membranes by the thinning of the lipid bilayer (Sokolov, Kozak, Kayed, Chanturiya, Glabe, & Hall, 2006) (Hane, Drolle, Gaikwad, Faught, & Leonenko, 2011).

7) Modification of DNA structure by attachment (Geng, Zhao, Ren, & Qu, 2010).

In the past, researchers believed that amyloid plaques, made of mature amyloid fibrils, were the toxic species implicated in AD; however, it has become apparent recently that oligomers, rather than fibrils, are the toxic amyloid species. This has led some researchers to theorize that amyloid plaques (made of mature fibrils) are in fact a, "last ditch cellular attempt to wall off potentially toxic AB oligomers" (Grenough, Camarakis, & Bush, 2012).

While the misfolding of Aβ42 has been shown to be causal to the pathogenesis of AD, attributing Alzheimer's pathology strictly to the presence of Aβ42 is problematic. Firstly, it is unknown why amyloid deposits are focused on the synapse and are not uniform in the cerebral parenchyma, especially because amyloid-β is uniformly expressed and Aβ42 is a normal

constituent of all cerebrospinal fluid. Secondly, amyloid deposition increases with age, yet amyloid production does not. It appears that processes which clear amyloid deposits are diminished with age as are mechanisms to protect against redox effects (Bush & Tanzi, 2008). A difference between Aβ production and Aβ clearance is likely an underlying factor in the AD disease process (Grenough, Camarakis, & Bush, 2012).

Even though there is only a two amino acid difference in the primary structure of Aβ40 and Aβ42, there is a distinct aggregation pathway (Bitan, Kirkitadze, Lomakin, Vollers, Benedek, & Teplow, 2003) and toxicity (Dahlgren, Manelli, Stine, Baker, Krafft, & LaDu, 2002). Aβ42 aggregates at a faster rate than Aβ40 making clearance of Aβ42 aggregates more problematic (Bush & Tanzi, 2008). While pathological Aβ42 concentration is only 10% that of Aβ40, Aβ42 is predominant in pathological amyloid plaques. An increase in the ratio of Aβ42:Aβ40 is associated with early onset AD because of a mutation of the amyloid precursor protein (APP) gene. This mutation results in an increased Aβ42:Aβ40 ratio, but not an increase in the total amount of Aβ produced. In addition, Aβ42 has been shown to be more neurotoxic than Aβ40, likely because of its higher aggregation propensity and its higher reactivity with metal ions (Bitan, Kirkitadze, Lomakin, Vollers, Benedek, & Teplow, 2003) (Bush & Tanzi, 2008).

Amyloid-β can aggregate into different oligomeric structures, each with varying levels of toxicities (Klug, Losic, Subasinghe, Aguilar, Martin, & Small, 2003). The structure of an amyloid tetramer determines whether an amyloid-β alloform becomes a pathological dodecamer or is non-pathological. Small folding differences of monomers are amplified by aggregation (Bernstein, et al., 2009). Amyloid-β has been shown to produce channel-like tetrameric and hexameric structures when incorporated into lipid membranes. Tetramers and hexamers appear

to be most stable in lipid membranes. Lal and colleagues predicted the presence of hexameric structures in a lipid environment using molecular dynamics simulations and demonstrated these predictions by observing images of amyloid-β in lipids with resolved channel-like structures of four and six subunits (Lin, Bhatia, & Lal, 2001). Amorphous amyloid plaques do not appear to be neurotoxic where compact amyloid deposits appear to have higher neurotoxicity (Klug, Losic, Subasinghe, Aguilar, Martin, & Small, 2003). Stable oligomers are expected to become highly neurotoxic and are fifty times more likely to induce neuronal apoptosis than amyloid fibrils consisting of wild-type Aβ42 (Sandberg, et al., 2010). Cross-linked amyloid-β oligomers are consistently more neurotoxic than fibrils (Ono, Condron, & Teplow, 2009) (Yu & Zheng, 2011). Trimers have a toxicity three times higher than that of monomers, where tetramers have a toxicity 13 times greater than monomers. Unfractionated cross-linked oligomers have a toxicity three times greater than that of monomers (Ono, Condron, & Teplow, 2009). The order of toxicity related to structure is tetramers > trimers > dimers > fibrils > monomers (Ono, Condron, & Teplow, 2009). The exposure of hydrophobic motifs in oligomers, rather than their size and secondary structure is the primary determinant of neurotoxicity (Campioni, et al., 2010). A higher crossing angle of beta sheets result in higher curvature forming pores by creating a hole along the helical axis of the toxic amyloid-β fibrillar oligomers (TABFO) (Stroud, Liu, Teng, & Eisenberg, 2012). TABFO's are toxic to HeLa and PC12 cells at micromolar concentrations (0.5 μM) (Stöhr, et al., 2012).

The addition of metals such as Cu^{2+} appears to greatly increase the neurotoxicity of amyloid-β. Aβ42 fibrils are toxic to PC12 cells (40% viability) , whereas Aβ42 with Cu2+ ions added result in a viability of PC12 cells of only 4% (Sarell, Wilkinson, & Viles, 2010).

Post-translational pyroglutamylated forms of amyloid-β (pE-Aβ) are structurally distinct and more toxic than normal amyloid-β (1-42) on its own. pE-Aβ oligomerizes with Aβ42 to form low-n oligomers (LNO's) which are far more neurotoxic than LNO's made from amyloid-β on its own (Nussbaum, et al., 2012). pE-Aβ triggers tau dependent neuronal apoptosis that proliferate in a prion like manner (Nussbaum, et al., 2012). As a result, a small concentration of pE-Aβ radically increases the neurotoxicity of amyloid-β oligomers.

Peroxidation of lipids is a major sign of elevated levels of oxidative stress in the brain which has been found in the brains of Alzheimer's patients. This phenomenon is likely caused by reactive oxidative species such as free radicals resulting in increased apoptosis (Zhao, Long, Mu, & Yue Chew, 2012). Oxidative stress may also lead to abnormal protein structure and function leading to pathological symptoms (Abdul & Butterfield, 2007). Anti-oxidant foods such as walnuts and curcumin have been shown to prevent oxidative stress brought on by amyloid-β (Mathaiyah, Essa, Chauhan, & Chauhan, 2011).

Up until the last decade, there was an active debate amongst researchers as to whether accumulated tau protein or amyloid plaques were causal to AD pathology. These two camps were whimsically referred to as the Tauists and the βAptists (Huang T.-H. J., 2001). Despite a decrease in the published literature supporting the tau protein hypothesis, a brief overview is warranted. Tau protein is important for the stability of the cytoskeletal and axonal transport as it controls microtubule assembly maintaining the structure of the cytoskeleton. The accumulation of phosphorylated tau leading to neurofibrillary tangles (NFT's) has been shown to contribute to neuronal apoptosis (Lovestone & Reynolds, 1997). The aggregation of amyloid-β is implicated in signalling and mediating the hyperphosphorylation of tau leading to intracellular NFT's (Hernendez, Gomex de Barreda, Fuster-Matanzo, Lucas, & Avila, 2010). In addition, amyloid

neurotoxicity is compounded by the expression of hyperphosphorylated tau (Nussbaum, et al., 2012).

1.3. Amyloid-β Aggregation

The correct folding of a protein into a physiologically functional structure is not a sure thing: proteins may misfold and aggregate into a non-functional or even a toxic structure. Often, this aggregation is the result of an alpha helical structure misfolding into a β-sheet. This misfold is referred to as the toxic amyloid fold which is responsible for amyloid aggregation and toxicity (Kayed, 2003). These beta sheets can then aggregate into non-functional oligomers or amyloid fibrils.

1.3.1. Amyloid-β Misfolding and Amyloidosis

Amyloidosis is defined as an abnormal molecular process in which a protein, normally in an alpha-helical state, unfolds, re-conforms in a β-sheet conformation and aggregates to form insoluble fibril-like structures forming pathogenic amyloid plaques (Serpell, 2000). These amyloid fibrils are then deposited either systemically or in specific organs, destroying surrounding cells through apoptosis (Johannson, 2005). Amyloid plaques, the visible end-product of the amyloidosis process, can be observed by staining with the Congo Red dye and showing birefringence under polarized light. Despite significant research into the amyloidosis process, no clear reason has emerged on the formation and kinetics of this process (Carrell & Gootu, 1998). This amyloidosis process is implicated in at least twenty seven different pathologies, each one affected by the aggregation of a different protein. These diseases include the neuro-degenerative disorders Alzheimer’s, Huntington's, Parkinson's, and Creutzfeld-Jacob's.

Although much research has been conducted on the conformational change of amyloid-β, a clear answer as to why this protein and other proteins misfold still eludes the research

community. While the question is often asked why some proteins misfold, research has shown that any protein can misfold: the misfolding process is an intrinsic property of the polypeptide backbone (Bucciantini M. , et al., 2002) and is believed to be the structure associated with the global energy minimum of the protein folding free energy landscape (Percel, Hudaky, & Palfi, 2007). So rather than "why do some proteins misfold?", a more relevant question is, "why don't all proteins misfold?"

Amyloid-β fibril formation has been shown to involve an α-helix to β-sheet transition. However, not all proteins form amyloid deposits by this conformational change: α-synuclein has no defined structure in its native state, yet still forms amyloid fibrils (Johannson, 2005). Certain proteins show very similar secondary structures once the amyloid process is complete despite radically different primary structures. This suggests that the amyloidosis process for each different protein involves a different biochemical mechanism than ordinary protein folding mediated by side chain interaction (Booth, et al., 1997) such as a polypeptide backbone mediated process. In solution, amyloid-β readily transforms into a β-sheet conformation (Szyperski, Vandenbussche, Curstedt, Ruysschaert, Wuthrich, & Jan, 1998) despite the theoretical predictions that show that the helices are resistant to unfolding (Kovacs, Mark, Johansson, & van Gunsteren, 1995).

The initial aggregation step of amyloid-β occurs with the 16-23 and 28-35 alpha helical regions forming beta strands and folding back on one another to "self-dimerize" into a double layer hairpin-like monomeric structure stabilized by hydrophobic interactions and a salt-bridge on residues D23-K28 (Sciarretta, Gordon, Petkova, Tycko, & Meredith, 2005) (Rauk, 2009).

Following the initial misfold, the next step in the aggregation process is the dimerization of two monomers, the initial process resulting in neurotoxicity (Barz & Urbanc, 2012). MD

simulations conducted by the Urbanc and Zheng groups demonstrated that the formation of amyloid oligomers is driven by the shielding of hydrophobic residue side chains by the solvent. The extra two hydrophobic residues in Aβ42 results in a higher solvent exposure and therefore higher aggregation propensity (Barz & Urbanc, 2012) (Yu & Zheng, 2011). In addition, these MD simulations have shown that amyloid-β dimers are the smallest building blocks in higher ordered oligomers. During the aggregation process, these hairpin-like monomers dimerize and eventually aggregate into various amyloid structures, including oligomers, molten globules, and fibrils aligned in a parallel and antiparallel conformations (Ma & Nossinov, 2002). The stability (ie. propensity to dissociate) of larger oligomers in not a function of the size of the oligomer: dimers are less stable than oligomers (Narayan, et al., 2012).

Amyloid fibril formation has been described as a two-step process involving a nucleation phase and a growth phase. During the slow nucleation phase, alpha helical or random coil amyloid-β changes conformation into a beta sheet structure. Once this nucleus has formed, adding additional beta sheet monomers becomes thermodynamically favourable (Huang T.-H. J., 2001) and the fibril grows in either width or length or both. Because of hydrophobicity of the peptide, the aggregation of amyloid-β in solution makes kinetics experiments difficult.

The “Dock and Lock” mechanism of fibril elongation attempts to explain how monomers are added to a growing amyloid fibril. This mechanism posits that elongation is mediated by two distinct kinetic processes. In the first conformational selection phase (dock), there is a reversible process in which monomers are added to the amyloid seeds. During the second (induced fit optimization (lock) phase, additional monomers are added irreversibly in a time-dependent manner (Esler, et al., 2000) (Massi & Staub, 2001).

As a protein folds, misfolds or aggregates, it is said to flow down an energy landscape. Local minima correspond to stable states. The amyloid fibril occupies one of these minima, the oligomer another minima. Moving along different pathways is a function of the solvent properties (temperature, ionic strength, pH) and intrinsic structural features of the peptide such as amino acid mutations. Concentration may also affect its location on the energy landscape (Chiti & Dobson, 2006) (Stefani, 2012). The aggregation side of the free energy landscape is poorly defined due to the inherent instability and dynamic nature of oligomeric structures which have similar free energies. In contrast, fibrils are far more defined and stable resulting in a more pronounced free energy landscape (Stefani, 2012).

The tendency of proteins to assemble into fibrils is a general property of the polypeptide backbone (Bucciantini M. , et al., 2002) (Chiti & Dobson, 2009) (Nelson, Sawaya, Balbirnie, Madsen, Riekel, & Eisenberg, 2005) caused by the tendency of polypeptide chains to assemble into fibrils stabilized by inter-molecular hydrogen bonds between peptide bonds in parallel or anti-parallel structured beta-sheets referred to as a cross-beta structure (Stefani, 2012). When exposed to certain environments, peptides may externalize their normally buried polar side chains allowing interaction with the environment. This results in protein aggregations that are more energetically favourable, and different than those occurring in bulk solution (Suetherman & Belfort, 2005) (Stefani, 2012). Both double sheet and triple beta sheet conformations have been suggested for amyloid fibrils (Ma & Nussinov, 2012). Despite past orthodoxy that amyloid oligomers are merely small fibrils or intermediates along the fibril pathway, recent advances suggest that some annular oligomers, such as annular protofibrils may be structural end products of their own aggregation pathway as opposed to structural intermediates enroute to a fibrillar

structure (Kayed R. H., 2003) (Stefani, 2012) (Bitan, Kirkitadze, Lomakin, Vollers, Benedek, & Teplow, 2003).

Work by Giles and colleagues showed that injecting transgenic mice with amyloid-β initiated the aggregation process. The authors claimed that this was incontrovertible evidence that amyloid-β are in fact prions (Stöhr, et al., 2012). It is worthwhile to remember that amyloid-β aggregates do seed further aggregates. Whether this qualifies these peptides to be classified as prions is a matter of current debate. It does however, explain why extensively researched amyloid vaccines have been unsuccessful thus far.

Even though the primary structure sequence between Aβ42 and Aβ40 are very similar, the two alloforms oligomerize much differently. From conducting numerous cross-linking experiments, Teplow and colleagues were able to identify that Aβ42 oligomers appear as multiples (dodecamer) of small species such as hexamers by a method of self-association of smaller units (Bitan, Kirkitadze, Lomakin, Vollers, Benedek, & Teplow, 2003). Larger oligomers, such as dodecamers were found primarily in the Aβ42 alloform. At similar concentrations, oligomers of Aβ40 did not form, revealing why there is a difference between amyloid toxicity depending on which of the alloforms is present in pathological cases (Bitan, Kirkitadze, Lomakin, Vollers, Benedek, & Teplow, 2003).

Research by Merzel and colleagues showed that the kinetics of amyloid-β aggregation may be a function of ionic strength: at low ionic concentrations, electrostatic repulsion between the monomer and the fibril allows for polymerization where the monomer binds the end of the fibril. At high ionic concentrations, hydrophobic interactions drives interaction at both the end of the fibril and the lateral edges making the fibril more broad (Zidar & Merzel, 2011).

1.3.2. Evidence for Separate Aggregation Pathways

Earlier reports often assumed that the amyloid fibril pathway is a single pathway which travels through intermediates such as oligomers, protofibrils and finally to a full mature amyloid fibril. An increasing body of evidence suggests that "intermediate" species of amyloid-β are not actually intermediates, but rather lie along a separate reaction coordinate, with its divergence from the fibrillar pathway occurring early in the aggregation process. However, it is still a matter of debate whether oligomers, and perhaps which species of oligomers, are on-pathway products (grow by a direct addition of monomers) or off-pathway, meaning they occupy a minima on the free energy landscape of amyloid fibrils (Bitan, Kirkitadze, Lomakin, Vollers, Benedek, & Teplow, 2003) (Necula, Kayed, Milton, & Glabe, 2007) (Stefani, 2012) (Petkova, Leapman, Guo, Yau, Mattson, & Tycko, 2005). No standardized nomenclature has been developed for amyloid intermediates or off-pathway structures. While research by the Glabe group uses the terms fibrillar oligomer and prefibrillar oligomer, other terms found in the literature include protofibrils, unstructured oligomers (Bieschke, et al., 2012) among others.

Small and colleagues used PAGE to observe different aggregation patterns in amyloid-β. Small showed that one of the pathways was inhibited by metal ions and slowly generates stable species detectable by PAGE. Along another pathway, unstable species that rapidly disaggregate are generated; these are not detectable by PAGE. Neurotoxicity studies show that amyloid-β which is slow to aggregate is more neurotoxic than the unstable species which aggregates more rapidly (Klug, Losic, Subasinghe, Aguilar, Martin, & Small, 2003).

Research by the Glabe laboratory has identified species of oligomers based on their reaction with antibodies (Glabe, 2008). Glabe has demonstrated that once the monomer misfolds, the aggregation pathway begins with a divergence depending on the conformation it adopts. The products along this reaction pathway include prefibrillar oligomers and fibrillar oligomers.

Products on this pathway are reactive to either antibody A11 or OC. Prefibrillar oligomers (PFO) are A11+ and OC-. These prefibrillar oligomers can then continue along their reaction pathway to form protofibrils and eventually amyloid fibrils. The second pathway, that of fibrillar oligomers (FO), is OC+ and A11- and represents fibril nuclei. The elongation of fibrils is a result of the addition of monomers until they become amyloid fibrils (Glabe, 2008). The fact that there is a difference in antibody binding to different oligomer structures suggests that there is a fundamental structural difference between the prefibrillar oligomer and the fibrillar oligomer (Glabe, 2008). However, Glabe and colleagues also showed that not all oligomers necessarily lie on the pathway to fibril formation (Necula, Kayed, Milton, & Glabe, 2007) (Kayed R. , et al., 2009) (Chen & Glabe, 2006). β-sheet–rich spherical oligomers lie along the fibril reaction pathway whereas unstructured oligomers are off-pathway (Ahmed, 2010). The hypothesis that various species lie along different pathways is supported by the observation that at high concentrations of urea, oligomers do not yet form amyloid fibrils still form. Certain oligomeric species such as spherical oligomers are observed at intermediate times of incubation during amyloid fibrillogenesis resulting in the conclusion that oligomers lie along the fibrillization pathway (Glabe, 2008). Further research by Glabe demonstrated that amyloid fibrillar oligomers do not seed Thioflavin T (ThT) positive amyloid fibrils. These fibrillar oligomers nucleate soluble oligomers which are OC positive and ThT negative (Wu, et al., 2010). By using ThT fluorescence, Glabe showed that fibrillar oligomers seed other fibrillar oligomers rather than amyloid fibrils and the kinetics of fibrillar oligomer formation is faster than fibril formation. Glabe concluded that soluble fibrillar oligomers are distinct from prefibrillar oligomers and mature fibrils with distinct structural and antibody reactive properties.

The work by Glabe is supported by observations by Dobson and Härd who used protein engineering to study the aggregation pathways of amyloid-β. Härd and colleagues found that amyloid-β can aggregate along at least two different aggregation pathways. By blocking amyloid fibril formation, toxic oligomers are transiently formed (Sandberg, et al., 2010). Härd deduced that the higher neurotoxicity of oligomers is a function of its aggregation pathway compared to the fibril forming pathway. By modifying the amyloid-β peptide, Härd demonstrated that a disulfide bridge between Cys21 and Cys30 prevented the formation of amyloid fibrils and formed stable oligomers which are indistinguishable from wild-type amyloid oligomers and contained dimeric and trimeric structures which have been shown to be neurotoxic.

Hoshi and colleagues used fluorescence correlation spectroscopy and TEM to uncover a novel amyloid species referred to as amylospheroids (ASPD). The pathways to ASPD's is off-pathway to fibrils. ASPD's initiate with trimerization as opposed to dimerization and their most toxic forms are 128 kDa 32-mer as opposed to the initial dimerization of fibrils (Matsumura, et al., 2012). ASPD's are not incorporated during fibrillogenesis and have different morphology from amyloid derived diffusible ligands (ADDL's) and protofibrils as well as different immunoreactivity profiles of the oligomeric antibody A11. Hoshi and colleagues provided some evidence that ASPD's are the amyloid species directly casual to neuronal apoptosis (Matsumura, et al., 2012). In contrast to fibrils, ASPD's do not form at lower pH. The assembly of various species may not be a linear process, but rather the result of the integration of various kinetic pathways.

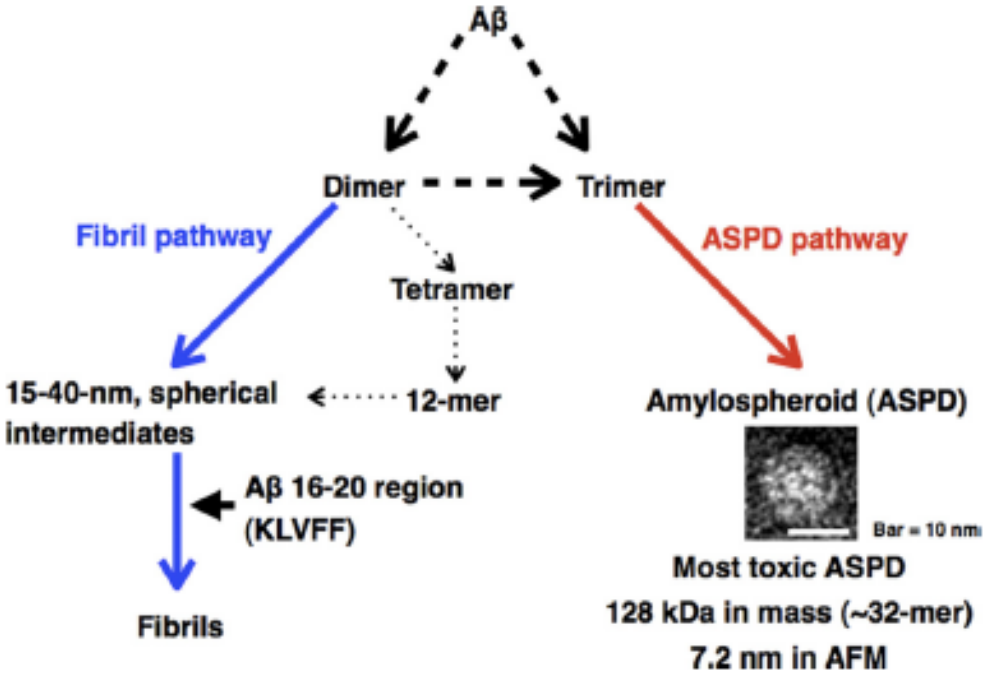

Figure 4 - Possible divergence pathway of fibrils and ASPD's. Figure reprinted with permission from (Matsumura, et al., 2012). Copyright 2012, the Journal of Biological Chemistry.

Molecular dynamics simulations by Shea and colleagues demonstrated a "rich diversity" of aggregation pathways (Bellesia & Shea, 2009). Shea demonstrated that these pathways occur via three mechanisms. The first is ordered oligomers assembling into fibrils, the second is the aggregation of on-pathway non-fibrillar aggregates; the third is the reorganization of amorphous aggregates into fibrils (Bellesia & Shea, 2009). All beta rich sequences resulted in non-fibrillar annular barrel-type structures (perhaps those observed by Lal (Connelly, et al., 2012) Glabe (Kayed R. , et al., 2009) or Teplow (Bernstein, et al., 2009) or fibrils. As the beta-sheet propensity of the peptide increased, the number of possible aggregation pathways was reduced. The barrel type structure appeared to be off-pathway and never evolved into fibrils. Furthermore, by increasing the flexibility of the peptide backbone, the number of possible end products is increased.

Theoretical predictions by Yu and Zheng demonstrated a unique conformation of amyloid oligomers which occur on a different reaction pathway than the fibrillar pathway, suggesting different kinetics between the two amyloid species (Yu & Zheng, 2011). The fibril pathway occurs as a two-step process with a lag phase in which nucleation occurs, and a growth phase associated with the elongation of the amyloid fibrils. Oligomers (called globulomers by Yu) on the other hand, form by interacting with other monomers and oligomers and occur rather quickly. Residues are packed in an out-of register fashion between the twisted beta strands. These globulomers have a measured diameter of 4nm with a molecular weight of 64 kDA corresponding to a 12-16 monomeric units/globulomers (Yu & Zheng, 2011). Yu determined the interaction energy of dimerization between the different species of amyloid aggregates and found that the parallel conformation dimer is more favoured than the out of register dimer conformation associated with the globulomers.

The aggregation pathway which amyloid-β travels appears to be concentration dependent. Aβ42 has been shown to form prefibrillar oligomers at concentrations below 30 μM while forming fibrils at higher concentrations. Tessier and colleagues demonstrated the conversion of a prefibrillar oligomer into an oligomer which is less toxic than the amyloid-β monomer and unable to disrupt the lipid bilayer. The authors proposed that peptide-lipid interaction is a function of the exposed hydrophobic segments (Ladiwala, et al., 2012).

By adding a novel amyloid antibody, KW1, to an incubation of amyloid-β, the addition of 1% preformed fibrils to the monomeric solution resulted in a 50% decrease in the lag curve; however, adding preformed oligomers to the incubation solution resulted in no change in the lag curve (Morgado, et al., 2012). This indicates that KW1 can accelerate the aggregation of amyloid fibrils but not oligomers.

Lastly, Aβ40 and Aβ42 have been demonstrated to aggregate along separate pathways despite an identical hydrodynamic radius (Chen & Glabe, 2006). The initial folding structures of Aβ40 and Aβ42 are different and effect the peptides pathway to form higher order fibrillar structures. This difference is attributed to Aβ40 and Aβ42 having different aggregation pathways (Chen & Glabe, 2006). Data collected by Teplow and colleagues suggest that the difference in fibril assembly occurring between Aβ40 and Aβ42 begins immediately after peptide translation (Bitan, Kirkitadze, Lomakin, Vollers, Benedek, & Teplow, 2003). Further research by the Glabe lab demonstrated that Aβ42 tends to form trimers and tetramers with a higher free energy than Aβ42 which remains in monomeric forms (Chen & Glabe, 2006). In addition, ASPD's from Aβ42 formed much faster than those from Aβ40 and were two orders of magnitude times more toxic (Matsumura, et al., 2012).

This difference in aggregation pathways between the two alloforms could be responsible for the pathological difference between the two alloforms: an overexpression of Aβ40 does not result in Alzheimer's symptoms whereas low levels of Aβ42 results in amyloid pathology (Chen & Glabe, 2006). This can be attributed to the difference in secondary structure between the two. Aβ40 is found to be largely in a monomeric form containing extensive random coil regions, but is not completely unfolded and likely adopts a two state unfolded monomer to monomeric model (Chen & Glabe, 2006). Consistent with the predictions made by Shea, as the beta-sheet content increases, the number of possible aggregation pathways decreases (Bellesia & Shea, 2009) leading to a higher probability of Aβ42 travelling along a pathogenic pathway.

1.3.3. Aggregation Kinetics

Amyloid aggregation follows a sigmoidal growth curve characteristic of nucleation dependent polymerization. Seeding the solution with preformed fibrils tends to result in a

hyperbolic growth curve (Hurshman, White, Powers, & Kelly, 2004). However hyperbolic curves have been demonstrated in some non-seeded experiments as well (Crespo, Rocha, Damas, & Martins, 2012). There are many different amyloid forming proteins each of which have their own individual kinetic and aggregation properties (Bellesia & Shea, 2009), however, the basic principles of aggregation kinetics apply to all of them.

The conformational change of a protein from its native state is the initiating step in protein aggregation (Chiti & Dobson, 2009). As the peptide begins to aggregate, a critical nucleus is formed. Repeated observations that adding fibrillar seeds to monomeric solutions eliminates the lag phase in the sigmoidal growth curve creating a hyperbolic growth curve (Crespo, Rocha, Damas, & Martins, 2012) supports the hypothesis that the formation of a critical nucleus is the rate limiting step in fibril formation and is responsible for the lag phase of growth kinetics (Stefani, 2012). In addition to seeding aggregates *in vitro*, adding pre-formed fibrils has been shown to accelerate the deposition of amyloid oligomers leading some researchers to conclude that amyloid forming proteins such as amyloid-β are in fact prions (Stöhr, et al., 2012). MD simulations by Urbanc showed that when the primary sequence of Aβ40 is modified slightly to form a D23-K28 covalent bridge, fibrils formed at a rate three orders of magnitude faster than the wild type protein. The authors suggest that the increase in kinetics is a result of a bypass of a rate limiting nucleation process (Barz & Urbanc, 2012).

Whether amyloid fibril formation is a one-step or two-step nucleation process is a question of contemporary debate and closely related to the debate of on- and off-pathway intermediates. Recently, Kashchiev and colleagues developed a model showing that the kinetic pathway is a function of both temperature and amyloid concentration in solution (Auer, Ricchiuto, & Kashchiev, 2012). Amyloid fibrillization can proceed in either a one-step

nucleation pathway where monomers directly become fibrils or along a two-step nucleation pathway where monomers become oligomers which then become fibrils. The conclusions derived from this kinetic model agree with the phenomenological observations made by Glabe (Glabe, 2008). At lower concentrations (<20 μM), OC+ fibrils tend not to form, but rather A11+ unstable oligomeric structures (Ladiwala, et al., 2012). The critical concentration of an amyloid forming protein is the concentration at which the rate of fibril formation is equal to the rate of fibril dissolution (Andreu & Timasheff, 1986). The aggregation process is a function of the initial protein concentration and depends on whether the concentration is greater than or less than the critical protein concentration (Lomakin, Chung, Benedek, Kirschner, & Teplow, 1996). Fibril nucleation is much slower than oligomer formation because of the greater entropic barrier needing to be overcome during fibrillar self-assembly (Lansbury, Costa, Griffiths, Simon, & Auger, 1995).

Hoshino and colleagues put forth a model for amyloid-β aggregation whereby the lag phase is caused by association events between amyloid-β molecules. Covalent disulfide linking between two separate peptides results in an increased local concentration leading to an increased rate of aggregation and an increase in the formation of ThT active aggregates (Yamaguchi, Yagi, Goto, Matsuzaki, & Hoshino, 2010). This state has a different morphology than amyloid fibrils even though it is ThT positive. These protofibrils aggregates are not the most thermodynamically stable, but occupy a kinetically trapped state.

The pathway leading to amyloid fibrils is not a direct one. Monomers can rapidly become paranuclei which can oligomerize further to form beaded structures or protofibrils at a slower rate. Finally, the protofibrils can irreversibly become mature fibrils (Bitan, Kirkitadze, Lomakin, Vollers, Benedek, & Teplow, 2003).

Bernstein and colleagues showed how tetramers, hexamers and dodecamers all lie along the neurotoxic pathway (Bernstein, et al., 2009). Figure 5 shows a cartoon of proposed different aggregation pathways. In the top random coiled pathway, the aggregates end up as non-fibrillar aggregates which bind to the A11 antibody. These aggregates are less structured than their fibrillar counterparts. The lower pathway travel along a β-sheet pathway with a neurotoxic fibril end product (Sandberg, et al., 2010).

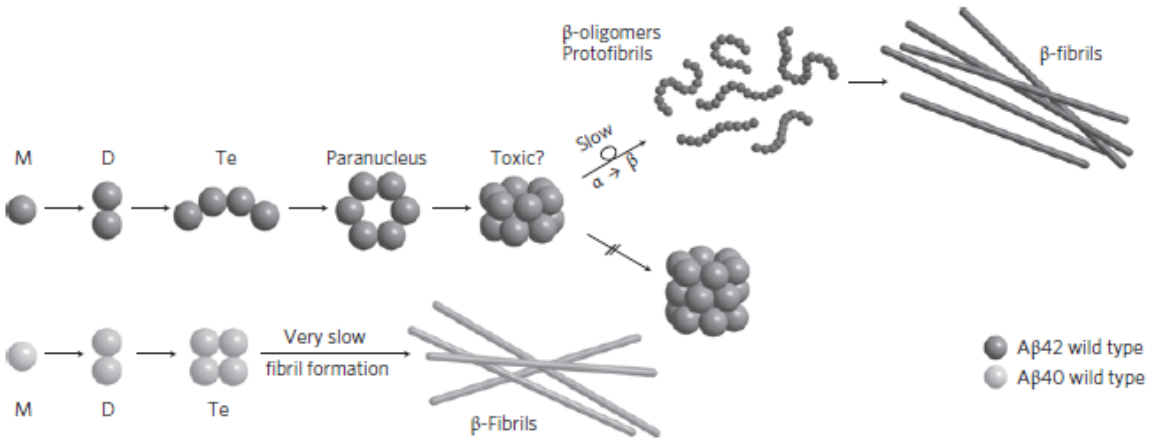

Figure 5 - Suggested amyloid aggregation pathway. Figure reprinted with permission from (Bernstein, et al., 2009). Copyright 2009, Nature Publishing Group.

Work by Lindquist and colleagues (Krishnan, et al., 2012) demonstrated that in the multitude of amyloid pathways, certain pathways result in OC+ aggregates (fibrils) and other pathways in A11+ aggregates (oligomers). Labeling the peptide with these antibodies directs the aggregation pathway along its respective pathway. There is a direct pathway to amyloid fibrils, but many secondary pathways result in a local minima in the free energy landscape.

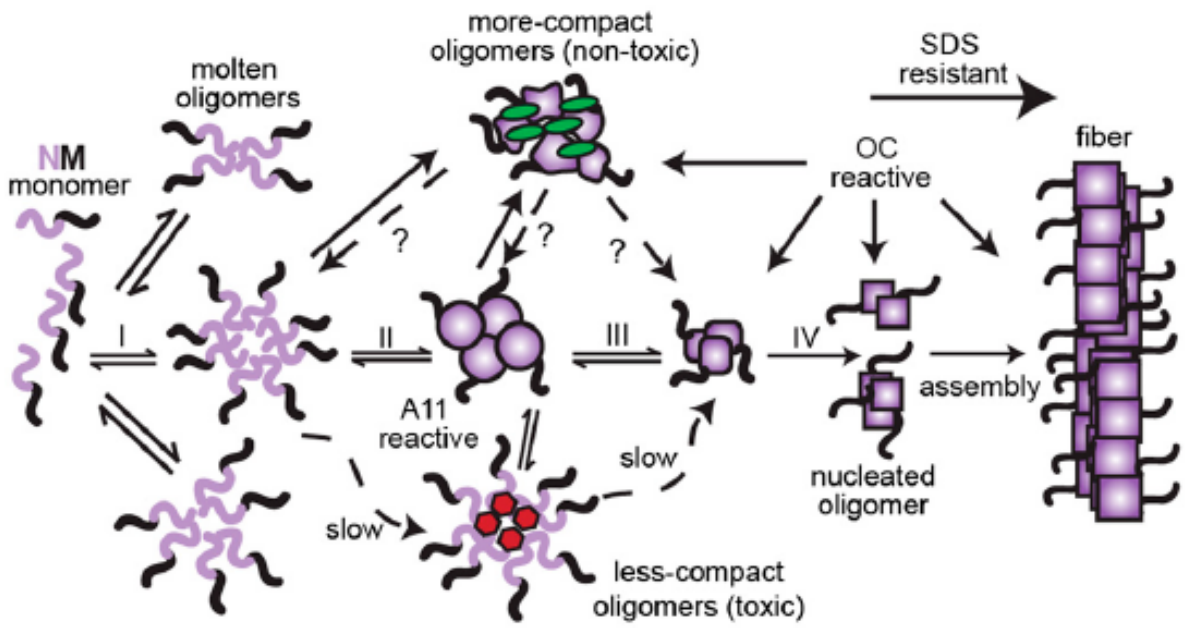

Figure 6 - Possible aggregation pathways. Figure reprinted with permission from (Krishnan, et al., 2012). Copyright 2012, National Academy of Sciences, USA.

Observations by a number of groups have demonstrated that even if amyloid species proceed along one pathway, they can readily change conformation and follow another pathway. For example, prefibrillar oligomers (PFO's) are A11+ and appear early in incubation. When exposed to hydrophobic-hydrophilic surfaces, or during longer incubation, PFO's can form annular protofibrils (APF's) which are circular PFO subunits and form pore forming ion channels (Kayed R. , et al., 2009). Fibrillar oligomers are A11- and OC+ and eventually seed amyloid fibrils and are thought of as small amyloid fibrils (Butterfield & Lashuel, 2010). During oligomer to fibril transition, there is a 90° rotation of the β-strands suggesting an intra- to inter-molecular hydrogen bond conversion. It is believed that this switch occurs as protofibrils mature into mature amyloid fibrils (Scheidt, Morgado, & Huster, 2012).

Different amyloid-β alloforms have different motifs, and as a result, different kinetic pathways (Côté, Laghaei, Derreumaux, & Mousseau, 2012). Despite similar primary structure,

Aβ40 and Aβ42 do not proceed along similar pathways. Aβ40 does not readily form typical amyloid fibrils: rather, it forms shorter protofibrils aggregates without any detectable lag period (Yamaguchi, Yagi, Goto, Matsuzaki, & Hoshino, 2010). A kinetic barrier for the formation of β-sheet makes Aβ40 more prone to form along the coil pathway rather than a toxic oligomeric pathway. This may explain why Aβ42 is more toxic than Aβ40 (Sandberg, et al., 2010). Aβ42 aggregates at a faster rate than Aβ40 because of a kinetic barrier in the Aβ40 pathway (Bitan, Kirkitadze, Lomakin, Vollers, Benedek, & Teplow, 2003) (Bernstein, et al., 2009).

Changes in kinetic properties of amyloid-β aggregation (ie. On rate) are not necessarily a function of thermodynamic effects (such as structural changes, solubility, etc). For example, the apoE3 gene reduces the rate of amyloidosis in Aβ40 without affecting the structure of the fibrillar end product (Evans, Berger, Cho, Weisgraber, & Lansbury, 1995).

Both the nucleation rate and the growth rate affect the fibrillization of proteins. Teplow and co-workers have argued that the terms “inhibition” and “promotion” describing external agents are overly simplistic because an “inhibitor” may inhibit nucleation, thereby reducing the number of fibrils, resulting in longer fibrils (Lomakin, Chung, Benedek, Kirschner, & Teplow, 1996).

Work by Roberts and colleagues (Ryan, Friedhube, Lind, Howlett, Masters, & Roberts, 2012) examined the kinetics of Aβ42 fibril formation in the presence of 96 different amphipathic molecules. Compounds such as sodium salt of deoxycholic acid maximized fibril formation whereas sodium dodecyl sulfate (SDS) maximized oligomer formation. The authors suggest that the amyloid-β binding site contains at least one small molecule binding site which modulates peptide aggregation. Human serum albumin inhibits the kinetics of amyloid fibrillization by increasing the lag time associated with fibril formation acting somewhat analogous to

competitive inhibitor in the aggregation pathway (Stanyon & Viles, 2012). In addition, human serum albumin (HAS) reduces the total number of fibrils generated as reflected in the reduced fluorescence signal. The authors suggest that HSA binds to amyloid-β molecules trapping them in a non-fibrillar form effectively preventing them from forming fibrils. It is interesting to note that while the binding affinity of HSA to amyloid-β is unremarkable (K_d=5μM), the concentration of HSA in the cerebrospinal fluid (CSF) is 3μM resulting in a reduction of amyloid-β able to aggregate.

1.3.4. Aggregation Statistical Mechanics

Looking at the amyloid cascade hypothesis through the lens of energy landscape theory raises some interesting observations. Firstly, a sufficient amount of amyloid-β protein must be present for nucleation to occur above and beyond the "saturation point", where the saturation point is the concentration at which, above, aggregation will occur. Secondly, a sufficient number of oligomers must be present and escape their free energy "reservoir" to support the elongation of fibrils. The protein diffuses down the free energy landscape as the aggregation process progresses with oligomers and fibrils occupying local or global minima (He, Giurleo, & Talaga, 2010). Disordered free structures have a high free energy while mature fibrils occupy a lower free energy state. By probing their locations on the free energy landscape, toxic oligomers and the critical nucleus required for aggregation have different energy landscapes.

There is a significant reduction in the free energy upon monomer to dimer conversion (Barz & Urbanc, 2012). The relationship between various amyloid intermediaries can be determined by probing their locations on the free energy landscape (He, Giurleo, & Talaga, 2010). Different secondary structures (parallel vs. antiparallel) in amyloid fibrils result in different potential energies (Han, Wang, & Yang, 2008). The formation of higher order

structures is a function of the concentration of reservoir oligomers. Elongation of fibrils or the formation of higher order structure requires the depletion of the reservoir of intermediate structures. The filling of the reservoir with intermediates may be the rate limiting step in any aggregation process (He, Giurleo, & Talaga, 2010). It is generally agreed that the amyloid fibril occupies the global free energy minima and is therefore the most stable structure both in a vacuum and in aqueous environments (Stefani, 2012) (Perczel, Hudaky, & Palfi, 2007). In particular, double or multiple stranded fibrils are the most stable structures. Theoretical work by Shea and colleagues showed that barrel-like aggregates have nearly identical potential energy as mature, triple layered fibrils (Bellesia & Shea, 2009).

A more flexible peptide results in a greater diversity of structures. The effect of β-sheet propensity and temperature has the greatest impact on the final oligomeric or fibrillar structure. A lower temperature and a high propensity of β -sheet structures is associated with a higher probability of forming highly ordered, triple layered amyloid fibrils. Amorphous structures occupy the phase space where temperature is highest and β-sheet propensity is lowest (Bellesia & Shea, 2009).

The aggregation process is driven by thermodynamics: once aggregation begins, there is no thermodynamic reason for the process to cease (Perczel, Hudaky, & Palfi, 2007) other than the structure finding a local minima. However, given the roughness of the free energy landscape, any increase in enthalpy would result in the protein coming out of its well, and further proceeding down the free energy landscape.

There is no primary amino acid sequence that codes for the amyloid fibril, rather, the aggregation of proteins is an inherent property of the polypeptide backbone (Perczel, Hudaky, & Palfi, 2007).

Antiparallel structures are preferred to parallel structures in amyloid aggregates when metals are added (Han, Wang, & Yang, 2008). Using MD simulations, the potential energy of antiparallel structures is predicted to be approximately 25% lower than that of parallel structures.

A greater proportion of hydrophobic residues exposed to the solvent correlate with increased propensity for aggregation. Aβ42 dimers showed a greater number of shallow local minima compared to Aβ40 (Barz & Urbanc, 2012). Aβ42 dimers show a greater structural diversity than Aβ40 (Barz & Urbanc, 2012). Using this reasoning, a mutation that induces aggregation would be expected to lower the energy barrier associated with aggregation (He, Giurleo, & Talaga, 2010).

Talaga and colleagues used a statistical mechanical method to quantify the aggregation of β-lactoglobulin, an amyloid forming protein. Talaga defines the term 'reservoir oligomer' as a structure occupying a local energy minima. Sufficient energy is required for the structure to escape the reservoir ie. overcome an energy barrier (He, Giurleo, & Talaga, 2010).

1.4. Amyloid-β-Metals Interactions

The presence of metals in amyloid plaques has long been attributed to a link between amyloid fibril formation and metal ions. In fact, in times past, physicians even recommended that people shouldn't cook in aluminum pans for fear of aluminum residues entering the body and making their way to the brain and inducing AD. Recent scientific advances have calmed the fears of gastronomers everywhere: cooking with aluminum pans has been disproven as contributing to Alzheimer's disease. Amyloid-β has a unique affinity to metal ions such as copper and zinc coordinated at the imidazole groups of His6, His13 and His14 (Faller & Hureau, 2009) (Hou & Zagorski, 2006) (Shin & Saxena, 2008) via a cross-linking action (Han, Wang, & Yang, 2008).

The brain uses more oxygen than any other organ in the body; it accounts for 20% of oxygen consumption but only accounts for 2% of the body's mass (Smith, Cappai, & Barnham, 2007). Amyloid deposits are focused in the synapses and lamina media of the cerebrovasculature and are not distributed uniformly despite the fact that APP is uniformly expressed rendering the theory that elevated amyloid-β levels the sole determinant of amyloid deposition highly improbable (Bush & Tanzi, 2008). Concentrations of metals in the brain are regulated at the blood brain barrier (Grenough, Camarakis, & Bush, 2012).

There appears to be a number of different mechanisms in which metal ions aggravate Alzheimer's disease (Faller & Hureau, 2009). Copper tends to drive the aggregation of amyloid-β towards the anti-parallel conformation which has a potential energy of approximately 25% lower than the parallel structure resulting in the formation of toxic oligomers rather than inert fibrils. Even sub-molar concentrations of copper ions released from synapses are sufficient to induce amyloid aggregation (Jun & Saxena, 2007) (Tougu, Karafin, & Palumaa, 2008). Redox active Fe(III) and Cu(II) have been shown to be neurotoxic via a Fenton reaction, while Zn(II) is believed to be neuroprotective or neurotoxic dependant on its concentration (Nair, Perry, Smith, & Reddya, 2010). Depending on concentration, zinc has been shown to stabilize amyloid oligomers preventing further aggregation into fibrils (Nair, Perry, Smith, & Reddya, 2010) or induce aggregation, but direct the aggregation pathway towards amorphous end products (Karr & Szalai, 2008). Cu(II) binding has K_d values several orders of magnitude lower than Zn(II) binding indicating a much stronger affinity (Faller & Hureau, 2009).

Rat and mouse amyloid-β has substitutions that reduce the affinity for metals (Bush, Pettingell, & Multhaup, 1994) leading some researchers to speculate that this is why these animals do not have amyloid deposits with advanced age (Bush & Tanzi, 2008).

Aβ42 has a greater binding affinity for Cu(II) than Aβ40 providing another possible explanation of why Aβ42 may be more neurotoxic than Aβ40 (Curtain, Ali, & Volitakis, 2001).

1.4.1. Chemistry of Amyloid-β-Copper Interactions

The brain has many different ways to regulate free copper ions. These include circulating albumin to bind copper, rendering it unavailable for forming amyloid complexes (Hartter & Barnea, 1988) (Lutsenko, Bhattacharjee, & Hubbard, 2010), and the limited uptake of free copper across the blood-brain barrier (Choi & Zheng, 2009) (Eskici & Axelsen, 2012).

His13 and His14 are the main ligands involved in metal coordination in amyloid aggregation. Cu binds to the imidazole ring of the histidine residues at the nitrogen atoms (Miura, Suzuki, Kohata, & Takeuchi, 2000). The specific atoms involved in binding metal ions are the N atom from the imidazole ring of His residues, N of the deprotonated amide of His, the O of the carboxyl group, N of the deprotonated amide of the main chain and O of water. Metals such as Cu(II) and Zn(II) can bridge peptide chains via tetrahedral coordination (Han, Wang, & Yang, 2008). Glu3, Glu11, Glu23, Asp1, Asp7, Asp23 and Tyr10 may also be involved in metal complexing (Nair, Perry, Smith, & Reddya, 2010) (Han, Wang, & Yang, 2008). Asp1 has been shown to form stable complexes with the His residues and Cu(II) however, Asp1 does not bind Cu(II) if there is any His binding (Azimi & Rauk, 2011). Cu(II) is more efficient in histidine binding than Fe(III) which is more efficient than Zn(II) (Cu>Fe>Zn) explaining why Cu(II) displays higher levels of peptide-metal complexing (Nair, Perry, Smith, & Reddya, 2010) than the other two metal ions. Copper binding to amyloid-β is dependent on pH with an increasing affinity with a drop in pH (Syme, Nadal, Rigby, & Viiles, 2004).

Various laboratories have shown that Cu(II) affinity towards amyloid-β varies from attomolar (Atwood, et al., 2000) to micromolar (Garzon-Rodriguez, Yatsimirsky, & Glabe,

1999). The difference in environmental conditions may account for some of these differences (Tougu, Tiiman, & Palumaa, 2011). Cu(I) appears to bind Cu with much higher affinity (femtomolar) then Cu(II) (Feaga, Maduka, Foster, & Szalai, 2011) (Azimi & Rauk, 2011).

There has been considerable controversy in the literature regarding the effects of Cu(II) ions as a function of their concentration. Substoichiometric levels of Cu(II), which are physiologically relevant, increase amyloid neurotoxicity (Sarell, Wilkinson, & Viles, 2010). However, as the concentration of Cu increases, the aggregation pathway tends to form neurotoxic non-fibrillar aggregates such as protofibrils and ADDL's (Eskici & Axelsen, 2012).

The potential energy of an amyloid-β dimer coordinated with Cu(II) is lower in an anti-parallel conformation compared to parallel. This difference is attributed to the difference in potential energies of the secondary structures and the planar structure of the metal bridge bonds in antiparallel structures which serve to further stabilize the structure. It is unlikely that Cu(II) is involved in parallel β-sheet structures because the Cu associated His13 and His14 residues would lie on opposite sides of the β-sheet and would be unable to interact with copper (Eskici & Axelsen, 2012).The formation of a bridge induced by metal binding results in a drop in the potential energy from -36.40 kcal/mol to -405 kcal/mol with Zn (II) binding and -281 kcal/mol with Cu (II) binding stabilizing the peptide structure (Han, Wang, & Yang, 2008).

The cleaving of APP is a function of γ-secretase and β-secretase activity. The cleavage site determines whether the amyloid-β will have a propensity to aggregate (Aβ42) or not (Aβ40). The presence of copper is one of the factors (via other copper binding proteins) that influences the cleaving sites of the secretases (Thinakaran & Koo, 2008). APP has a copper binding domain at 124-189 and 376-554 which lies outside the domain cleaved for amyloid-β (Eskici & Axelsen, 2012). The copper binding domain of APP demonstrates a K_d value of 10nM indicating a strong

affinity for Cu (Smith, Cappai, & Barnham, 2007). Figure 7 shows the three possible coordination geometries of the APP protein. 7A shows a 5 coordinate geometry of a crystal structure of the Cu binding domain. Figure 7B shows a tetrahedrally distorted square planar geometry in APP. 7C shows square planar coordination geometry in amyloid-β involving His6, His 13, and His14 (Eskici & Axelsen, 2012).

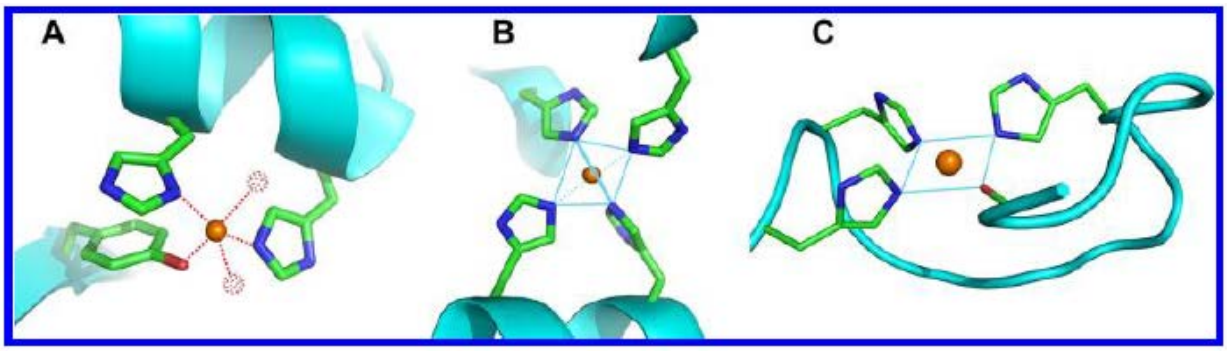

Figure 7- APP-Cu coordination geometries. Figure reprinted with permission from (Eskici & Axelsen, 2012). Copyright 2012, American Chemical Society.

1.4.3. Chemistry of Amyloid-β-Zinc Interactions

The amyloid-β zinc coordination is similar to that of the amyloid-β copper coordination. Reddya and colleagues demonstrated a 1:2 stoichiometry of Zn:histidine residues with an octahedral structure (Nair, Perry, Smith, & Reddya, 2010) likely made up of 4-6 ligands including His6, His13, His14 and possibly Asp1 (Faller & Hureau, 2009). However, other side chains such as Asp and Glu and the hydroxyl group of Tyr may contribute to Zn binding affinity (Nair, Perry, Smith, & Reddya, 2010). Zn can destabilize and break the loop region formed by Asp23 and Lys28 by forcing these residues into conformations where salt bridge formation is not favourable (Mayeux, Tang, & Mehta, 1999) while leaving the cross-β structure of fibrils intact (Mithu, Sarkar, Bhowmik, Chandrakesan, Maiti, & Madhu, 2011). Amyloid-β forms a cross-β structure regardless of whether or not exposed to Zn. Zn ions bring more order to the side chains

of the histidine residues at the metal binding site. Furthermore, Zn removes the salt bridge at Asp23 and Lys38 by altering the side chain conformation into non-bridge forming conformations which may result in the higher neurotoxicity of amyloid-β when exposed to high concentrations of Zn. Mutants with ill-defined salt bridges have been shown to be more neurotoxic than salt bridge forming wild type (Mithu, Sarkar, Bhowmik, Chandrakesan, Maiti, & Madhu, 2011).

Some reports have shown that Zn at concentrations below 10mM reduces amyloid-β toxicity by destabilizing toxic intermediates (Garai, Sahoo, & Maiti, 2007) while higher concentrations of Zn appears to increase toxicity by increasing aggregation (Lovell, Xie, & Markesbury, 1999).

1.4.2. Effect of Metals on Amyloid-β Aggregation

Extensive research has been conducted on the effect of metals on amyloid-β aggregation by Bush (Bush & Tanzi, 2008), Faller (Faller & Hureau, 2009), and Smith (Bonda, Lee, Blair, Zhu, Perry, & Smith, 2011) all of which have shown that both Cu(II) and Zn(II) accelerate amyloid-β aggregation (Ha, Ryu, & Park, 2007). Amyloid aggregation starts instantly when amyloid-β is in the presence of Cu(II) (Pedersen, Østergaard, Rozlosnik, Gammelgaard, & Heegaard, 2012) compared to a lag period in the absence of copper.

Both metal ions disrupt the formation of fibrillar forms of amyloid with some concentrations completely abolishing the formation of amyloid-β. Hou and Zagorski have shown that after amyloid-β binding to Cu(II) ions, the amyloid-β peptide undergoes rapid aggregation, but does not form fibrils (Hou & Zagorski, 2006). Some groups have not reported fibril growth in the presence of Cu(II), but rather amorphous precipitates (Ha, Ryu, & Park, 2007) (Tougu V. , et al., 2009) likely the result of using higher concentrations of Cu(II) (Innocenti, et al., 2010). The effects of the metals on amyloid aggregation are largely a function of the concentration of

the peptide and metal ion. In dilute conditions, rapid fibril formation was detected in a copper environment, however, at higher concentrations, no fibrils were detected (Sarell, Wilkinson, & Viles, 2010). Even substoichiometric concentrations of metal ions induce and accelerate amyloid aggregation: substoichiometric levels of Cu(II) doubles the rate of fibril nucleation and elongation (Sarell, Wilkinson, & Viles, 2010). At micromolar concentrations of amyloid-β Cu(II) does not form cross linked species with amyloid-β, and coordination geometry in the monomer and fibril is identical ruling out copper bridging to form cross-linked amyloid-β (Sarell, Wilkinson, & Viles, 2010). Substoichiometric concentrations of Cu(II) (between 0.2 and 0.4 mol eq) show the largest effect on the growth rates of fibrils (Sarell, Wilkinson, & Viles, 2010). Viles and colleagues suggest that substoichiometric levels of Cu(II) nucleate fibrils formation and suggested that the binding of Cu(II) increases the isoelectric point approaching physiological levels inducing self-association.

Cu(II) increases the nucleation and elongation rate of fibril formation. For Aβ40, there is predominantly a reduction in lag time with the addition of Cu(II). For Aβ42, lag times are not affected as greatly, but rather, there is an increase in the elongation rates (Sarell, Wilkinson, & Viles, 2010). Fibrils formed in Cu(II) solution are able to seed fresh fibrils in non-copper solutions with an associated reduction in lag time (Sarell, Wilkinson, & Viles, 2010). Zn(II) ions completely inhibit amyloid fibril formation at 3μM. Cu(II) ions form an intramolecular complex with amyloid-β whereas Zn(II) forms an intermolecular complex cross-linking between the two histidine residues on multiple amyloid-β peptides (Minicozzi, et al., 2008) (Faller & Hureau, 2009) (Sarell, Wilkinson, & Viles, 2010). Acidic conditions aggravate the effects of Cu on the aggregation of amyloid-β (Bin, Chen, & Xiang, 2013).

The ratios of copper and amyloid-β are different in different tissues (Eskici & Axelsen, 2012). Physiologically, the concentration of copper is much greater than the concentration of Aβ: Cu concentrations in CSF are in the order of 0.1-4.0 µM (Bogden, Troiano, & Joselow, 1977) whereas the concentration of amyloid-β is in the order of nM (Oe, et al., 2006). In extracellular fluid, the concentration of amyloid-β is 10% of that in CSF (Cirrito, et al., 2003) while copper concentrations are up to 2 orders of magnitude higher (Kardos, Kovacs, Hajos, Kalman, & Simonyi, 1989). In extracellular fluid, the concentration of amyloid-β is approximately one tenth the concentration in CSF (Cirrito, et al., 2003); however, some reports have shown that copper concentrations may be as high as 100 µM (Kardos, Kovacs, Hajos, Kalman, & Simonyi, 1989). Micromolar concentrations of synapse released copper is sufficient to induce amyloid-β aggregation (Ha, Ryu, & Park, 2007) (Tougu, Karafin, & Palumaa, 2008). Fibrils tend to form in the extracellular fluid as opposed to the CSF. It is worth to note that in the ECF, the concentration of amyloid-β is lower and the Cu:Aβ ratio is higher (Eskici & Axelsen, 2012). Metal ions induce amyloid-β insertion into lipid vesicles. In the absence of metal ions, the peptide is only able to insert at pH values below 5.5 (Curtain, Ali, Smith, Bush, Masters, & Barnham, 2003).

Heegaard and colleagues reported on the aggregation kinetics of amyloid-β in a copper environment (Pedersen, Østergaard, Rozlosnik, Gammelgaard, & Heegaard, 2012). The concentration of Cu:Aβ ratio is a major determinant of the aggregation pathway. Heegaard, along with previous researchers reported that three different kinetic pathways can occur for amyloid-β in a copper environment. The first pathway occurs at low ratios of Cu(II):Aβ form by the complexes quickly forming a critical nucleus followed by the slow addition of peptide-metal complex to form an amyloid fibrils (Bush, Pettingell, & Multhaup, 1994) (Sarell, Wilkinson, &

Viles, 2010). These fibrils may slowly form amorphous aggregates. The second pathway involves the formation of amyloid fibrils in the presence of copper (Ha, Ryu, & Park, 2007). At equimolar concentrations, there is a fast irreversible aggregation into peptide-metal oligomers which slowly bind together resulting in amorphous aggregates leading to spherical oligomers. The third pathway, as identified by Heegaard, alters the kinetic pathway of amyloid-β and develops into both fibrillar and oligomeric forms of amyloid-β. As the Cu(II):Aβ ratio increases, the pathway is shifted from fibrillar to non-fibrillar indicating a destabilizing effect of Cu(II) on the structure of amyloid aggregates (Pedersen, Østergaard, Rozlosnik, Gammelgaard, & Heegaard, 2012). The third pathway (at high Cu(II):Aβ ratios) is similar to the second pathway, but there is a fast reversible process that adds additional copper molecules to the oligomer increasing the Cu(II):Aβ ratio to 1.4:1 (Pedersen, Østergaard, Rozlosnik, Gammelgaard, & Heegaard, 2012). In the presence of copper, fibrils grow by the addition of monomers to an end of a fibril which eventually bundle into full mature fibrils stabilized by inter-fibrillar interactions. Agitation of the solution increases the kinetic rate of formation (Tougu, Tiiman, & Palumaa, 2011).

Heegaard reported that at higher Cu(II):Aβ40 ratios, 65% of the peptide aggregated within 2 hours. After this initial aggregation, the rate decreased so that after 50 hours of incubation, there was still a detectable amount of monomeric peptide (Pedersen, Østergaard, Rozlosnik, Gammelgaard, & Heegaard, 2012). It is believed that the aggregation of Cu:Aβ complex is the rate limiting step as opposed to the formation of the amyloid-metal complexes themselves. Analysis of Cu:Aβ kinetics indicates that the peptide-metal complex aggregates in a two-phase kinetic fashion. At supra-equimolar ratios, the Cu:Aβ ratio in aggregates has been shown to be 1.4:1, implying another binding site is present in aggregates, whereas at Cu:Aβ <1,

the ratio appears to be 1:1. Even in the presence of Cu(II), shorter Aβ16 peptides do not aggregate because they are missing the critical 23-27 sequence needed for self-assembly (Balbach, et al., 2002) (Pedersen, Østergaard, Rozlosnik, Gammelgaard, & Heegaard, 2012). The thermodynamic equilibrium between oligomers and monomers is a function of the peptide concentration to the power of the number of monomers per oligomer (Tougu, Tiiman, & Palumaa, 2011).

Copper has been shown to decrease the hydrophobic residues exposed to the surface (thereby forcing them towards the center of the peptide) possibly explaining why Cu:Aβ demonstrate increased solubility in aqueous solutions (Chen, Liuo, Yu, Cheng, & Cen, 2011).

Zn ions can promote aggregation, but may not be neurotoxic. The late Dr. Mark Smith has frequently commented that this aggregation can serve as a neuroprotective mechanism, whereas the toxic peptide aggregates further along its pathway to form inert aggregations (Smith, Cappai, & Barnham, 2007). Cu(II) ions can inhibit Zn(II) induced aggregation (Suzuko, Miura, & Takeuchi, 2001) (Tougu, Tiiman, & Palumaa, 2011).

A number of important findings can be noted from the available literature. Monomeric amyloid-metal complex can be formed with synaptic Cu and Zn ions. All known structures (monomeric, oligomeric, fibrillar) of amyloid-β can bind metals. Fibrillar amyloid-metal complexes are resistant to metal chelator likely because the metal ions are trapped inside the fibrillar structure. Cu ions can generate ROS in the presence of H_2O_2 and other reducing agents (Tougu, Tiiman, & Palumaa, 2011).

1.4.3. Redox Effects of Metals Contributing to Neurotoxicity

The presence of oxidative stress in the Alzheimer's brain has been universally acknowledged[3] , but it is still unclear whether the oxidative stress is a cause of Alzheimer's symptoms or just a consequence (Eskici & Axelsen, 2012). Numerous effects of oxidative stress brought on by the generation of reactive oxidative species (ROS) have been identified. These include an increased level of protein, lipid and DNA oxidation in the brain, resulting in deleterious cell signaling and function, decreased production of cytochrome C oxidase, and the formation of inflammatory cytokines including interkeukin-6 (Jomova, Vondrakova, Lawson, & Valko, 2010). Oxidative stress plays a role in the normal process of human aging (Doraiswamy & Finefrock, 2004) (Pearl, 1928).

Oxidative stress to the brain is one of the earliest signs of Alzheimer's disease (Smith, Numomura, Zhu, Takeda, & Perry, 2000) demonstrated by the presence of oxidatively damaged macromolecules and inflammation preceding the presence of amyloid aggregations (Zhu, Lee, Perry, & Smith, 2007) (Pimplikar, 2009). The binding of copper to amyloid-β correlates with the generation of hydrogen peroxide (Bonda, et al., 2010) (Bonda, Lee, Blair, Zhu, Perry, & Smith, 2011). There is a minority opinion advocated by researchers such as Atwood and Smith who have proposed that amyloid plaques act as a metal "reservoir" intended to trap metals that, if not trapped, would catalyze oxidative reactions (Atwood, et al., 2012). In essence, the formation of amyloid plaques is a compensatory mechanism to remove ROS rather than a pathological mechanism. This hypothesis is the minority view (Eskici & Axelsen, 2012), but may have some merit because trace metals are embedded deep within amyloid fibrils (and therefore plaques) unable to interact with their environment and produce ROS. Smith and colleagues argue that the removal of amyloid-β as proposed by numerous groups may in fact have a deleterious effect on the symptoms of Alzheimer's disease since there would no longer be an agent removing reactive

[3] See extensive list of references in (Eskici & Axelsen, 2012).

oxygen from the system (Atwood, et al., 2012). However, the majority of evidence supports the hypothesis that amyloid-β peptides promote oxidative stress mediated by metals such as Cu(II) bound to amyloid-β (Eskici & Axelsen, 2012).

The effect of free radicals and oxidative damage to the brain influenced by amyloid-β is extensive. A free radical is a molecule containing one or more unpaired electrons allowing them to react readily. In biological systems, species derived from oxygen are the most common free radicals (Cadenas & Davies, 2000). The oxidative injury associated with AD is mediated by H_2O_2 which, via a Fenton reaction, produces the OH radical which is highly reactive. H_2O_2 is membrane permeable and is able to react with reduced metal ions such as Cu(II) and Fe(II) to produce OH. The hydroxyl radical is able to initiate a number of biochemical reactions including post translational protein modifications, DNA damage and lipid peroxidation (Markesbury & Lovell, 2007). The brain has natural defense systems for scavenging excess H_2O_2 such as catalase, glutathione peroxidase, and superoxide dismutase, which may be rendered inoperative by the sheer amount of H_2O_2 generated by the amyloid-metal complex (Bush & Tanzi, 2008). Cerebral content of oxidative stress inducing agents such as Cu and Fe have been documented to be elevated in post mortem examination of brains of Alzheimer's patients (Jomova, Vondrakova, Lawson, & Valko, 2010). Copper-amyloid binding leads to the production of ROS. If no other molecule is involved in oxidation, it is the amyloid-β side chains which may become oxidized (Puglielli, Freidlich, & Setchell, 2005). The binding of amyloid-β, especially the Aβ42 alloform (Huang, Cuajungco, & Atwood, 1999), to metal ions Cu(II) or Fe(III) produces H_2O_2 by a double electron transfer reaction, reducing the metal ions in favour of O_2 oxidation (Tabner, Turnbull, & El-Agnaf, 2002) (Dikalov, Vitek, & Mason, 2004) which is mediated by Met35 and Tyr10 (Barnham, Haeffner, & Ciccotosto, 2004). Oxidation of Tyr10 can result in stable, but highly

neurotoxic forms of amyloid-β (Atwood, et al., 2004). The electron implicated in the reduction of the metal ion could be from amyloid-β, from Met35 or from reducing agents such as dopamine and ascorbate (Opazo, et al., 2002). H_2O_2 can also be formed by the cycling of metals bound to amyloid-β using electron donors without oxidation of the peptide. The reducing agents implicated are sterols such as cholesterol and long-chain fatty acids (Murray, Sindoni, & Axelsen, 2005). The chemistry of H_2O_2 and $OH^{\bullet}$ production proceeds by Fenton and Haber-Weiss reactions as outlined below (Markesbury, 1997) (Liochev, 1999).

The reduction of the metal ion proceeds along by the reaction,

$$A\beta + M^{(n+1)+} \rightarrow A\beta + M^{n+}$$

Where M is the metal and n the charge. Oxygen is reduced via the reaction,

$$M^{n+} + O_2 \rightarrow M^{n+1} + O_2^-$$

The production of hydrogen peroxide proceeds by,

$$O_2^- + O_2^- + 2H \rightarrow H_2O_2 + O_2$$

Fenton chemistry mediates the reaction between metals and hydrogen peroxide to produce hydroxyl radicals,

$$M^{n+} + H_2O_2 \rightarrow OH^{\bullet} + OH^- + O_2$$

Lastly, Haber-Weiss chemistry reacts oxygen with hydrogen peroxide to produce free radicals,

$$O_2^- + H_2O_2 \rightarrow OH^{\bullet} + OH^- + O_2$$

From this chemistry, it appears that metals are required to produce ROS in Alzheimer's disease by oxidizing another moiety (Smith, Cappai, & Barnham, 2007).

While there is some controversy over whether or not amyloid-β has a neuroprotective effect, this effect tends to be dependent on the *in vivo* concentration of amyloid-β. Nanomolar

concentrations appear to have a neuroprotective effect (Whitson, Selkoe, & Cotman, 1989) while micromolar concentrations appear to induce neurotoxicity via oxidative mechanisms (Ueda, Fukui, & Kageyama, 1994). Cu(II) ions tend to increase amyloid toxicity while Zn(II) decrease toxicity (Cuajunco, et al., 2000). Viles and colleagues have identified two reasons why toxicity is enhanced in amyloid-β in the presence of Cu(II) ions. The first is that monomeric amyloid-β binds substoichiometric Cu(II) at the cell surface generating H_2O_2 and hydroxyl radicals leading to lipid peroxidation compromising cell integrity. The second reason is that copper near the neuronal synapse may promote aggregation of monomeric amyloid-β causing increased cytotoxicity (Sarell, Wilkinson, & Viles, 2010). If the pathogenesis of the metals hypothesis of Alzheimer's disease was as simple as the generation of ROS by copper, it would be expected that neurotoxicity would be a function of metal concentration. However, Viles and colleagues showed that smaller concentrations of Cu(II) ions are more toxic than metal solutions 50 times more concentrated. This provides evidence that the ability of Cu(II) to promote amyloid aggregation has a major role in the etiology of Alzheimer's disease beyond that of simply forming ROS (Sarell, Wilkinson, & Viles, 2010).

1.5. Alzheimer's Disease Pharmaceuticals

The following possible strategies have been identified to prevent the aggregation of amyloid-β (Härd & Lendel, 2012) (Sokolov, Kozak, Kayed, Chanturiya, Glabe, & Hall, 2006):

1) Stabilizing or sequestering the native state of the protein.

2) Stabilizing or promoting off pathway aggregates which may have reduced toxicity.

3) β-sheet breakers than end fibril elongation or stop aggregation.

4) Disassembling amyloid aggregates.

5) Preventing oligomer-cell membrane interactions.

6) Preventing amyloid induced membrane thinning.

In addition, the promotion of clearance mechanisms have recently shown promise (Cramer, et al., 2012).

Currently there are only five pharmaceuticals used to treat AD which are approved by the Food and Drug Administration. All have limited efficacy- none reverse the course of disease progression or result in any sustained delay of symptoms (Karran, Mercken, & Stooper, 2011) (Skaat, Chen, Grinberg, & Margel, 2012). The first four are acetylcholinesterase inhibitors (donepezil, galantamine, rivastigmine, tacrine) and the fifth is memantine, an N-methyl D-aspartate (NMDA) antagonist. These medications relieve some of the symptoms associated with AD, but do not alter the course of the illness or provide any curative mechanism (Neugroschl & Sano, 2010).

1.5.1. Mechanism of Action

Cholinesterase inhibitors combat amyloid toxicity by slowing the degradation of acetylcholine after release at the synapse. Memantine prevents overstimulation of the NMDA glutamate receptors (Mattson M. , 2004). Both acetylcholinesterase inhibitors and memantine, often used together, have shown moderate effects on cognitive function and behavioural scores (Roberson & Mucke, 2006). Many AD patients also take antipsychotics and antidepressants to manage psychiatric issues associated with AD. Non-steroidal anti-inflammatories (NSAID) have been demonstrated to have some anti-Alzheimer's benefits (Townsend & Pratico, 2005).

Another possible strategy for the treatment of Alzheimer's disease involves compounds that can prevent the misfolding and aggregation of amyloid-β. A number of these beta sheet breakers have been identified with limited success in clinical trials. Methylene Blue has been demonstrated to inhibit the aggregation of both amyloid-β (Necula, Kayed, Milton, & Glabe,

2007) and tau (Wischik, Edwards, Lai, Roth, & Harrington, 1996). The anti-leprosy drug rifampicin has been identified to inhibit amyloid aggregation. The mechanism of action is believed to be related to its ability to scavenge free radicals and stabilize amyloid oligomers (Härd & Lendel, 2012) (Li, Zhu, Ranjamani, & Uversky, 2004). The dye Orange G inhibits fibril formation, but does not inhibit the formation of amyloid oligomers (Necula, Kayed, Milton, & Glabe, 2007). The research group of Arvi Rauk has synthesized a few novel peptides referred to as SG1 and SG2 (Roy, 2010). These peptides have the potential to prevent any further aggregation by binding to the amyloid-β self-recognition site and therefore interfering with the dimerization of the peptide. Other inhibitors are based on the actual amyloid-β peptide, but the terminals are modified to prevent their aggregation. Shin and colleagues tested a multitude of steryl benzene derivatives which have excellent binding affinities to amyloid fibrils and oligomers preventing further aggregation (Lee, et al., 2012) (Lee V. , 2002). Ferulic Acid, an antioxidant inhibits fibril formation and mitigates amyloid toxicity (Ono, Hirohata, & Yamada, 2005). Curcumin, common in tumeric, has been demonstrated to directly bind small amyloid oligomers preventing further aggregation. Curcumin is also a powerful antioxidant suppressing oxidative damage and inflammation (Yang, et al., 2005). Epidemiological studies have shown a correlation between tumeric consumption and reduced risk for AD (Ganguli, et al., 2000). Phenolic compounds such as myricetin and rosmarinic acid have been shown to inhibit amyloid aggregation. These compounds have been demonstrated to reduce synaptic dysfunction by blocking early assembly processes (Ono, et al., 2012). Dimers, trimers and tetramers have all been demonstrated to be cytotoxic (Ono, Condron, & Teplow, 2009) leading some researchers to suggest that pharmaceuticals should be targeting monomeric forms of amyloid-β to ensure that dimerization does not occur (Ono & Yamada, 2011). Results obtained by Yamada and

colleagues showed that at lower ratios (5:2) of Aβ42:myricetin, there was a moderate inhibition of oligomerization with the elimination of pentamers and hexamers and tetramers. At higher ratios (1:4 Aβ42:myricetin) there was no inhibition of oligomerization. A similar result was observed for rosmarinic acid (Ono, et al., 2012). Yamada and colleagues concluded that the following phenolic compounds inhibit amyloid oligomerization with decreasing efficacy: myricetin, rosmarinic acid, nordihydroguaiaretic acid (NDGA), furulic acid (FA), curcumin with NDGA and FA having similar efficacies (Ono, et al., 2012). Engineered polymer nanoparticles have been demonstrated to slow the transition from random coil to β-sheets of Aβ40 slowing fibrillization kinetics (Skaat, Chen, Grinberg, & Margel, 2012). The rate of fibrillization decreased, but fibrils still formed eventually. This inhibition is attributed to hydrophobic interactions between the double phenylalanine residues of the nanoparticles and residues of amyloid-β aggregates. Another possible mechanism proposed by researchers is that instead of attempting to inhibit amyloid fibril formation, fibril formation could be promoted so that toxic oligomers would not be formed, or if formed, would quickly develop into a low toxicity reservoir in the form of fibrils (Bieschke, et al., 2012).

Polyphenols, such as resveratrol, have been demonstrated to have extensive antioxidant and anti-inflammatory properties and inhibit amyloid fibril formation and reduce cell death induced by amyloid-β (Riceevans, Miller, Bolwell, Bramley, & Pridham, 1995) (Jang & Surh, 2003).

Three mechanisms of action have been identified for amyloid-β targeted immunotherapy. The peripheral sink hypothesis states that binding of monomeric amyloid-β in the blood to antibodies alters the transport of amyloid-β across the blood-brain barrier (BBB). The second hypothesis is that antibodies may cross the BBB to alter the aggregation process. Lastly,

antibodies that bind fibrils can trigger Fc-mediated phagocytosis to clear plaques (Härd & Lendel, 2012).

Amyloid immunotherapy is currently the subject of intense research. A number of antibodies are in late clinical trials (Pul, Dodel, & Stangel, 2011). However, it has come to light that many of these pharmaceuticals, while successful in laboratory trials, are failing and in some cases even increase, the toxic effects of amyloid-β (O'Nuallain, Hrncic, Wall, Weiss, & Solomon, 2006) (Lord, Gumucio, Englund, Sehlin, Sunquist, & Soderberg, 2009). These deleterious effects have been attributed to the suggestion that amyloid-β are in fact prions and the body cannot develop an immunity to them (Stöhr, et al., 2012). Cognitive improvements in mice models were demonstrated following passive immunizations with amyloid antibodies (Bard, et al., 2000) suggesting antibodies could cross the blood brain barrier and clear amyloid via phagocytosis by microglia. Antibodies specific to the N-terminus only recognize and promote amyloid clearance (Bard, Barbour, Cannon, Caretto, Fox, & Games, 2003) correlating with previous observations that the N-terminus is not part of the core of amyloid fibrils and therefore accessible to binding (Petkova, et al., 2002). Macao and colleagues demonstrated that the novel ZAβ3 affibody clears Aβ from the brain of the *D. melanogaster* fly (Luheshi, Hoyer, Barros, Härd, Brorsson, & Macao, 2010).

The use of statins to prevent AD is based on the hypothesis that amyloid uses cholesterol as scaffolding on neuronal membranes. If cholesterol is removed, perhaps amyloid binding to membranes in minimized. However, a meta-analysis demonstrated that the use of statins to prevent AD is not supported by concrete evidence (Zhou, Teramukai, & Fukushima, 2007).

Docosahexanoic Acid (DHA) is an omega-3 polyunsaturated fatty acid found in relatively high quantities in fish. AD patients have been shown to have lower plasma DHA levels

leading to studies showing that patients with very mild cognitive decline benefit from the consumption of omega-3 fatty acids. There was no effect on patients with moderate levels of cognitive decline (Freund-Levi, Eriksdotter-Jonhagen, & Cederholm, 2006).

Studies of efficacy of ginkgo biloba in reducing AD demonstrated no statistically different results between patients given ginkgo biloba and those given a placebo (Dekosky, Williamson, & Fitzpatrick, 2008).

Both red wine (Wang, Ho, & Zhao, 2006) and resveratrol was shown to reduce amyloid plaque formation in transgenic mice (Karuppagounder, Pinto, Zu, & al, 2009).

Melatonin has been demonstrated to mitigate the toxic effects of amyloid-β in vitro (Zatta, Tognon, & Carampin, 2003) by preventing free radical formation caused by amyloid-metal interactions. Furthermore, melatonin demonstrated a reduction in fibril formation (Cheng, Feng, Zhang, & Zhang, 2006) and reduction in oxidative stress in mice models.

The use of Human Serum Albumin is currently in a phase 2 clinical trial. HSA has been shown to bind free amyloid "removing" it from the system (Stanyon & Viles, 2012). In addition, HSA is able to freely pass through the blood brain barrier.

PBT2, an 8-hydroxyquinoline derivative of clioquinol, has been shown to reduce levels of Aβ42 in the CSF, but not serum concentrations. There was some improvement in cognitive measures (Lannfelt, et al., 2008).

The amyloid-β degrading enzyme neprilysin is regulated by the phosphorylation state of the intracellular domain. In turn, neprilysin modulates extracellular concentrations of amyloid-β. Saido and colleagues have proposed that enhancing the cell surface activity of neprilysin either by activating phosphatases or inhibiting the kinase responsible for phosphorylation is a possible method of reducing amyloid-β aggregation (Kakiya, et al., 2012).

A variety of treatment strategies have been proposed which are related to amyloid-β: the inhibition of the β- or γ- secretases or promotion of the α-secretase which would alter the primary structure of the toxic Aβ42 alloform, inhibiting aggregation, promoting amyloid degrading proteases such as neprilysin and immunotherapy (Citron, 2004) (Citron, 2010). Myr can act as a β-secretase inhibitor that reduces cellular amyloid-β production in vitro (Shimmyo, Kihara, Akaike, Niidome, & Sugimoto, 2008).

1.5.2. Current Research

Research by Ravindranath and colleagues has demonstrated a remarkable effect of the Withania root on the reduction of levels of amyloid-β and improvement of cognitive function in laboratory mice within 14-21 days (Sehgal, et al., 2012). The authors attribute this effect to the up-regulation of liver lipoprotein receptor related protein (LRP) and protease neprilysin enhancing clearance of amyloid-β.

Desferrioxamine (DFO) an approved drug for iron overload disease has demonstrated to slow the progression of AD. These effects have been attributed to its metal chelating properties which clear metals from the brain preventing the formation of free radicals and thus neuronal oxidative damage (Liu, Men, Perry, & Smith, 2010).

A recent clinical trial has been completed for the monoclonal antibody, solanezumab with mixed results: although cognitive decline decreased in patients with mild cognitive decline, no statistically significant results have been obtained for patients with moderate cognitive decline (Health, 2012). These results suggest than solanezumab will join the list of failed Alzheimer's drugs making an effective treatment even more elusive (Kambhampaty, 2012).

1.6. Atomic Force Spectroscopy

Atomic force spectroscopy is a process used to measure extremely small forces using the atomic force microscope or optical tweezers. Interest in this technique was piqued when Strunz and colleagues used an atomic force microscope to pull the two complementary strands of DNA apart and measured the unbinding force of each base pair separating (Strunz, Oroszlan, Schafer, & Guntherodt, 1999). Other force spectroscopy experiments have measured antibody-antigen unbinding forces (Riener, et al., 2003), protein unfolding forces (McAllister, et al., 2005) (Harris, Song, & Kiang, 2007) (Schlierf & Rief, 2006), and peptide-lipid interactions (Rico, Oshima, Hinterdorfer, Fujiyoshi, & Scheuring, 2011), to name a few.

Using single molecule force spectroscopy, the substrate is typically chemically modified to attract one half of the system being studied (i.e. one peptide terminus). The cantilever is chemically modified to attract the other half of the system, which may be another peptide or the other terminus of a protein. The cantilever is lowered and the two peptides (or other molecules) are allowed to bind. The cantilever is then retracted and a force as a function of distance recorded. Typically, an experiment will involve hundreds or thousands of such approaches and subsequent retractions yielding a much smaller fraction of actual rupture events. This fraction is termed the experimental yield. Rupture forces are placed in a histogram and statistics of the force distributions are taken.

1.6.1. Effect of Mechanical Manipulation on Binding Kinetics

As a chemical system proceeds along a reaction coordinate from states A → B, it must overcome an energy barrier of height ΔG located at a location x_β from A, the initial state. Thermal fluctuations in the system allow individual molecules to overcome this activation barrier in order for the chemical reaction to complete. The rate at which molecules overcome this energy

barrier is referred to as the association rate (also referred to as the on-rate). Similarly, thermal fluctuations can cause the reaction to occur in reverse and molecules to proceed back to A at the dissociation rate (also referred to as the kinetic off rate).

Generally, receptor-ligand systems interact non-covalently and their kinetics are similar to covalently bound compounds. Assume two interacting molecules, *X*, and *Y*. *X* and *Y* bind together to form a complex *XY*. However during the course of the reaction, *X* and *Y* are not completely consumed in favour of product *XY*. Rather, the reaction lies at some equilibrium where *X*, *Y* and *XY* are all present. This reaction is represented by the equation:

$$X + Y \underset{k_{on}}{\overset{k_{off}}{\rightleftharpoons}} XY$$

Where k_{off} is the kinetic off (dissociation) rate and k_{on} is the kinetic on (association) rate. By determining these two kinetic rates, the affinity of two molecules can be determined by the equilibrium dissociation constant, $K_d = k_{off}/ k_{on}$.

By increasing the heat in the system, the thermal fluctuations are greater, and generally, the reaction speed is increased in an Arrhenius-like fashion. However, temperature is not the only variable which increases reaction kinetics: the mechanical force separating the two molecules have also been shown to change both the height of the energy barrier and the kinetic off rate (Merkel, Nassoy, Leung, Ritchie, & Evans, 1999).

As force is applied to a receptor-ligand complex, the height of the energy barrier decreases as a function of the force applied and distance from the energy barrier in accordance with the equation (Dudko, Hummer, & Szabo, 2006),

$$U(x) = U_0(x) - Fx$$

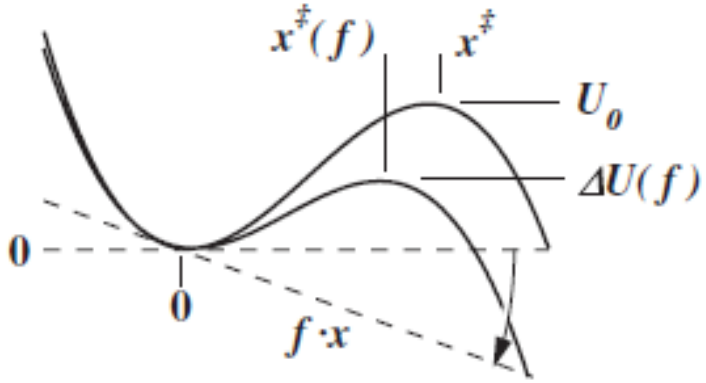

Figure 8- Effect of force on energy barrier. Figure reproduced with permission from (Friddle, 2008)

As shown in figure 8, the free energy surface, U(x), is equal to the intrinsic free energy surface $U_0(x)$, and reduced proportional to the force, F.

By conducting AFS at a variety of loading rates, the intrinsic energy barrier and kinetic off rates can be established.

1.6.2. Surface Chemistry

Force spectroscopy requires both the substrate and the tip to be chemically modified for the system to bind on one terminus to the substrate and the other terminus to the cantilever tip. Protocols for the modification of the surfaces vary from simple (Schwaiger, Kardinal, Schleicher, Noegel, & Rief, 2004) to complex (Guo, Lad, Ray, & Akhremitchev, 2009). In one common surface modification protocol, a polyethylene glycol (PEG) linker is bound to the substrate via a silanated surface modification. This linker provides extra space between the surfaces (substrate and tip) and the system to be studied, preventing damage to the system. A typical set up is shown in figure 9 below.

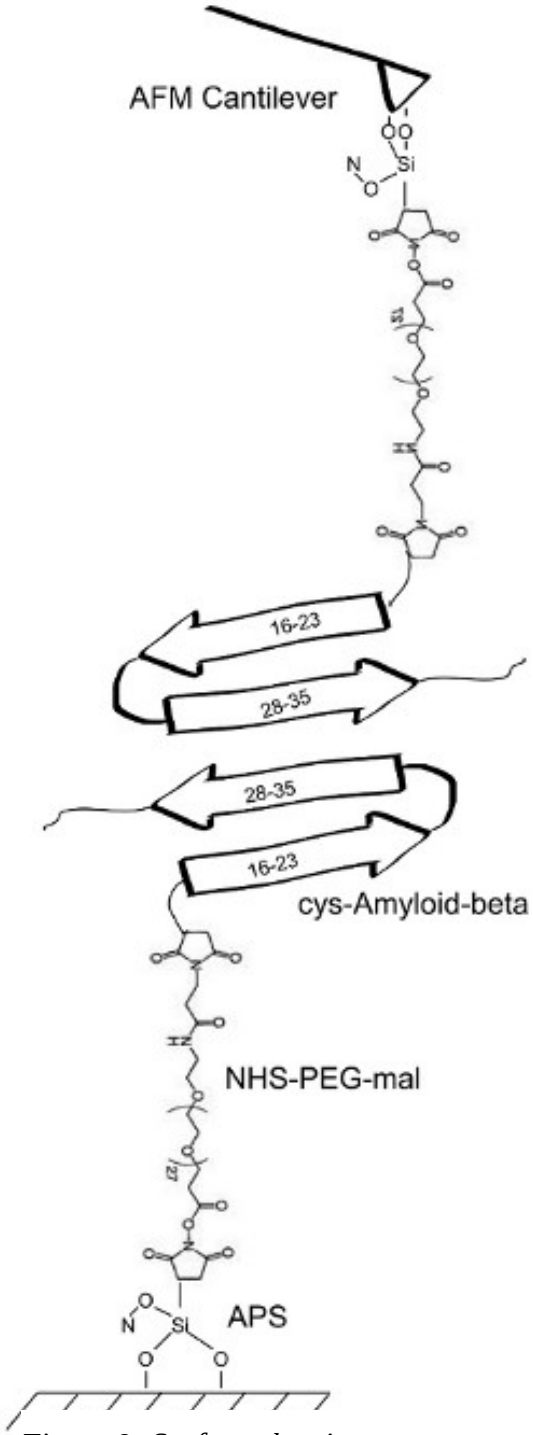

Figure 9- Surface chemistry cartoon. Figure reprinted with permission from (Hane, Tran, Attwood, & Leonenko, 2013).

In our lab we modified the protocol developed earlier (Yu, Malkova, & Lyubchenko, 2008). The protocol begins by freshly cleaving mica and cleaning a Bruker MLCT AFM tip by placing the tip in an ethanol bath for 15 minutes, washing in water and drying in a gentle stream of nitrogen. The tip is placed under UV light for 30 minutes to remove any remaining organic matter.

All immersions are done by cutting the cap off a centrifuge microvial and placing the appropriate liquid (HEPES, ethanol, etc) into the caps. The caps are then placed inside of a petri dish. After the appropriate liquid was placed into the caps, curved blunt nose tweezers are used to lift the cantilever chips out of their storage container and into the appropriate liquid taking care to ensure the cantilever chip is completely immersed in the liquid prior to releasing the grip on the tweezers.

Aminopropyl silatrane (APS) which was synthesized in accordance with (Shlyakhtenko, Gill, Filonov, Cerovac, Lushnikov, & Lyubchenko,

2003) and dissolved in water at a concentration of 167µM.. Both surfaces are silanated by immersing the tip and mica in APS.

When APS is allowed to react with the mica and water, the silicon covalently binds with the oxygen atoms on the mica surface preparing the surface for a hetrobifunctional crosslinker (such as N-hydroxysuccinimide-PEG-maleimide) (Shlyakhtenko, Gill, Filonov, Cerovac, Lushnikov, & Lyubchenko, 2003).

The mica and tip are further modified by placing them in a solution of N-hydroxysuccinimide-PEG-maleimide (NHS-PEG-mal) at a concentration of 167µM in dimethylsulfoxide (DMSO) for a period of 3 hours. Depending on the manufacturer, NHS is also referred to as succinamide valerate (SVA). Both tips and mica are washed with DMSO and dried under a gentle stream of nitrogen.

Cys-amyloid-β (1-42) (Anaspec, Freemont, CA) is prepared by dissolving the peptide to a concentration of 1 mg/mL in DMSO. The cys-amyloid-β is diluted in HEPES (pH 7.4, 50 mM, 150mM NaCl) for a final peptide concentration of 20nM. An equal volume of 200nM tris(2-carboxyethyl)phosphine (TCEP) is added to the amyloid solution to prevent aggregation and the solution is stored for 10-15 minutes. The amyloid-β is centrifuged for 15 minutes at 15k RPM driving high molecular weight peptides to the bottom of the centrifuge tube. Amyloid-β near the top of the tube is removed and allowed to soak the tips and mica for 30 minutes. The tips and mica are rinsed 3 times with HEPES. To prevent unwanted binding events to unreacted maleimide groups, the surfaces were immersed in beta-merceptoethanol, a short chain thiol ethanol which quenches unreacted maleimide groups. The surfaces are rinsed with HEPES and are ready for force spectroscopy in HEPES solution.

1.6.3. Conducting Force Spectroscopy Experiments

Once surface chemistry is complete, the tip and mica are loaded into the atomic force microscope. The AFM cantilever is calibrated using the thermal noise method as directed by the manufacturer to calculate the cantilever spring constant. Typical force spectroscopy settings are Igain 40, pgain 0.0048, set point 10 nN, relative set point 0.9. Approach and retract speeds are in the order of nanometers/sec to micrometers/sec and will vary greatly during dynamic force spectroscopy. A 0.5 second pause is set to allow the peptides to bond to one another. Usually 900 force curves are taken per 100 μm area with a 30x30 grid (30 points taken in each row, with 30 rows sampled).

Experimental yield (number of binding events/number of binding attempts) varies from 2.5% to 30% depending on conditions. Sample force curves are shown below. As the tip is retracted from the sample, if a binding event occurs, the tip is deflected. A worm like chain (WLC) fit can be used to model a variety of natural phenomenon including the extension of polymers and the bending of structural beams under load. At molecular rupture, the cantilever no longer is subjected to any force and the cantilever returns to a neutral position. The WLC model envisions an isotropic continuously flexible rod. The deflection of the WLC model is in accordance with the following equation.

$$\frac{Fl_p}{k_B T} = \frac{1}{4}\left(1 - \frac{x}{L_c}\right)^{-2} - \frac{1}{4} + \frac{x}{L_c} \qquad \text{eq. 1}$$

Where F is the force, l_p is the persistence length of the polymer, k_B is Boltzmann constant, T the absolute temperature, x is the length of stretching and L_c the contour length (Bustamante, Marko, & Smith, 1994). The persistence length is a method of quantifying the stiffness of a polymer. If the length of a polymer is less than its persistence length, the polymer acts as a flexible elastic rod. If the length of the polymer is greater than its persistence length, its

properties cannot be described dynamically. The contour length of a peptide is the maximum length the peptide can physically be extended.

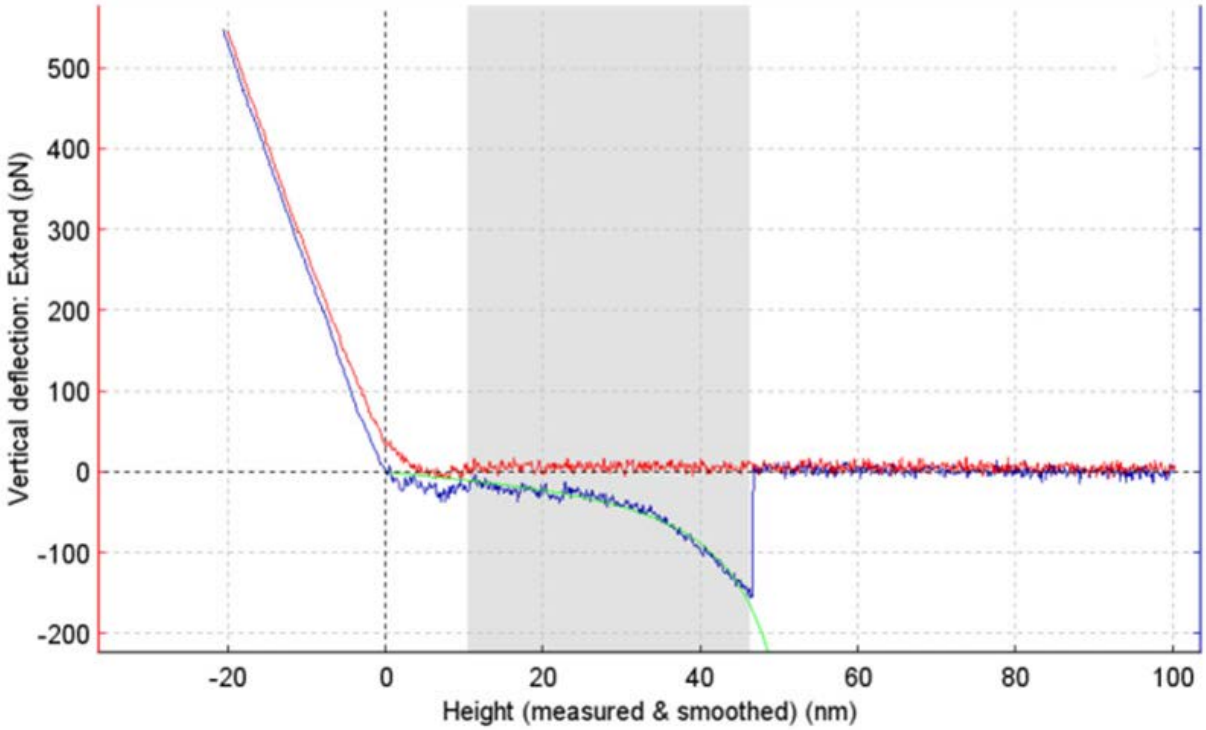

Figure 10 - Sample force curve showing an approach, retract and rupture of a chemical bond. Figure reprinted with permission from (Hane, Tran, Attwood, & Leonenko, 2013).

1.6.4. Data Analysis

Once data are collected, JPK data processing software is used to analyze the force curves. Force curves are zeroed so the distant approach and retract line is on the x-axis. The force curve is smoothed and the vertical deflection is calibrated using the sensitivity settings collected during cantilever calibration. A WLC model is then applied to the force curve. The software calculates the rupture force, contour length, loading rate and persistence length (JPK Instruments AG, 2007). Rupture forces are recorded in a spreadsheet and histograms are plotted. We can obtain the mean and median of the force curves to determine the most probable unbinding force but

using a Gaussian fit to the histograms or a probability density function yields a more rigorous result.

1.6.5. Dynamic Force Spectroscopy

Dynamic force spectroscopy (DFS) is a variation of atomic force spectroscopy whereby the retraction velocity, and therefore the loading rate is changed to obtain a force spectra as a function of the loading rate as shown in figure 11. DFS may be used to extract kinetic or thermodynamic information about protein unbinding or unfolding events such as the kinetic off rate and the height and width of the energy barriers (Hinterdorfer & Dufrêne, 2006) (Allison, Hinterdorfer, & Han, 2002). This kinetic information can then be used to elucidate thermodynamic information about the protein such as the free energy of an unbinding barrier and the location of this barrier along a reaction coordinate. DFS utilizes the AFS technique, but instead of a single set of data being collected at a given speed and thus loading rate, unbinding forces at multiple loading rates are collected. The loading rate is the spring constant of the cantilever multiplied by the retraction speed. The "apparent" loading rate is obtained by obtaining the slope of the cantilever position with respect to time, dx/dt, at the rupture event and multiplying by the cantilever spring constant.

To extract kinetic data from the unbinding experiments, a number of analytical models have been proposed to fit the experimental data. While the Bell-Evans model (Evans & Richie, 1997) (Evans E. , 2001) is the oldest and most highly cited model, an argument can now be made questioning the interpretation of some experimental results which have utilized this model (Friddle, Noy, & De Yoreo, 2012).

1.6.6. Bell-Evans Model

The Bell-Evans model is the most cited method of extracting kinetic information from DFS data. The origins of the Bell-Evans theory began with the work by Bell in 1978 (Bell, 1978) who proposed a phenomenological method for the analysis of the adhesion of cells to other cells. The Bell-Evans model was the result of Evans' adaptation of the work introduced by Bell in 1978 (Bell, 1978) and adapted for atomic force spectroscopy (AFS) (Evans & Richie, 1997) (Evans E. , 2001). This model posited that the rupture force between two cells was proportional to the natural logarithm of the loading rate during retraction. In 1997, Evans and Richie built upon Bell's model to extract kinetic information from the dissociation of individual macromolecules such as proteins (Evans & Richie, 1997). The theoretical work developed by Evans and Richie became known as the Bell-Evans model.

The Bell-Evans model is based on the assumption that for non-covalent bonds, molecules in solution bond and dissociate continuously when no force is force applied to them. By introducing a force field to the system, there is a reduction in the ratio of bound-to-free molecules. The mean lifetime of one of these non-covalent bonds is referred to as τ_{off}. If the bond is pulled apart faster than τ_{off}, the bond resists rupture (Evans E. , 2001). On a single molecule level, we can deduce that as a force is applied quicker to the molecules (the loading rate), the unbinding force required to dissociate the bond is increased. The rate constant of this dissociation, $k_{off,}$ is given by the equation $k_{off} = 1/ \tau_{off}$.

Every metastable chemical system contains some thermodynamic energy barrier which needs to be overcome in order for a reaction to proceed along the reaction coordinate. If an external force is applied to this system, the energy landscape barrier is reduced and therefore τ_{off} is decreased. If we conduct multiple experiments, we can obtain a most probable rupture force at

a given loading rate. By repeatedly conducting this experiment at loading rates with difference of orders of magnitude and plot the most probable rupture force on a log scale of loading rates, the most probable unbinding force at each loading rate is obtained (Evans E. , 2001). An example of such a loading rate plot is shown in figure 11.

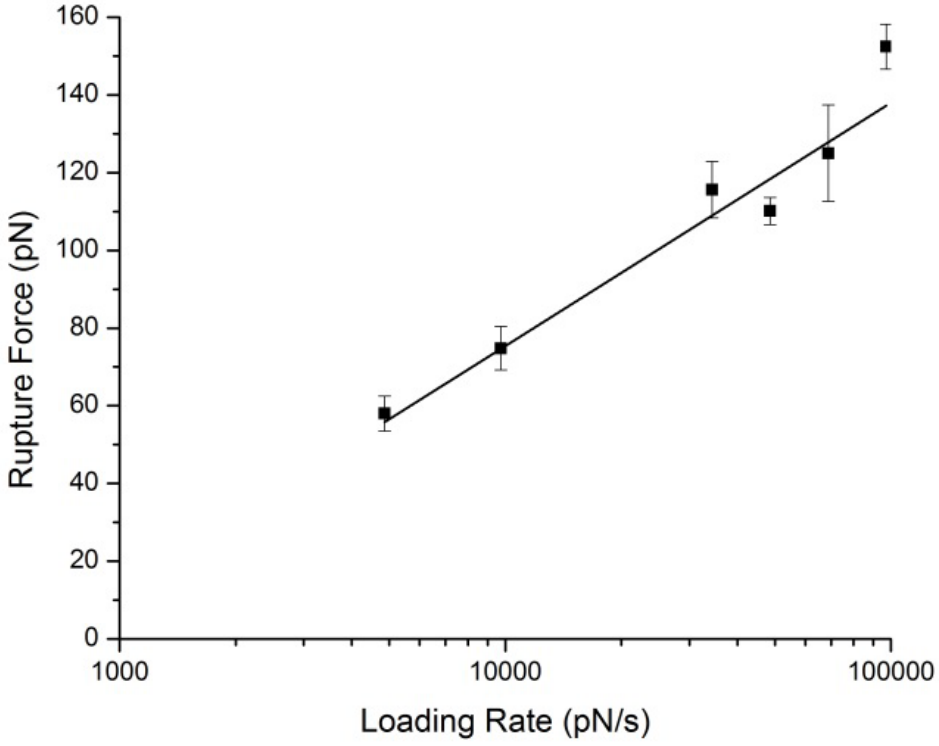

Figure 11- Most probable rupture force as a function of loading rate.

When the most probable unbinding force is determined from plotting all unbinding events at a given loading rate on a histogram, and the most probable unbinding force is plotted against the loading rate on a log scale, a straight line results, the slope of which is the location of the transition barrier, $x_{\beta,}$ and the y-intercept being the height of the energy barrier, ΔG (Evans E. , 2001). Using Bell-Evans equation (eq.1) (Evans & Richie, 1997) (Evans E. , 2001),

$$F\,(r) = \left(\frac{k_B T}{x_\beta}\right) \ln \frac{r\, x_\beta}{k_0\, k_\beta T} \qquad \text{eq. 2}$$

where F(r) is the most probable rupture force, k_B, Boltzman's constant, T, temperature in Kelvin, x_β, the location of the energy barrier, r, the loading rate, and k_0 the off rate constant at zero force. Once k_0 is determined, ΔG can be calculated using following equation (eq.2) (Evans & Richie, 1997) (Evans E. , 2001).

$$-\Delta G = k_B T \ln \frac{k_0 h}{k_B T} \qquad \text{eq. 3}$$

Some DFS experiments yield multiple slopes of the rupture force plots. Common orthodoxy interprets this as an additional energy barrier to be overcome however this paradigm has recently come under heavy criticism (Kim, Palermo, Lovas, Zaikova, Keana, & Lyubchenko, 2011) (Evans E. , 2001) (Friddle, Noy, & De Yoreo, 2012).

1.6.7. The Dudko-Hummer-Szabo Model

While the Bell-Evans model has received widespread acceptance within the force spectroscopy research community, it has received criticism that its assumptions are overly broad (Hummer & Szabo, 2003) (Dudko, Hummer, & Szabo, 2006). A number of groups have suggested modifications to the Bell-Evans model. The most commonly accepted DFS analysis technique which corrects for the inadequacies of the Bell-Evans model is that proposed by Dudko, Hummer and Szabo (Dudko, Hummer, & Szabo, 2006) which in turn is based on the work solely by Hummer and Szabo (Hummer & Szabo, 2003) based on Kramers' kinetic diffusion model of gases (Kramers, 1940).

Both the Bell-Evans model and Dudko-Hummer-Szabo models can be reduced to a similar expression, $\langle F \rangle \sim (\ln v)^a$, where $\langle F \rangle$ is the average rupture force of an ensemble of measurements, v the pulling speed, and a, an arbitrary exponent equal to 1 in the Bell-Evans model (Evans & Richie, 1997), ½ by Garg (Garg, 1995) and 3/2 by the Hummer-Szabo model (Hummer & Szabo, 2003).

Modifying the Bell-Evans model above, Szabo and colleagues determined an arbitrary exponential scaling constant to obtain the equation (eq.4) (Dudko, Hummer, & Szabo, 2006),

$$\tau(F) = \tau_0 \left(1 - \frac{aFx_\beta}{\Delta G}\right)^{1-1/a} e^{\Delta G\left[1-\left(1-\frac{aFx_\beta}{\Delta G}\right)^{1/a}\right]} \qquad \text{eq. 4}$$

Where τ is the bond lifetime, a is a power scaling factor corresponding to ½ for a cusp-like barrier, 3/2 for a linear-cubic barrier, and 1 for a recovery of the Bell-Evans model.

Szabo and colleagues reduced the Bell-Evans model to its approximate limit using a stochastic model of a spring (Hummer & Szabo, 2003) and used Kramers' theory of diffusion (Kramers, 1940) to determine kinetic constants. Szabo and colleagues later updated this model by adding an exponential constant of 1/2 to create a cusp-like model to better approximate kinetic parameters such as the kinetic off rate and location of the energy barrier (Dudko, Hummer, & Szabo, 2006).

The Bell-Evans model assumes that $k_{off}(F)$ scales linearly with $\exp(Fx_\beta)$, so $k(F)=k_0e^{Fx\beta}$. However, this assumption has been shown to be an oversimplification (Dudko, Hummer, & Szabo, 2006): this phenomenological approximation holds as $\Delta G \rightarrow \infty$, but with ΔG of realistic values the unbinding process can be better modeled using Kramer's theory of diffusive barrier crossing. The Dudko-Hummer-Szabo model modifies the Bell-Evans model above and applied Kramer's theory to extract more rigorous kinetic and thermodynamic parameters (Hummer & Szabo, 2003) (Dudko, Hummer, & Szabo, 2008).

The loading rate during a rupture event has been estimated as $r = k_c v$ where r is the loading rate (N/s), k_c the cantilever spring constant (N/m) and v the retract velocity (m/s). Dudko showed that the molecular linker can be incorporated into the loading rate calculation (Dudko, Hummer, & Szabo, 2008). Dudko and colleagues showed that the loading rate of two molecules

connected by a linker following worm like chain (WLC) dynamics can be modelled by equation 5:

$$r(F) = v\left[\frac{1}{k_c} + \frac{2\beta L_c l_p\left(1+\beta F l_p\right)}{3+5\beta F l_p + 8\left(\beta F l_p\right)^{5/2}}\right]^{-1} \quad \text{eq. 5}$$

Where v is the retraction velocity, L_c is the contour length, β is $k_B T^{-1}$, and l_p is the persistence length of the system consisting of the linker and peptide. The persistence length is the length at which, when greater, the system deforms in a classical manner. The first term within the brackets represents the cantilever's contribution to the loading rate and the second term represents the molecular linker's contribution to the loading rate. The addition of the two terms is multiplied by the retraction velocity.

The bond lifetime, τ(F), is approximated by the equation 6:

$$\tau(F) \cong \frac{\left[\frac{\pi}{2}\left(\langle F^2\rangle - \langle F\rangle^2\right)\right]^{1/2}}{r(F)} \quad \text{eq. 6}$$

Where $\langle F^2\rangle$ is the mean squared rupture force at a given loading rate r(F).

1.6.8. Friddle-De Yeoreo Reversible Binding Model

In the past, it has often been assumed that multiple slopes on the rupture force – loading rate plot was to be interpreted as multiple energy barriers. Often DFS experiments result in apparent multiple slopes in the unbinding force/loading rate plots (Merkel, Nassoy, Leung, Ritchie, & Evans, 1999). Given early avidin-biotin experiments and their known multiple unbinding properties, experiments on simpler systems have also interpreted these non-linearity's as complex systems with multiple kinetic barriers with some barriers occurring at impossible distances of significantly less than 1 Å (Friddle, Noy, & De Yoreo, 2012).

Recently De Yoreo and colleagues challenged the assumption made by these earlier models that no reversible binding occurs during force experiments and that multiple spectra are the result of different energy barriers resulting from the mechanically induced deformation of the protein structure (Friddle, Noy, & De Yoreo, 2012). By challenging this assumption, De Yoreo was able to explain away some of the more peculiar conclusions reached by previous groups such as the complexity of very simple system and energy barriers of orders of magnitude less than 1 Å. As De Yoreo so aptly stated, "*If fitting is the only criterion, then the multi-barrier hypothesis can never be rejected, because this segmented approach can be tailored to fit any force spectrum*."

De Yoereo and colleagues attribute the phenomenon of multiple "slopes" to reversible binding at low loading rate- a very plausible scenario (Seifert, 2002) or fluctuations of several independent interactions (Seifert, 2000) (Erdmann & Swartz, 2004).

In the Friddle-De Yoreo interpretation, a system of two bodies being pulled apart passes through two phases: an equilibrium phase at lower pulling velocities where the molecules can rebind, and a kinetic phase at higher loading rates where molecules unbind irreversibly. The equilibrium phase is associated with a shallow slope and the kinetic phase, a steeper slope. Both cases result in the system moving through two states – an equilibrium state characterized by a finite force and a kinetic state where the system displays a weak dependence on loading rate, F ~ ln v.

The force at which the dissociation rate and the association rate cross is given by the equilibrium equation,

$$f_{eq} = \sqrt{2k_c \Delta G} \qquad \text{eq. 7}$$

Where k_c is the spring constant of the cantilever and ΔG the height of the activation barrier.

The unbinding force, F(r), is approximated by the equation,

$$\langle F(r) \rangle \cong f_{eq} + f_{\beta} \ln\left(1 + \frac{re^{-\gamma}}{k_{off}(f_{eq})f_{\beta}}\right) \quad \text{eq. 8}$$

Where γ is Euler's constant, 0.577. The thermal force scale, f_{β} is given by the expression $f_{\beta}=k_BT/x_{\beta}$. $k_{off}(f_{eq})$ is the dissociation rate at the equilibrium force, f_{eq}, the force at which the system transitions from the equilibrium regime to the kinetic regime. F(r) is the mean rupture force as a function of the loading rate, r, corrected for the effect of the PEG linkers as demonstrated in (Dudko, Hummer, & Szabo, 2008).

From f_{β}, the width of the energy barrier, $x_{\beta,}$ can be calculated as,

$$x_{\beta} = \frac{k_BT}{f_{\beta}} \quad \text{eq. 9}$$

The dissociation rate at force F, $k_{off}(F)$ is given by the function,

$$k_{off}(F) = k_0 \exp\left[\beta\left(Fx_{\beta} - 1/2k_c{x_{\beta}}^2\right)\right] \quad \text{eq. 10}$$

The association rate (on-rate), $k_{on}(F)$, is given by the function,

$$k_{on}(F) = k_{on}(0) \exp\left[-\frac{\beta k_c}{2}\left(\frac{F}{k_c} - x_{\beta}\right)^2\right] \quad \text{eq. 11}$$

$$k_{on}(F) = k_0 \exp\left[\beta\left(\Delta G - \frac{F^2}{2k_c}\right)\right]$$

1.6.9. Eliminating Errors in Force Spectroscopy Experiments

Force spectroscopy data analysis assumes that for every rupture event, only one pair of molecules bind. In reality this assumption is often not true. On occasion, two molecules bind

simultaneously resulting in abnormally high forces shifting force histograms high. The determination of the number of double ruptures is given by the equation,

$$P = 1 - \left(\frac{1}{\rho} - 1\right) ln\left(\frac{1}{1-\rho}\right) \qquad \text{eq. 12}$$

where P is the probability of a multiple rupture event and ρ is the experimental yield of the experiment (Tees, Waugh, & Hammer, 2001).

It is accepted practice to truncate the highest rupture forces from the force histogram. For example, if we conduct 1500 approaches yielding 125 usable force curves the resulting experimental yield, ρ=0.083. We calculate the probability of obtaining simultaneous multiple unbinding events. In accordance with the above equation P=0.0425 The number of unbinding forces which are likely a double unbinding event is 125 x 0.0425 = 5.3. Truncating these 5 highest rupture forces from the rupture force histogram and excluding them from data analysis is an accepted practice within the force spectroscopy field (Evans, Halvorsen, Kinoshito, & Wong, 2009).

Akhrimitchev has suggested other ways to minimize the probability of multiple bond ruptures. These include a low peptide surface density (achieved by using nanomolar peptide solutions), using sharp AFM tips, using crosslinkers exceeding 20nm in length to facilitate identifying multiple bond ruptures, and using cantilevers with high spring constants for experiments where high rupture forces are anticipated (Karacsony & Akhrimitchev, 2011).

Chapter 2
Research Objectives

2.1.Objectives of Research

This research began with an objective of probing the binding forces of amyloid-β peptides, and testing the effects of copper ions and inhibitors on amyloid-β unbinding as well as determining the height and width of the energy barrier of amyloid-β dimerization. These objectives have been met.

In this work, I show the forces involved in the unbinding of an amyloid-β dimer with and without the mediating effects of copper ions. I expand on these force experiments by probing the kinetics and thermodynamics of the initial dimerization and aggregation process on a single molecule level and comparing a variety of dynamic force spectroscopy models. Lastly, I demonstrate the effect of amyloid aggregation inhibitors on the unbinding force of the amyloid dimer.

2.2.Hypothesis

I hypothesize the following explanation of the etiology of Alzheimer's disease: the normal body produces a normal amount of amyloid-β cleaved from the amyloid precursor protein. These amyloid-β monomers are routinely cleared by the body as a normal part of recycling proteins. Certain individuals have genetic mutations that allow the body to produce abnormally high amyloid peptide or disproportionately high levels of AB42 to AB40. As these individuals age, the ability of the body to clear amyloid is hindered and these monomers aggregate. People with genetic mutations in APP, PSEN1 or PSEN2, APOE4 are at additional risk for AD because the inability to clear AB is compounded by excess AB production. In addition, aging and unidentified genetic factors allow the accumulation of trace amounts of metal

ions such as copper. The increase in metal ions leads to higher amyloid-amyloid affinity accelerating the kinetics of amyloid aggregation and lowering the free energy required for the initial dimerization of the amyloid peptide.

Once oligomers have formed, the oligomers thin the neuron membrane or produce small ion channels in the membrane disrupting regular cell function. The addition of metals, while already accelerating amyloid aggregation, further compounds the progression of AD by destroying the neuronal membrane by lipid peroxidation.

Specific to the experiments I have proposed, I make the following hypothesis':

Adding trace amounts of metals will result in higher amyloid-amyloid unbinding forces. Amyloid aggregation is characterized by a sinusoidal aggregation curve with a lag phase prior to appreciable aggregation. The higher amyloid-amyloid unbinding forces correlate with a decrease in the lag time associated with amyloid aggregation. The lag phase is characterized by the amyloid overcoming an energy barrier during the dimerization process.

Amyloid oligomers and amyloid fibrils lie on separate pathways. An amyloid dimer can dimerize in a variety of different conformations including a β-hairpin and N-terminal-N-terminal. The conformation of this dimer determines the pathway the amyloid will take- either destined to become an oligomer or destined to become a fibril.

Adding metals to the system will result in the peptide to travel along an oligomeric rather than fibrillar pathway.

Adding metals to the system lowers the activation barrier and deepens the free energy well associated with dimerization, thereby accelerating the aggregation kinetics.

Adding amyloid aggregation inhibitors to the system will result in no dimerization of the amyloid peptide, preventing any further aggregation.

2.3. Relevance of Research

Alzheimer's disease affects 12 million people worldwide. By 2050, this figure is destined to triple to nearly 36 million people. Alzheimer's patients do not suffer alone - the estimated health care costs by 2050 are estimated of approaching $1.1 trillion. Despite millions of dollars in funding and millions of man-hours spent on research, the best Alzheimer's treatments so far only delay the onset of symptoms of by a few months.

Copper has long been implicated in AD. By understanding the single molecule interactions in a copper environment, researchers may be able to target metal chelators more efficaciously, perhaps by using our AFS based screening technique.

Our attempt to standardize dynamic force spectroscopy (DFS) experiments will allow researchers to compare data obtained from single molecule force spectroscopy (SMFS) experiments using the same data analysis techniques.

The research contained within this thesis addresses the issues surrounding AD etiology at its very initial stages – the point where two amyloid-β peptides bind to form a neurotoxic dimer. By understanding what molecular events occur during the progression of AD on a single molecule level, other researchers may eventually be able to develop therapeutic strategies to slow the progression of AD.

Chapter 3
Cu(2+) Affects Amyloid-β (1-42) Aggregation by Increasing Peptide-Peptide Binding Forces

This chapter is reprinted with permission from Hane, et al. PLoS ONE. *(2013).*

The link between metals, Alzheimer's disease (AD) and its implicated protein, amyloid-β (Aβ), is complex and highly studied. AD is believed to occur as a result of the misfolding and aggregation of Aβ. The dyshomeostasis of metal ions and their propensity to interact with Aβ has also been implicated in AD. In this work, we use single molecule atomic force spectroscopy to measure the rupture force required to dissociate two Aβ (1-42) peptides in the presence of copper ions, Cu^{2+}. In addition, we use atomic force microscopy to resolve the aggregation of Aβ formed. Previous research has shown that metal ions decrease the lag time associated with Aβ aggregation. We show that with the addition of copper ions the unbinding force increases notably. This suggests that the reduction of lag time associated with Aβ aggregation occurs on a single molecule level as a result of an increase in binding forces during the very initial interactions between two Aβ peptides. We attribute these results to copper ions acting as a bridge between the two peptide molecules, increasing the stability of the peptide-peptide complex.

Author Contributions:

- Designed Experiments: Zoya Leonenko, Francis Hane
- Performed Experiments: Francis Hane, Gary Tran, Simon Attwood
- Analyzed Data: Francis Hane, Gary Tran, Simon Attwood
- Wrote the Manuscript: Francis Hane, Simon Attwood, Zoya Leonenko

3.1. Introduction

The mechanism for Aβ misfolding has not yet been identified. The initial misfolding of amyloid-β onto itself occurs through the folding of amino acid sequences 16-23 onto 28-35 to form a β-sheet structure (Rauk, 2009). It is now accepted that the oligomers, which may form along a distinct pathway, are more neurotoxic than the relatively inert amyloid fibrils (Arispe, Pollard, & Rojas, 1993) (Lin, Bhatia, & Lal, 2001) (Necula, Kayed, Milton, & Glabe, 2007). Despite extensive research, the mechanism of action of Aβ is not clearly understood.

The factors affecting AD are diverse and their interrelatedness remains elusive. Genetic factors (Bertram & Tanzi, 2005), metals (Bush & Tanzi, 2008), and vascular deficiencies (Roy & Rauk, 2005) have been found to be associated with AD. Also, the Alzheimer's afflicted brain has been shown to suffer from severe oxidative stress (Markesbury, 1997) and inflammation (Akiyama, Barger, Barnum, Bradt, & Bauer, 2000). In post-mortem brains of AD patients, amyloid plaques were laden with trace metals such as copper, zinc, and iron at concentrations up to 400 μM, 1 mM, and 1 mM, respectively (Lovell, Xie, & Markesbury, 1999). Extensive research has been conducted on the role of metal ions in the formation of reactive oxygen species (ROS), and amyloid-metal complexes that increase amyloid toxicity by ultimately promoting apoptosis (Huang, Cuajungco, & Atwood, 1999) (Jomova, Vondrakova, Lawson, & Valko, 2010) (Liu, Men, Perry, & Smith, 2010) (Sayre, Perry, & Smith, 1999) (Smith, Numomura, Zhu, Takeda, & Perry, 2000).

Aβ aggregation begins with a lag phase at which point the peptide progressively aggregates to form nucleation seeds (Harper, Liber, & Lansbury, 1997). The addition of metal ions has been shown to reduce the lag phase associated with Aβ aggregation (Sarell, Wilkinson, & Viles, 2010). Aβ has been shown to bind metal ions, such as copper, zinc, and aluminum,

yielding amyloid-metal complexes with varying effects (Lovell, Xie, & Markesbury, 1999) (Curtain, Ali, Smith, Bush, Masters, & Barnham, 2003). The binding of Aβ to copper allows the peptide to insert into lipid membranes more readily (Curtain, Ali, Smith, Bush, Masters, & Barnham, 2003), while aluminum-Aβ complexes have been shown to disrupt lipid membranes (Suwalsky, Bolognin, & Zatta, 2009).

The binding site of copper is believed to lie within the N-terminal portion of the peptide. Specifically, there is a salt bridge formed utilizing metals, such as zinc and copper, predominantly through a His(13)-metal-His(14) conformation as well as bridges with His(6) (Faller & Hureau, 2009) (Azimi & Rauk, 2011).

Previous research has shown that copper binds to these His co-ordination sites with greater affinity than zinc (Nair, Perry, Smith, & Reddya, 2010) and significantly stabilizes Aβ aggregates (Han, Wang, & Yang, 2008). The binding of copper causes Aβ to become redox active, which significantly contributes to the oxidative stress prevalent in AD (Rauk, 2009) (Markesbury, Oxidative stress hypothesis in Alzheimer's disease, 1997). The reduction of Cu^{2+}-amyloid complexes to Cu^{+}-amyloid complexes has been shown to produce hydrogen peroxide (Hewitt & Rauk, 2009) that in turn leads to the formation of pro-apoptotic lipid peroxidation products, such as 4-hydroxynonenal, which ultimately induces neuronal cell apoptosis (Jang & Surh, 2003). Thus, the binding of copper to Aβ not only increases neurotoxicity, but it has also been demonstrated to have kinetic and thermodynamic implications (Huang, Cuajungco, & Atwood, 1999).

In this work, we study the effect of copper ions on the peptide-peptide rupture force of the Aβ (1-42) peptide. We show that when copper ions are added to the Aβ force spectroscopy environment, the rupture force increases dramatically, which correlates with a higher rate of

aggregation shown by AFM imaging. This is the first single-molecule study which shows that Cu^{2+} increases the force of interaction between two single Aβ peptides; thus, affecting further aggregation.

3.2. Experimental Procedures

We used a widely accepted method of binding proteins through N-terminus to PEG heterobifunctional cross linkers (Allison, Hinterdorfer, & Han, 2002) (Hinterdorfer & Dufrêne, 2006), an experimental setup as previously described (Kim, Palermo, Lovas, Zaikova, Keana, & Lyubchenko, 2011). Detailed protocols are described in appendix A of this thesis. Briefly, the experimental procedures are outlined below.

3.2.1. Tip and Surface Modification

Bruker MLCT AFM cantilevers were cleaned by soaking in ethanol for 15 minutes, washed in ultrapure water and dried in a gentle stream of nitrogen and placed under UV light for 30 minutes. Mica was freshly cleaved. 3-aminopropyltriethoxy silane (APS) was synthesized as previously described (Shlyakhtenko, Gill, Filonov, Cerovac, Lushnikov, & Lyubchenko, 2003). The structure of APS was confirmed using NMR spectroscopy. The mica and cantilever were then immersed in 167μM APS for 30 minutes, rinsed with ultrapure water and dried under a gentle stream of nitrogen. The mica and cantilever were then placed in a 3400MW Polyethylene Glycol (PEG) solution (167μM in DMSO) (Laysan Bio, Alabaster GA) for 3 hours, than rinsed with DMSO. The cantilever and mica were washed and stored in HEPES buffer (50mM HEPES, 150mM NaCl, pH 7.4). We specifically chose HEPES buffer because of the absence of metal ions.

3.2.2. Aβ (1-42) Preparation and Surface Binding

Cys-Aβ (1-42) was purchased from Anaspec (Fremont, CA) and prepared in DMSO at a concentration of 1mg/mL. The Aβ stock solution was then diluted in HEPES buffer to a final concentration of 20nM. An equal volume of 200nM *tris*(2-carboxyethyl)phosphine (TCEP) was added to the dilute peptide solution to prevent aggregation. The Aβ solution was stored for 15 minutes and then centrifuged at 14000 RPM for 15 minutes to move monomeric forms to the top of the solution to ensure primarily monomeric forms of the peptide were used. The mica and cantilevers were soaked in the dilute Aβ solution for 30 minutes. The Aβ was rinsed with HEPES buffer, and the mica was treated for 10 minutes with β-mercaptoethanol to react with any available maleimide groups so as to prevent false rupture events. Both cantilever and mica were washed three times with HEPES buffer, and stored in HEPES buffer until use.

3.2.3. Atomic Force Spectroscopy

A JPK Nanowizard II atomic force microscope was used for all measurements. Cantilever spring constants were measured using Hutter's thermal noise method (Hutter & Bechhoefer, 1993), which requires both the normal sensitivity and the thermal resonance spectra. The sensitivity was obtained from the gradient of the contact portion of a force-displacement plot acquired on a mica surface. The thermal spectrum was obtained using the JPK software. The voltage response of the cantilever deflection measured using the photodiode was converted to units of force by multiplying by the normal sensitivity and the spring constant. Mica coated with Aβ as described earlier was placed on the stage in the liquid cell and immersed in HEPES buffer. A series of force curves were taken with an approach and retract velocity of 400 nm/s. A dwell time of 0.5 seconds was set to allow peptide-peptide binding events. For a single experiment approximately 1000 force curves were recorded, out of which approximately 10% of these

showed specific unbinding events. Each experiment was repeated four times with a different cantilever and substrate. For each repeat experiment at least 100 force curves were analyzed, a similar binary distribution was observed and representative experiments are presented. Solutions of Cu^{2+} (purchased from Sigma-Aldrich) in HEPES buffer were prepared at a concentration of 20nM and were added to the liquid cell for applicable experiments.

3.2.4. Force Curve Analysis

JPK data analysis software was used to analyze force curves. A worm like chain (WLC) fit was obtained for each force curve and rupture forces were obtained. Rupture force histograms were fitted with a sum of two Gaussian distributions, and minimized using the Levenberg-Marquardt non-linear least squares fitting routine in Matlab. Errors quoted for the most probable rupture force are evaluated as the standard deviation of each distribution, divided by the square root of the effective number of counts for each distribution (estimate of standard error). The effective number of counts was approximated by multiplying the total number of data points by the area fraction of the given Gaussian distribution.

3.2.5. Amyloid Incubation for AFM Imaging

Aβ (1-42) (purchased from rPeptide, Bogarta, GA) was pre-treated according to the Fezoui procedure (Fezoui, Hartley, Harper, Khurana, & Walsh, 2000) to ensure the monomeric form. The peptide solutions were prepared by adding HEPES buffer and either Cu^{2+} ions or an equal amount of buffer to produce the copper and control samples, respectively. The final concentration of amyloid-β (1-42) was 55 μM, and the final concentration of Cu^{2+} was 5.5 μM, which yielded a 10:1 amyloid-Cu^{2+} molar ratio. The solutions were incubated at room temperature for 1 hour, 6 hours and 24 hours. 50 μL aliquots were placed onto freshly cleaved

mica at the respective times for a 5 minute adsorption period. Excess amyloid solution was then washed with milliQ water and dried with a gentle stream of N_2 gas.

3.2.6. AFM Imaging

The mica slides with adsorbed amyloid were placed in a JPK Nanowizard II atomic force microscope and imaged in air in Intermittent Contact mode using cantilevers purchased from Nanosensors^{TM} (Non-contact/Tapping™ mode - High resonance frequency; non-coated; tip radius <10nm). All images were taken with a line rate of 0.5Hz, and the gains were adjusted to yield maximum image quality. 10x10μm and 5x5μm images were taken, and subsequently analyzed using JPK Data Processing Software. Each experiment was repeated at least twice and at least 3 images for each sample.

3.3. Results

We used a combination of single molecule atomic force spectroscopy and atomic force microscopy to probe the single molecule interactions of Aβ in the presence of Cu^{2+} ions. Statistical analysis was completed on force curves to determine the most probable rupture force and Gaussian curve width. Figure 9 illustrates a schematic of the force spectroscopy experimental set up. Notice that Aβ has been bound to both the tip and substrate through APS and a PEG linker, via a cys residue at the N-terminus.

Figure 12 shows a series of histograms of rupture events. For our control experiment without any copper added, we observed double Gaussian peaks centered on 66±1 pN and 132±4 pN. These figures are shown in Table 1. With the addition of copper, a much higher mean rupture force was observed, with copper yielding rupture forces with double Gaussian peaks at 83±3 and 164±5 pN and mean rupture force of 178.9±7 pN.

	Gaussian Peak 1 ± SE (pN)	Gaussian Peak 2 ± SE (pN)	Mean Rupture Force (pN)	Experimental Yield (%)
Aβ Control	66±1	132±4	125.2±5	14.3
Cu^{2+} added	83±3	164±5	178.9±7	14.2

Table 1 - Statistical Data of Force Spectroscopy Experiments

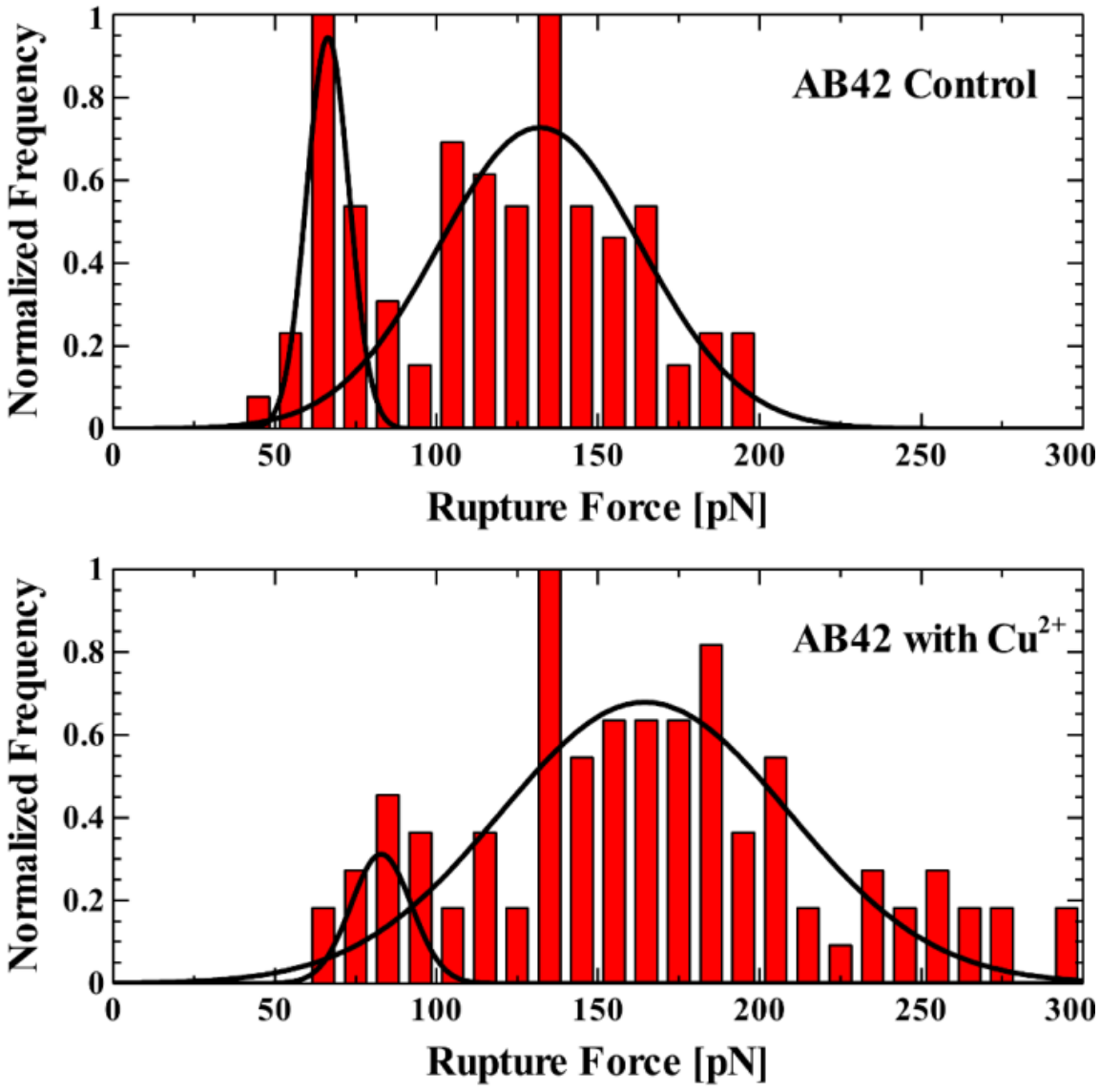

Figure 12- Histograms of rupture forces showing the distribution of forces required to rupture the peptide-peptide complex without copper (A) and with copper (B). Fits to the data are Gaussian distributions, the peaks of which represent the most probable rupture force.

Figure 13 shows sample force curves obtained with and without copper and occurring within both the higher and lower Gaussian peaks shown in figure 12.

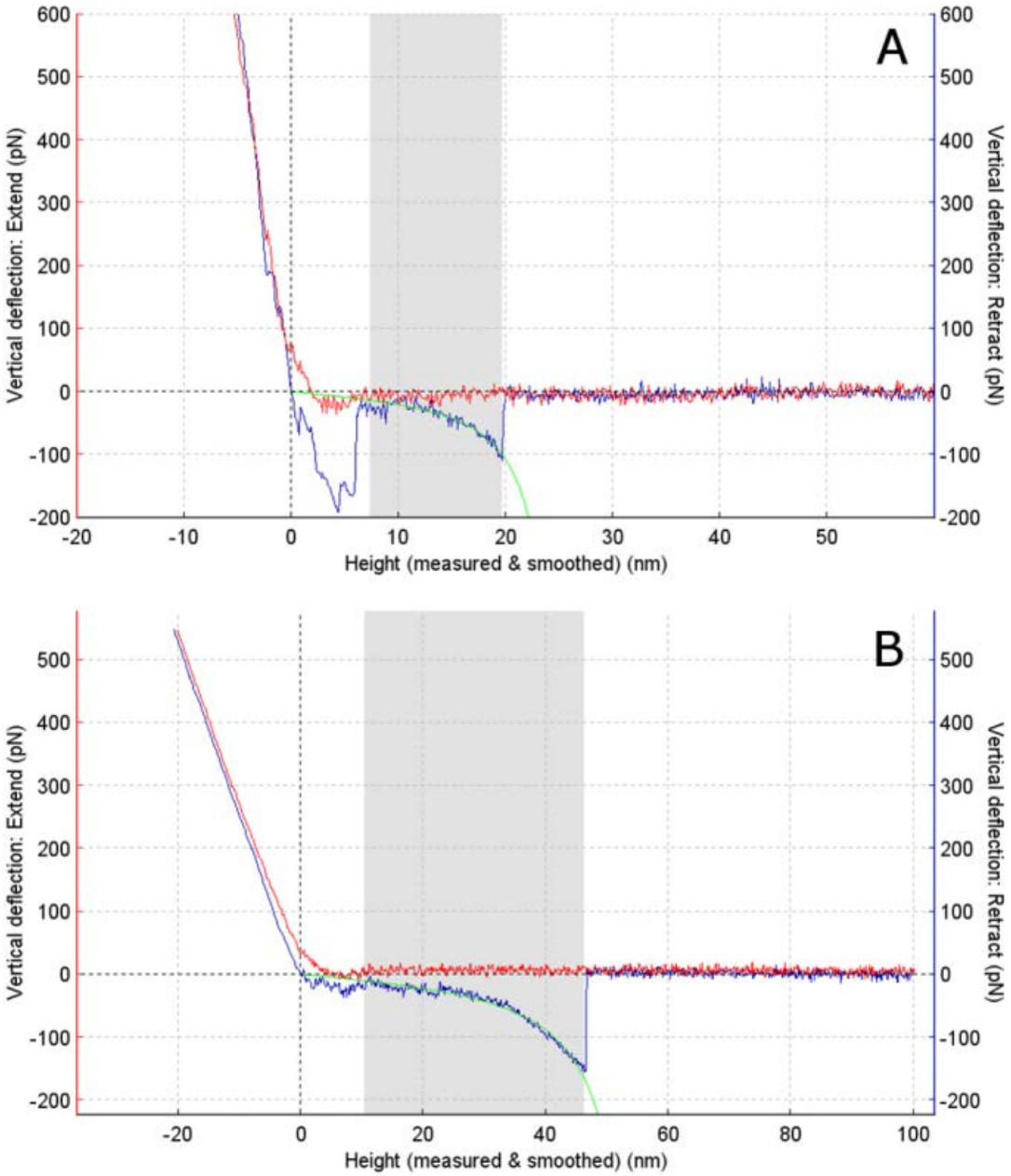

Figure 13- Representative force curves. Force curves showing rupture forces of an Aβ dimer without (A) and with (B) copper added at a retraction rate of 400 nm/s. Curves are shown as force vs. piezo z-displacement.

Figure 14 shows AFM images of amyloid aggregates formed in solution with and without copper ions added for incubation times of 1 hour, 6 hours and 24 hours. We observed oligomeric amyloid species with a mean height of 3.13 nm after an hour of incubation without copper, as seen in figure 14A. After 6 hours, the control experiment (figure 14B), revealed the formation of a mixture of oligomeric species, and short fibrils that had a mean height of 4.5 nm. At 24 hours of incubation (figure 14C), Aβ aggregated to dominantly fibrillar species with a mean height of 7.2 nm. The observed fibrils at 24 hours were significantly longer than those observed at 6 hours, extending up to 3 μm. Figures 14D-14F are representative images of the various structural conformations of the Aβ aggregates in the presence of one tenth Cu^{2+} molar concentrations under the respective times. Large amorphous aggregates with a mean height of 9.3 nm were formed after 6 hours, which coincided with the formation of the short fibrils as found in the respective control. After 24 hours, these unique aggregates remained the dominant species, and the populous fibrils that were observed in the control were not present.

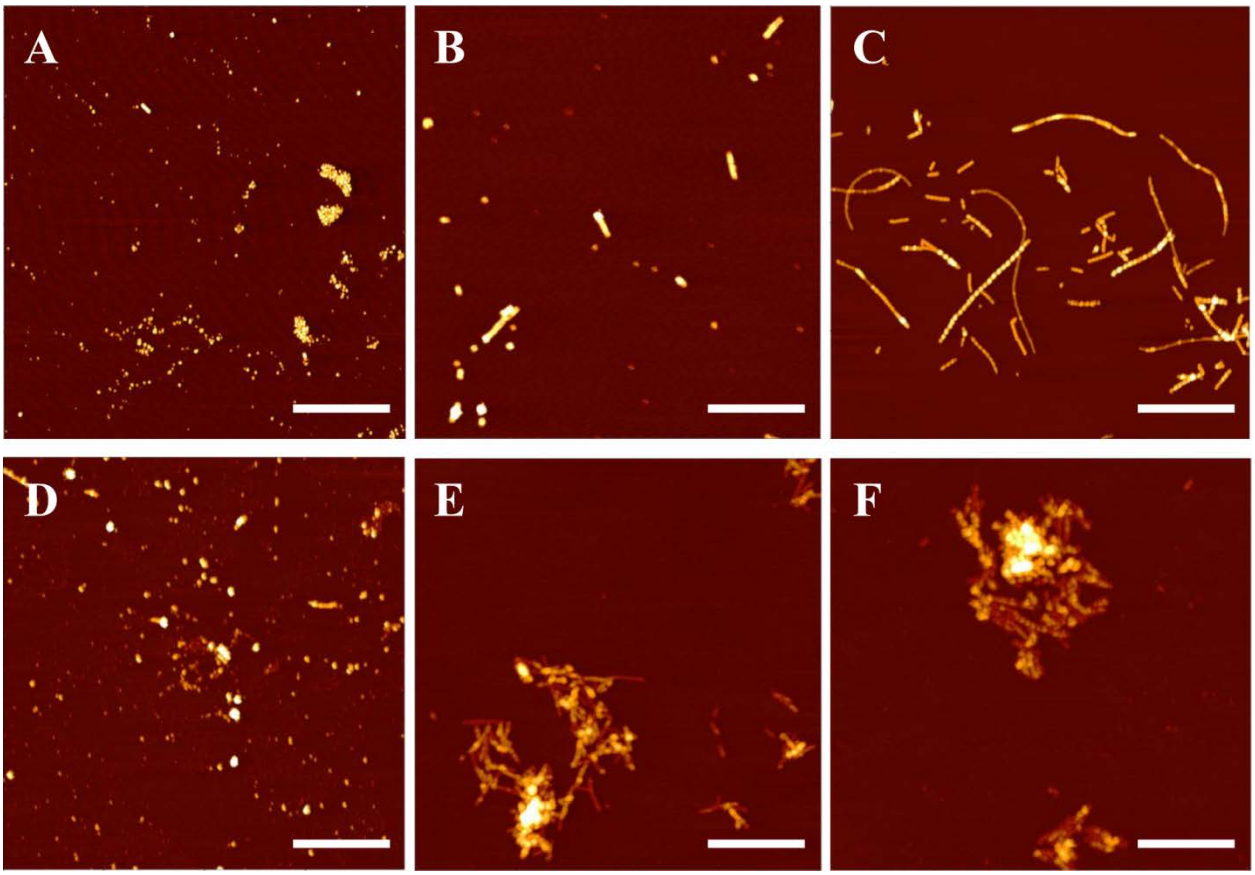

Figure 14- AFM images of amyloid-metal aggregates. AFM images of Aβ incubated without copper for periods of 1hr (A) 6hr (B) and 24hr (C), and with copper at a 10:1 molar ratio for 1hr (D), 6hr (E), and 24hr (F). The lateral scale bar is 1 µm.

3.4. Discussion

In a recent report, Sarell and colleagues (Sarell, Wilkinson, & Viles, 2010) attributed the increase in aggregation of Aβ with substoichiometric levels of Cu^{2+} to charge neutralization caused by the binding of copper ions to the copper binding site at the histidine residues resulting in a peptide more prone to self-association. In this work, we present for the first time measurements of the initial single molecule interaction between two Aβ peptides in the presence of Cu^{2+} ions. We show that with the addition of copper, the unbinding (rupture) force increases notably. The increase in unbinding force is consistent with the findings of other groups showing

a reduction of lag time in amyloid aggregation when copper is added to the system (Huang, Atwood, Moir, Hartorn, & Tanzi, 2004). This suggests that the reduction of lag time associated with Aβ aggregation occurs on a single molecule level as a result of the very initial dimerization interactions between the peptides.

The rate of aggregation of aggregation-prone proteins, such as Aβ (1-40) and α-synuclein, has been shown to be a function of the mean rupture force between two peptides (McAllister, et al., 2005) (Yu, Malkova, & Lyubchenko, 2008). It has been established that the acceleration of aggregation is the result of a decrease in the lag time associated with amyloid nucleation (He, Giurleo, & Talaga, 2010). Although the mechanisms involved during this lag time have previously been unclear, it is believed that the lag time is a result of the development of a significant amyloid nucleus onto which other peptides can bind to. We suggest that a reduction in lag time may occur as a result of the very initial nucleation process: the dimerization of two Aβ peptides.

The common theory of the aggregation of Aβ involves the oligomer cascade hypothesis (Hardy & Higgins, 1992). According to the oligomer cascade hypothesis, monomeric species form a dimeric nucleation site. Additional monomers are added to this nucleus to progressively form larger oligomers, protofibrils and finally, mature amyloid fibrils (Hardy & Higgins, 1992). This paradigm has recently come under review and a serious argument can now be made that pathological oligomers and inert fibrils may form along separate pathways (Yamaguchi, Yagi, Goto, Matsuzaki, & Hoshino, 2010). Necula and colleagues have suggested that several different oligomeric species may form following the misfolding of the Aβ monomer (Necula, Kayed, Milton, & Glabe, 2007). Only one of these oligomers may eventually form fibrils, with other oligomers remaining in the most stable oligomeric state. He and colleagues studied the amyloid

forming β-lactoglobulin protein and have suggested a bifurcation of its amyloid pathway at the 16mer point, where the aggregate may continue as an oligomer or begin to form a protofibril (He, Giurleo, & Talaga, 2010). Based on our data, we propose that, for Aβ, the divergence of this pathway begins much earlier: at the initial dimerization of the two Aβ peptides, where the structure of the initial dimer varies and determines the pathway followed. In our control experiments without copper, we observe two distinct force peaks most likely associated with different dimer configurations, possibly parallel and anti-parallel for two amyloid peptides interacting with each other at the self-recognition site as proposed by Tjernberg (Tjernberg, Naslund, Lindquist, Johannsson, Karlstrom, & al, 1996) and illustrated in figures 15A and B. The anti-parallel dimer configuration (figure 15A) is the more stable of the two stabilized by salt bridges at each end (Mothana, Roy, & Rauk, 2009), and therefore, we assign this configuration to the stronger force observed (peak two, figure 12A). The first weaker force (peak one, Figure 2A) more likely corresponds to the parallel configuration (Figure 15B).

Our interpretation of the data collected is consistent with the results of Pedersen and colleagues (Pedersen, Østergaard, Rozlosnik, Gammelgaard, & Heegaard, 2012). Pedersen used bulk measurements of Aβ aggregation under the influence of Cu^{2+} and concluded that copper alters the aggregation pathway of Aβ. The interpretation of our data is consistent with Pedersen's conclusions. Our results build on this data and propose a structural model which is consistent with the observations provided by our groups.

The addition of copper ions significantly increases the unbinding forces of Aβ peptides, at the same time the two distinct peaks shift to a higher value (figure 12B). It was also apparent that though there is a shift in the two Gaussian peaks, the proportion of the number of binding events in the first peak to the second peak decreases when copper is added to the environment.

Based on our hypothesis that there are at least two different conformations of the Aβ dimer, we believe that the addition of copper increases the probability of Aβ to dimerize in a conformation correlating with the second peak, corresponding to a larger binding force. Given these differences in unbinding forces, we suggest that both the parallel and anti-parallel dimer conformations become stabilized by Cu^{2+} ions, which results in the shift of these peaks to higher forces. Considering the possibility of Aβ-Aβ binding both with and without Cu^{2+} ions, we suggest four possible complexes that can be formed in this case: Aβ-Aβ parallel, Aβ-Cu-Aβ parallel, Aβ-Aβ anti-parallel, Aβ-Cu-Aβ antiparallel. Our hypothesis is further supported by recent theoretical work by Mousseau (Côté, Laghaei, Derreumaux, & Mousseau, 2012) and Urbanc (Barz & Urbanc, 2012). Using molecular dynamics simulations, both groups independently demonstrated that Aβ (1-42) can dimerize in multiple conformations along multiple pathways. It stands to reason that different dimer conformations have different unbinding forces.

We considered alternative explanations to our hypothesis to explain the presence of two most probable force peaks. We considered that two distinct dimers are rupturing at the same time yielding one much larger force. Based on the probability of a binding and unbinding event, we applied the method proposed by Akhremitchev (Karacsony & Akhrimitchev, 2011) to determine the probability of two or more peptides being located in the same area and rupturing simultaneously. For our highest yielding experiments, where the most rupture events happened for a given number of approaches, we calculate this probability to be p=0.12. Consistent with previous analysis methods, the force curves with the (pn, n = number of force curves) highest rupture forces were discarded and not included in the rupture force histograms. Over several thousand collected force curves, we did indeed observe some double, and even triple, binding

events. However, given the inhomogeneity of the length of the PEG linkers, these events were identified by two force curves with the distance between them being a function of the difference in PEG linkers rather than one large force curve. Given our statistical observations, we conclude that any double unbinding event masquerading as a single force curve is so improbable as to be negligible, and certainly would not approach the greater than 50% of force curves that occur at the higher force.

Our second alternative explanation for the presence of these double force peaks is that instead of a monomeric peptide being bound at the end of the PEG linker, aggregation has occurred prior to attachment to the PEG linker and an amyloid oligomer was in fact bound at the end of the PEG linker. We closely followed the procedure developed by the Lyubchenko group, who repeatedly showed that when treated as noted in our methods and kept in such a dilute solution, Aβ will not aggregate (Kim, Palermo, Lovas, Zaikova, Keana, & Lyubchenko, 2011).

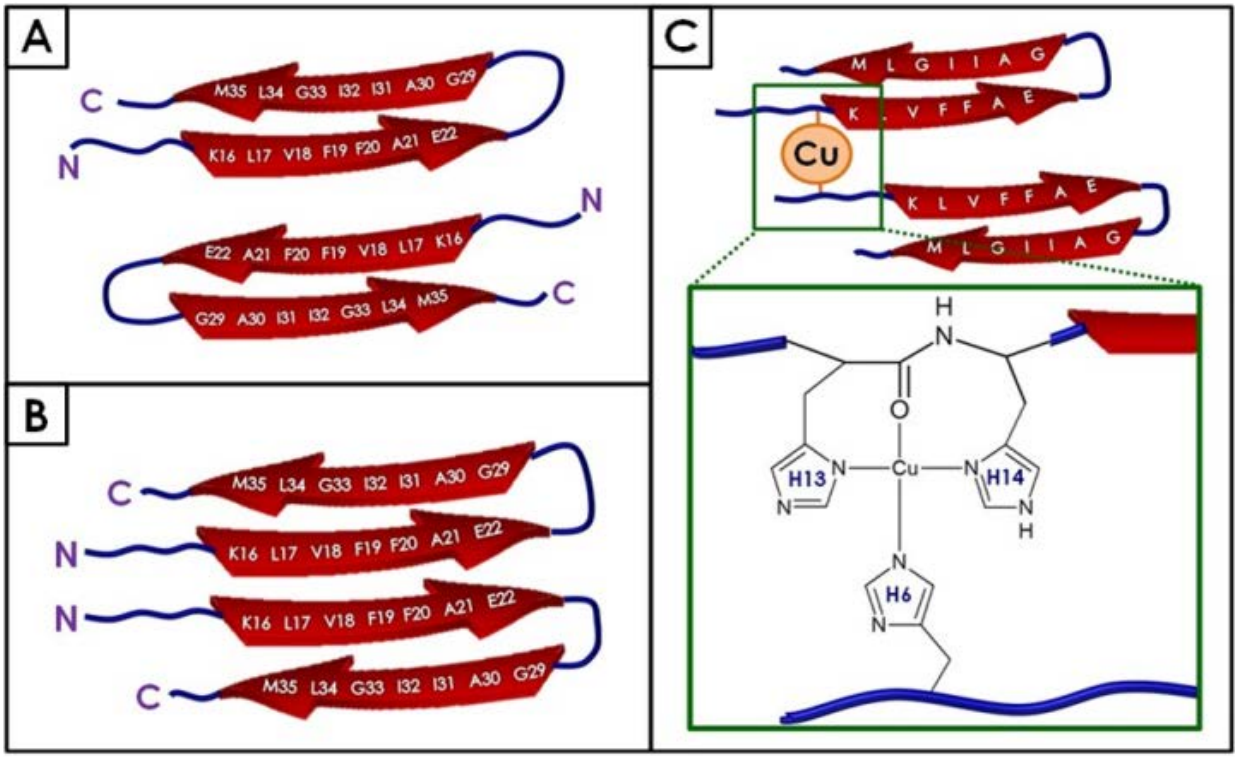

Figure 15- Schematic diagram of Aβ dimers with and without copper. Without copper, the most favorable conformation of the Aβ dimer involves an anti-parallel conformation (A). With the addition of copper, Aβ adopts a parallel dimer conformation (B) stabilized by the occupied copper binding sites (C).

Figure 16 shows plausible conformations of Aβ dimer with and without copper assembled from stable Aβ42 monomer structures (Raffa & Rauk, 2007). Each monomer has an internal antiparallel β-sheet between residues 18-21 and 30-33. The dimers are assembled by juxtaposition of the self-recognition site residues 18-21 in antiparallel (A, C) and parallel (B, D) orientation. Both orientations bring His6, His13 and His14 of each monomer into close proximity, requiring little reorientation to bind Cu^{2+} ions (filled green circles). Figure 16 A and B show plausible assemblies for the Aβ-Aβ complexes in antiparallel and parallel conformations without copper. Figure 16 C and D show two possible structures for Aβ-Cu-Aβ in anti-parallel and parallel conformations, respectively. The variety of possible structures and the strengthening

of each binding event by Cu^{2+} results in the broad distribution of unbinding forces we observed in the presence of Cu^{2+} ions (figure 12B).

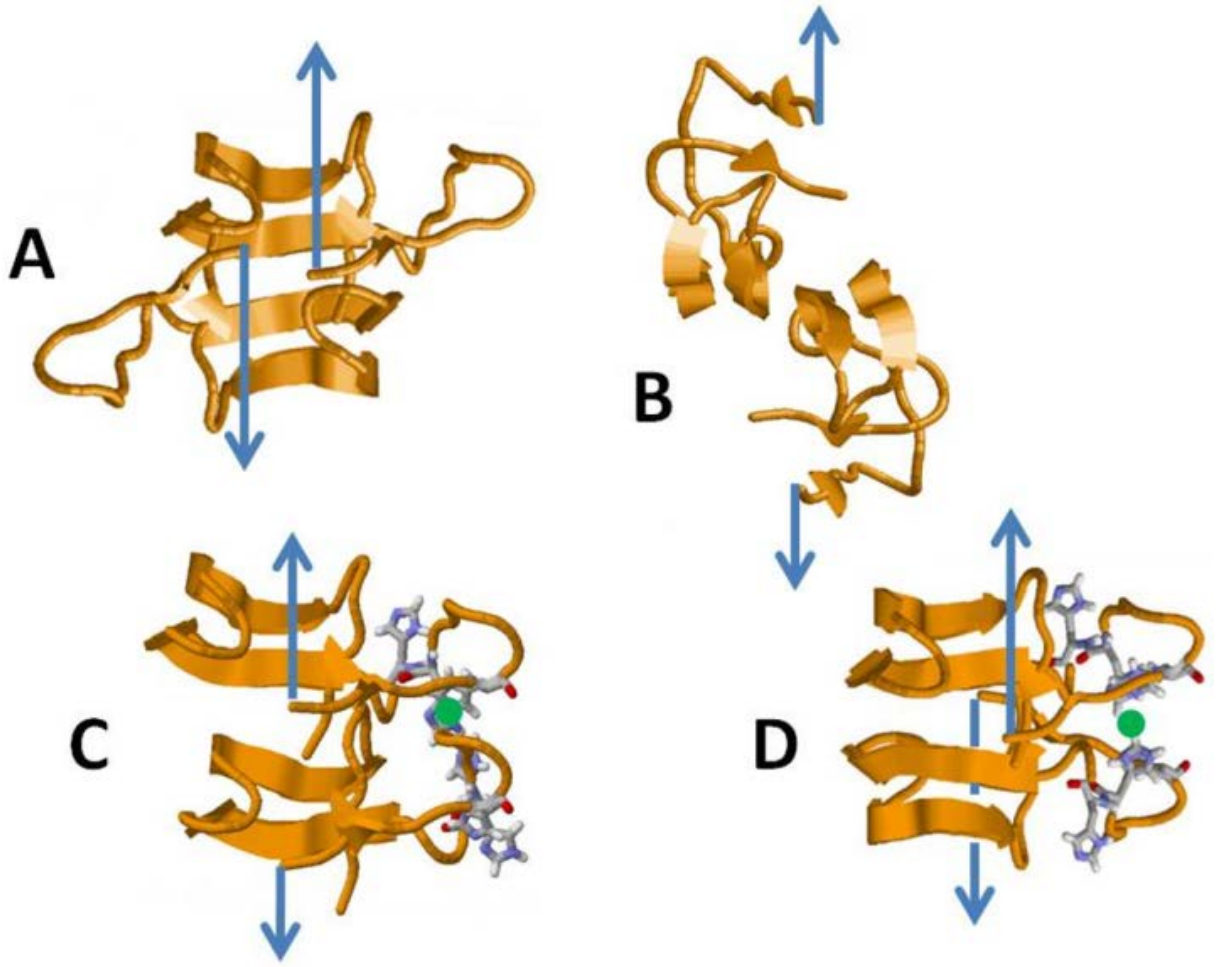

Figure 16 - Schematic diagram of Aβ dimers with and without copper assembled from stable Aβ42 monomer structures (Raffa & Rauk, 2007). Each monomer has an internal antiparallel β-sheet between residues 18-21 and 30-33. The dimers are assembled by juxtaposition of the self-recognition site residues 18-21 in antiparallel (A, C) and parallel (B, D) orientation. Both orientations bring His6, His13 and His14 of each monomer into close proximity, requiring little reorientation to bind Cu^{2+} ions (filled green circles). Proposed schematics are courtesy of A. Rauk, unpublished data, created using Raswin software.

Our AFM imaging shows that after 6 hours of incubation in the presence of copper, no amyloid fibrils were found in a significant amount. Rather, we observed large amorphous structures that indicate the presence of a copper-dependent Aβ aggregation pathway distinctive

from the aggregation pathway without Cu^{2+} which leads to fibril formation. The dominance of these amorphous amyloid aggregates in the presence of copper ions is consistent with previously published images of amyloid aggregation in the presence of Cu^{2+} (Ha, Ryu, & Park, 2007) (Innocenti, et al., 2010).

Trace amounts of metal ions have been shown to decrease the lag time associated with aggregation (Huang, Atwood, Moir, Hartorn, & Tanzi, 2004). Previously, it has been unclear why only substoichiometric amounts of metal ions were needed to reduce the lag time, and thus, increase aggregation. We believe that the reduction of lag time associated with amyloid aggregation in the presence of copper is a result of the very initial dimerization process immediately forming an aggregation nucleus which other peptide can bind onto.

In summary, we demonstrated that unbinding forces of two Aβ peptides without Cu^{2+} have two distinct force peaks, likely associated with parallel and anti-parallel configurations, and resulted in amyloid fibril formations as demonstrated by AFM imaging. The addition of Cu^{2+} ions resulted in a shift to higher force distributions and a higher proportion of unbinding events occurring in the higher force. As seen by the AFM imaging, this distinct force profile is correlated with the formation of amorphous aggregates. We assign this effect of Cu^{2+} to the strengthening of binding between two individual Aβ peptides and disruption of fibril formation pathway at a single molecule level.

3.5. Conclusions

In conclusion, we report that copper increases peptide-peptide binding forces at a single molecule level and changes aggregation observed at the microscale. Therefore, single molecule peptide-peptide interaction defines a pathway for amyloid aggregation. This finding leads to a better understanding of the role of biometals in the mechanism of amyloid fibril formation.

Chapter 4
Effect of Aggregation Inhibitors on Amyloid-β Peptide Unbinding Force

This chapter has been adapted from a manuscript which has been accepted for publication in the journal Biosensors and Bioelectronics.

Alzheimer's disease is a neurodegenerative disease with no known cure and few effective treatment options. The production of pharmaceuticals which prevent the aggregation of amyloid-β has long been a goal of researchers. The principal neurotoxic agent is an oligomeric form of the amyloid-β peptide and one of the treatment options currently being studied is the inhibition of amyloid aggregation. In this work, I tested a novel pseudopeptidic aggregation inhibitor designated as SG1 designed by the Rauk group. SG1 has been designed to bind at the amyloid-β self-recognition site and prevent amyloid-β from misfolding into beta sheet. I used atomic force spectroscopy, a nanoscale measurement technique, to quantify the binding forces between two single amyloid peptide molecules. I demonstrated that single molecule atomic force spectroscopy can be used to assess the effectiveness of amyloid aggregation inhibitors by measuring the experimental yield of binding and can potentially be used as a screening technique for quick testing of efficacy of inhibitor drugs for amyloid aggregation.

Author Contributions:

- Designed Experiments: Zoya Leonenko, Arvi Rauk, Francis Hane
- Performed Experiments: Francis Hane, Brenda Lee, Anahit Petoyan
- Analyzed Data: Francis Hane, Brenda Lee, Anahit Petoyan
- Wrote the Manuscript: Francis Hane, Zoya Leonenko, Arvi Rauk

4.1. Introduction

AD is a complex disease associated with a number of potential factors including aging (Bertram & Tanzi, 2005), genetics (Bertram & Tanzi, 2005), metals dyshomeostasis (Bush & Tanzi, 2008), protein-lipid interactions (DiPaolo & Kim, 2011), vascular disorders (Roy & Rauk, 2005), and loss of acetylcholine receptors (Whitehouse, et al., 1986). Pharmaceutical therapies have focused on attacking underlying factors associated with Alzheimer's (Roberson & Mucke, 2006). For example, γ-secretase inhibitors have been developed in an attempt to stop the cleaving of amyloid-β from its precursor protein, the amyloid precursor protein (APP) (Citron, 2004). Despite extensive research and funding, no therapy has yet been shown to reverse the symptoms associated with Alzheimer's in human trials, and even the most efficacious therapies are not curative, but only delay the onset of symptoms (Neugroschl & Sano, 2010).

Aβ begins its pathological aggregation by misfolding into an internal beta sheet between the amino acids 17-23- and 28-35. The amino acids (24-27) form a beta-hairpin to allow the peptide to fold back on itself (Petkova, et al., 2002) (Sciarretta, Gordon, Petkova, Tycko, & Meredith, 2005). After misfolding into a hairpin, the peptide may bind to another Aβ peptide, acting as a nucleus for further peptide aggregation. The self-recognition site (17-23) (Tjernberg, Naslund, Lindquist, Johannsson, Karlstrom, & al, 1996) is responsible for the aggregation of Aβ into dimers and higher oligomers. Blocking this site effectively prevents the misfolding and subsequent aggregation. In the absence of sufficient peptide clearance, this aggregation leads to the formation of toxic amyloid aggregates (Harper, Liber, & Lansbury, 1997).

The Aβ sequence (13-23), which incorporates the self-recognition site, has been a target for amyloid aggregation inhibitors (Mothana, Roy, & Rauk, 2009) which are designed to have a high affinity for the self-recognition site and "block" the peptide from self-dimerization. Rauk

and co-workers developed a series of pseudopeptidic novel amyloid inhibitors that bind to and act on this self-recognition site (Mothana, Roy, & Rauk, 2009) (Roy, 2010). These inhibitors consist of a series of modified amino acids including methylated amino acids. A structure of SG1 is show in figure 18b. These inhibitors were synthesized and tested using a combination of circular dichroism and thioflavin T fluorescence assay to look for evidence of peptide aggregation. These methods have a characteristically low throughput because a period of 24 hours or more is needed for the peptide to aggregate into a recognizable form to determine the effect of the inhibitor on the aggregation properties. We used atomic force spectroscopy to test the efficacy of a synthetic amyloid inhibitor termed SG1 (figure 18) and demonstrated that SG1 reduces the number of binding events between two Aβ peptides by as much as 81%. In addition, we used atomic force microscopy and molecular dynamics simulations for comparison with AFS data and demonstrated with all these methods that the aggregation of Aβ is greatly reduced in the presence of SG1.

4.2.Experimental Procedures

To follow the effect of SG1 on Aβ aggregation and fibril formation, AFM was used in both imaging mode and force spectroscopy mode. To measure single molecule binding forces between peptides, AFM was used in force spectroscopy mode, in which the AFM probe, with an Aβ peptide attached to it was moved repeatedly towards and away from the mica surface, also bound with peptides, and the interaction force was measured as a function of probe-sample separation at pN resolution. For these experiments attachment of the Aβ peptide to both AFM probe and the surface is required. Except as noted, we used chemical modification protocols as previously described (Hane, Tran, Attwood, & Leonenko, 2013) and in appendix A of this thesis.

4.2.1. Preparation of SG1 Inhibitor Solution

SG1 was synthesized using fmoc-chemistry method (Roy, 2010). SG1 was lyophilized and stored in powdered form in -20 °C. When ready for experimental use, SG1 was dissolved in HEPES buffer (50 mM, 150 mM NaCl, pH 7.4). A 2 μM stock solution was prepared using serial dilutions. From the stock solution, final aliquots of 20 nM, 40 nM and 200 nM were prepared for experimental force spectroscopy experiments.

4.2.2. AFM Imaging of Amyloid-β and SG1 incubated in solution

Aβ (1-42) was purchased in lyophilized powder from rPeptide (Bogart, GA), pretreated according to the Fezoui procedure (Fezoui, Hartley, Harper, Khurana, & Walsh, 2000) to ensure monomeric form. The Aβ was dissolved in HEPES buffer (20 mM HEPES and 100 mM NaCl, pH 7.4) and was immediately used to prepare the sample solutions at a final concentration of 110 μM Aβ (1-42). The inhibitor SG1 was added at a 1:1 molecular ratio of SG1 to Aβ. The control solution had no inhibitor added. Solutions were incubated at 1, 6, and 24 hours at room temperature. After each incubation period, 100 μL of each solution was deposited onto freshly cleaved mica slides and incubated at room temperature for 5 minutes. Mica slides were then rinsed 5 times with 50 μL aliquots of distilled H_2O, dried for 2 minutes with a gentle stream of nitrogen gas and imaged in air in intermittent contact mode using JPK Nanowizard II AFM. We used silicon AFM probes (VISTA), with a spring constant of 40 N/m, resonance frequency of 300 kHz, and an aluminum reflex coating. Multiple 50x50 μm images and 5x5 μm images were collected from each sample at a resolution of 2048x2048 pixels and used for statistical analysis. AFM images were analyzed to extract the size of oligomers, size of fibrils and the oligomer to fibril ratios using JPK image processing software and ImageJ v.1.43 software.

4.2.3. Molecular Dynamics Simulations

The initial structures of SG1, Aβ (13-23), Aβ (13-23)-Aβ (13-23), and SG1-Aβ (13-23) were obtained as described earlier (Mothana, Roy, & Rauk, 2009). The monomeric Aβ receptor model, Aβ(13-23), was acetylated at the N-terminus, residue 13 (His13) and N-methylated at residue 23 (Asp23). The SG1-SG1 dimer was determined as described previously (Mothana, Roy, & Rauk, 2009). All MD simulations were performed using the Gromacs 4.5 suite of software (Berendsen, van der Spoel, & van Drunen, 1995). Previously, the free energy perturbation technique called "Atomic Force Microscopy" or AFM was used to calculate the free energy of binding of different complexes (Mothana, Roy, & Rauk, 2009). The binding results presented in this work were reevaluated with the more accurate technique, "Umbrella Sampling," in which selected frames along the AFM potential curves are re-equilibrated and re-assembled into complete potential curves by the "Weighted Histogram Analysis Method" (WHAM). Each dimer had thirty windows and each window was equilibrated for 20ns with force constant 1000 kJ/ (mol nm^2) at physiological pH (7.4) and temperature (310 K).

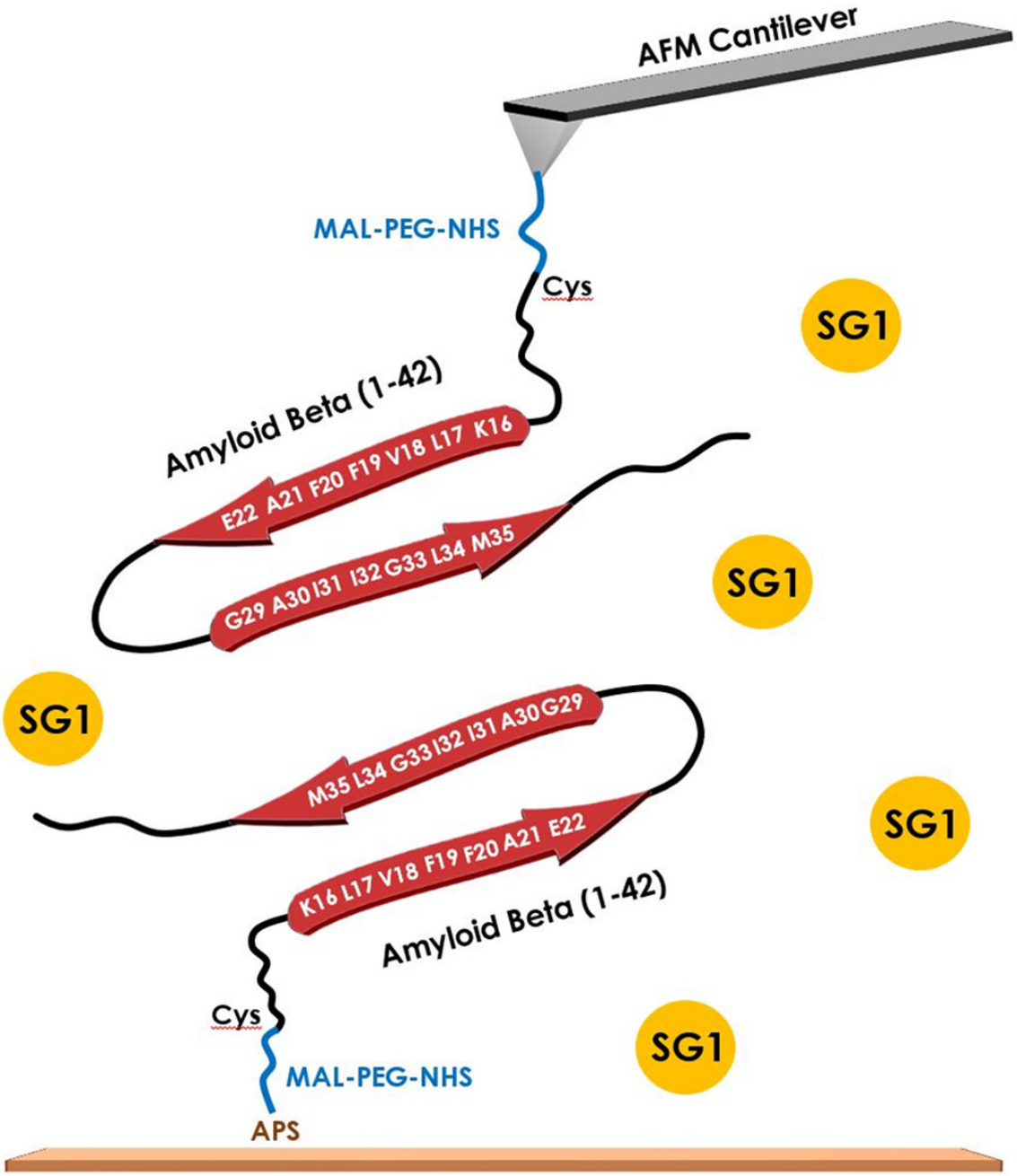

Figure 17- Schematic of Force Spectroscopy Experiment. A schematic of the experimental setup of force spectroscopy experiments, showing Aβ bound to the substrate and AFM tip via the PEG linker with aggregation inhibitor SG1 in the aqueous solution. A silanated surface is modified with NHS-PEG-maleimide. A cysteine residue is bound to the N-terminus of Aβ peptide to act as a binding site for the maleimide group of the linker molecule.

4.3.Results

A schematic of the experimental set up is shown in figure 17 with one Aβ peptide bound to the tip and another to substrate via intermediate PEG linkers.

Amyloid aggregation inhibitor SG1 binds to the Aβ self-recognition site (17-23), preventing the dimerization and further aggregation of Aβ. By binding to this site, the inhibitor physically prevents the two structured sections from coming into contact and forming the prerequisite hairpin. In figure 18a, the structure of most stable conformation of Aβ (13-23) is shown, which is folded conformation, stabilized by intramolecular H-bonds between Glu22 and the amido N-H of residues Val18 - A21. The most stable conformation of SG1 is a β-strand (figure 18b). SG1 is designed to make an antiparallel beta sheet with the self-recognition site, Aβ (17–23). The structure of the SG1 peptide shown in figure 18a was obtained by MD simulations and the binding between SG1 and Aβ (13-23) fragment responsible for beta-sheet formation was calculated. When SG1 binds to Aβ, N-methylation at one edge of the beta strand ensures that SG1 cannot propagate a beta sheet from that edge. Figure 18c shows the complex formed as a result of binding between SG1 and Aβ (13-23), which is predominantly an antiparallel β-sheet.

Figure 18d shows free energy curves for the dissociation of the Aβ (13-23) dimer, the SG1/Aβ (13-23) complex and the SG1 dimer obtained from MD simulations. The estimated free energies of dissociation are 62, 56, and 40 kJ/mol, respectively.

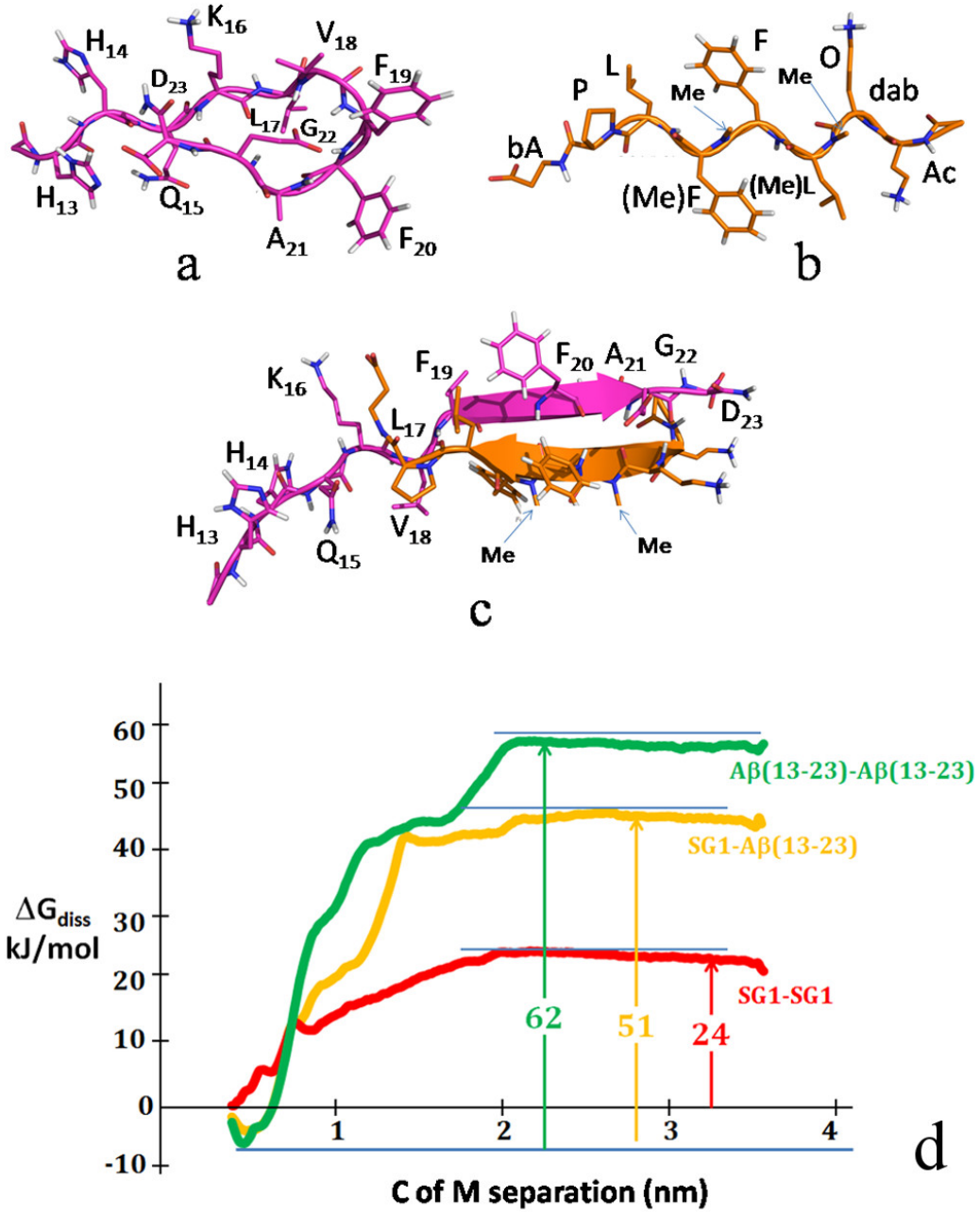

Figure 18- Molecular Dynamics Simulations Showing Mechanism of Action of SG1: a) the structure of Aβ (13-23) in its most stable conformation. b) the structure of SG1 in its most stable conformation (β-strand): SG1=Ac-dab-O-(Me)L-F-(Me)F-LP-bA-COOH where dab=diaminobutyric acid, O=ornithine, (Me)L=N-methylleucine, (Me)F=methylphenylalanine, and bA= β-alanine; c) The structure of the complex of SG1 (gold) and Aβ (13-23) (magenta). The complex is predominantly an antiparallel beta sheet. d) Free energies of dissociation (ΔG_{diss}) in kJ/mol, of Aβ(13-23)-Aβ(13-23), SG1-Aβ(13-23) and SG1-SG1. All form antiparallel dimeric complexes.

Using AFS we measured unbinding forces and observed a noticeable reduction in the experimental yield in the presence of SG1 (from 24% in control experiment to 11.2% with equimolar concentrations SG1). Higher inhibitor concentrations of 40 nM and 200 nM resulted in experimental yields of 7.9% and 6.9% respectively.

A typical force curve is shown in figure 19a, with adhesion peak in the withdraw part of the force plot (blue). The unbinding event starts at a ~65nm which correlates with the length of two PEG linkers (each ~35nm). MD data as shown in figure 18d do not include a PEG linker and separation is therefore considerably less.

Figure 19b and 19c display the results of a typical experiment with mean rupture force shown (figure 19c) and the experimental yield of this experiment (19b). While a significant reduction in the experimental yield was observed as a function of inhibitor concentration (figure 3b), a quasi-linear increase in the unbinding force was also observed at higher concentrations of SG1 (figure 19c). This experiment was repeated four times. Each time, the addition of SG1 resulted in a decrease in experimental yield. Other experiments (data not shown) resulted in decreases from 3.1% to 0.5%, 8.8% to 6.1% and 36.3% to 23.4% with the addition of inhibitor SG1.

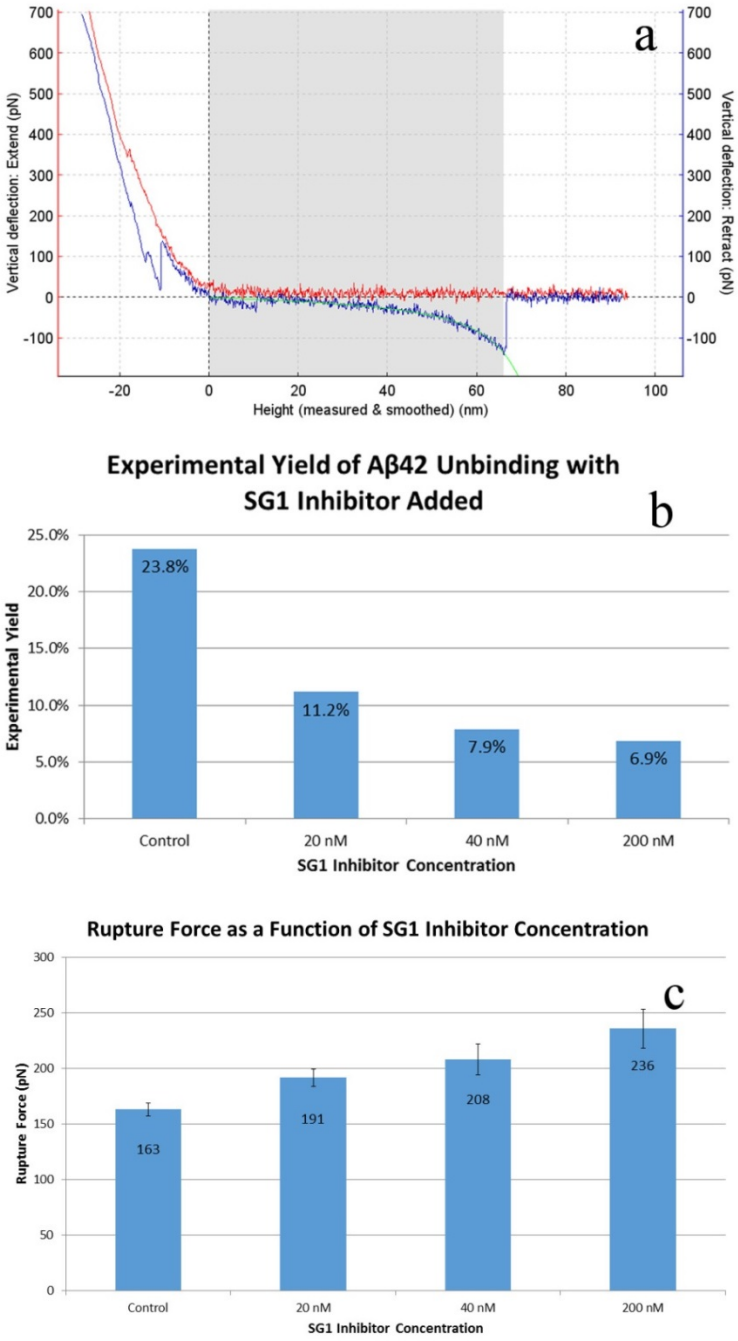

Figure 19 a). Typical unbinding force curve. The tip approaches the surface (red) until the AFM senses a repulsive force resulting from the tip interacting with the sample. The tip is then retracted (blue). As the tip is retracted, an interaction between the two molecules is measured until there is a sudden rupture at which point the cantilever returns to its original unbent position. If a binding event occurs, the retraction plot shows adhesion peak; b). Dependence of experimental yield of binding on concentration of SG1 inhibitor; c) Rupture force dependence on inhibitor concentration.

The effectiveness of the inhibitor was also validated by atomic force microscopy imaging. SG1 was added into the Aβ solution and after incubation for 1, 6 and 24 hours, the aggregates that were formed in solution were deposited on mica and imaged by AFM (figure 20) in air. In the absence of inhibitor, typical amyloid fibrils grew in width and length as a function of incubation time. When the aggregation inhibitor SG1 was added, a reduction in the number of fibrils was observed especially at earlier incubation times of 1 and 6 hours. We define the oligomer qualitatively as any of small globular structures not resembling a long fibrillar form. Other authors have referred to these structures as Aβ derived diffusible ligands (ADDL) (Lambert, et al., 1998), or prefibrillar oligomers (Glabe, 2008). Fibrils formed with inhibitor present were considerably smaller in length and width than the fibrils observed in the control samples. A statistical analysis of height distribution for Aβ control shows that the mean aggregate heights for 1, 6, and 24 hours were very similar: 6.47, 7.00, and 6.39 nm, respectively. For samples with SG1, the mean aggregate heights were changing with time: 3.13, 5.17, and 7.87 nm for 1, 6 and 24 hours, respectively.

The size of fibrils increased as a function of time for control samples. When SG1 inhibitor was added, fibril growth was considerably slower, and fibrils produced were shorter. The mean fibril lengths for amyloid-beta as 262, 571, 715 nm at 1, 6 and 24 hrs respectively. For the SG1 sample, we calculated mean fibril length of 83, 193, and 301 nm at 1, 6, 24 hrs respectively. We analyzed the images to deduce oligomer to fibril ratio (figure 21a). After 1 hour of incubation, both the control sample and the SG1 sample showed twice as much oligomers compared to fibrils. As incubation time increased, the control sample showed a large increase in the fibril/oligomer ratio to 10.3 indicating that there were 10 times as many monomers in fibrillar form than the oligomeric form. At 24 hours of incubation, the fibril to oligomer ratio increased to

12.5. With the SG1 present, the fibril to oligomer ratio was much lower: 0.5 at 1h and increased to only 9.7 after 24 hours of incubation (figure 21a).

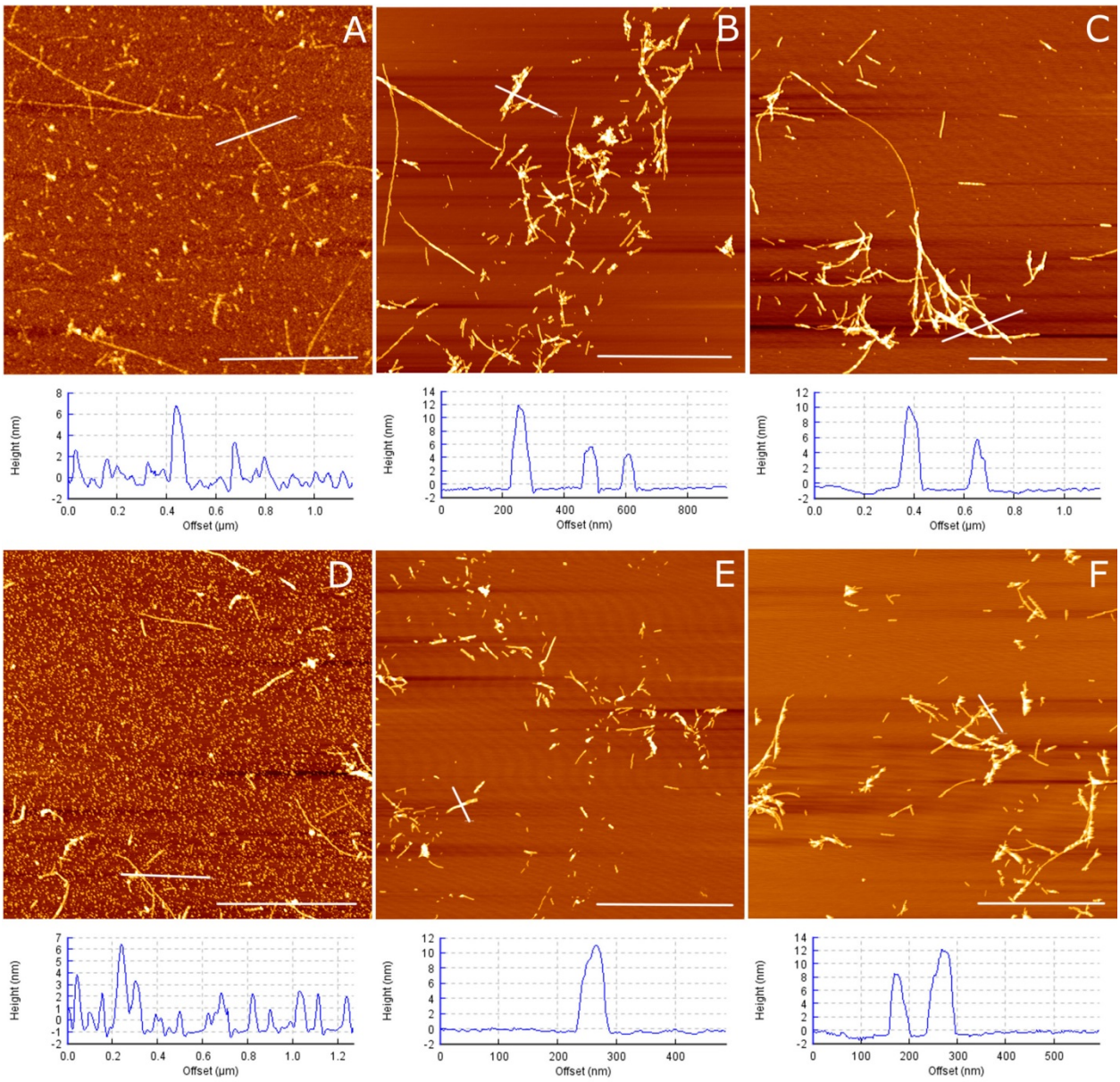

Figure 20 - AFM images of Amyloid Fibril Formation with and without Inhibitor. Aβ only (A, B, C) and Aβ with inhibitor SG1 incubated for 1, 6 and 24 hours respectively (D, E, F) and representative cross sections. SG1 and Aβ concentrations were both identical at 110 µM. After incubation for 1, 6, and 24 hours (images from left to right) at room temperature, 100 µL aliquots of each solution were deposited on freshly cleaved mica for 5 minutes, washed, dried and imaged in air. Below each image a cross-section is shown, indicating the height of the aggregates. The scale bar is equal to 1 µm.

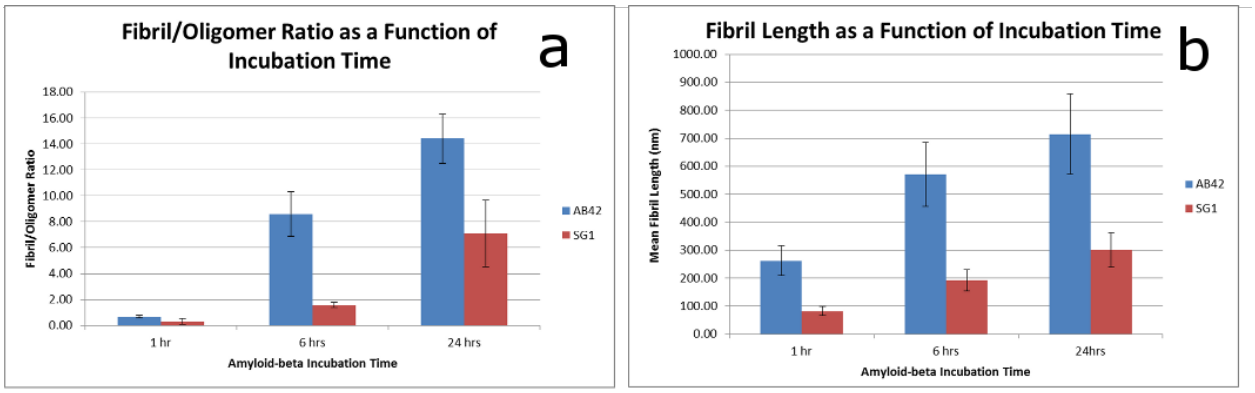

Figure 21- Analysis of AFM images. a) Fibril to oligomer ratio and b) Fibril length as a function of incubation time and presence of inhibitor.

4.4. Discussion

The goal of this study was to demonstrate that amyloid aggregation inhibitor SG1 can be used to slow the aggregation of the Aβ peptide. In addition, we wanted to show the potential of using AFS for quick testing of inhibitor drugs for amyloid fibril formation before they go to cellular, animal studies or clinical trials.

The first step in any aggregation process is the formation of a critical nucleus which begins with the dimerization of two molecules. If this initial process can be inhibited, aggregation will not occur, or at least the lag time associated with aggregation will increase or the aggregation rate will be lowered to allow for physiological clearance mechanisms to clear aggregates before they accumulate and become neurotoxic.

In past AFS experiments, the unbinding force itself has been used to characterize binding of molecules (Hinterdorfer & Dufrêne, 2006). In this work we show that the most useful parameter for testing inhibitors is the experimental yield of binding/unbinding events. Our objective was to determine a binary process: “binding” or “no-binding” event. We demonstrate that the greatest reduction in amyloid dimerization occurs when a small concentration (20 nM) of

SG1 inhibitor is present in the solution, followed by further reductions (though not to the same magnitude with increasing inhibitor concentrations (figure 19b). In correlation with experiments, the MD data demonstrate that SG1 binds to Aβ (13-23) fragment, a self-recognition part of Aβ (1-42), a slightly less strongly than Aβ binds to itself, but significantly stronger than SG1 binds to itself. The N-methylation pattern of SG1 ensures that when it binds at the self-recognition site of Aβ, it prevents the amino acid domains (16-22) and (29-35) from binding with one another- the initiating event of the aggregation cascade. An ideal inhibitor will result in no Aβ dimerization (no binding), but there is a limit to the inhibitor concentration able to bind to a very sparse coverage of surface bound peptides. The reason there are still amyloid-amyloid binding events in the inhibitor environment is because the inhibitor has not bound all available Aβ peptide. As the inhibitor concentration increases, the probability of an inhibitor molecule coming into contact with a surface or tip bound Aβ peptide increases. The difference between 40 nM and 200 nM concentrations of inhibitor is only 1% experimental yield making the inhibitor concentration dependence appear asymptotic. The AFM images in figure 20 show that some aggregation is still observed even with inhibitors present. Furthermore, we noticed that higher inhibitor concentrations resulted in an increase of unbinding force. From MD simulations we conclude that SG1 induces a conformational change in Aβ, converting the self-recognition region into a beta strand. This conformational change costs energy, making the calculated binding affinity less than the actual interaction between two beta strands. Once the energy cost has been paid, further interaction may appear to be stronger. This may cause the increase of the unbinding forces that we observe experimentally with the increase of concentration of SG1.

The analysis of AFM images indicates that the structure of the oligomers that were different when SG1 was present. Without the inhibitor, Aβ forms characteristic oligomers of

beta-sheet structure which grow in length to form long fibrils. When the inhibitor was present, characteristic Aβ-Aβ arrangement was disturbed, which resulted in the observation of different heights of oligomers and less fibril growth (figures 20 and 21). Extensive evidence suggests that the dimerization and further nucleation of an amyloid oligomer is the rate limiting step in the fibrillization process (Stefani, 2012). Our AFM data indicate that SG1 may not slow the nucleation of Aβ but rather inhibit the polymerization of oligomers into amyloid fibrils with beta-sheet structure. Thus, all three factors, the change in the unbinding force, the reduction of experimental yield of binding, and the decrease of fibril formation indicate that the SG1 inhibitor successfully suppresses the typical pathway of Aβ-Aβ interaction, which results in characteristic (Aβ-Aβ) unbinding forces and formation of fibrils and oligomers with β-sheet structure.

Alzheimer's disease does not usually occur as a result of excessive production of Aβ, but rather the ability of neurons to clear the peptide prior to aggregation is impaired (Mawuenyega, et al., 2010). Our data demonstrates that the addition of SG1 to a solution of Aβ slows the aggregation of Aβ possibly allowing the body's natural clearance mechanisms to "catch up". The slowing of aggregation may be sufficient for the physiological clearance of amyloid aggregates before they become pathological.

Previous methods used to test the effectiveness of amyloid inhibitors required several hours of preparation, followed by running an SDS-PAGE gel (Lee, et al., 2012), or incubation (in the case of AFM imaging) (Gestwicki, Crabtree, & Graef, 2004). In the case of single molecule AFS, a set of chemically modified cantilevers and substrates can be prepared in advance, and once the cantilever is loaded into the AFM two sets of experiments (control and inhibitor test) can be conducted within about 30 minutes. In this work we have shown a good correlation between experimental data obtained with force measurements (AFS), AFM imaging and

molecular dynamics simulations, which demonstrated that the SG1 synthetic inhibitor disrupts the typical Aβ-Aβ nucleation pathway.

4.5. Conclusions

We conclude that synthetic inhibitor SG1 successfully disrupts the typical Aβ aggregation pathway by inhibiting binding of individual Aβ peptide molecules. Single molecule atomic force spectroscopy can be used to test compounds which act as specific competitive inhibitors for amyloid fibril formation. Notably, we were able to test the efficacy of SG1 inhibitor in only 30 minutes. This approach can potentially be used by the pharmaceutical industry as a high throughput screening technique to rapidly test various inhibitors for amyloid aggregation as well as a wide variety of other drug candidates which block the interaction of two molecules.

Chapter 5
Comparison of three competing dynamic force spectroscopy models to study binding forces of amyloid-β (1-42)

This chapter has been adapted from a manuscript which has been submitted to the journal Soft Matter *for publication.*

A number of different models have been proposed to explain the increase in rupture force as a function of loading rate including the Bell-Evans model, Dudko-Hummer-Szabo, and the Friddle- De Yoreo. In this work I compare these three models by applying them to extract the free energy parameters of Aβ42 dimerization. I show that correcting the loading rate for the effect of the PEG linker is imperative to obtaining accurate kinetic rate information.

Author Contributions:

- Designed Experiments: Zoya Leonenko, Francis Hane
- Performed Experiments: Francis Hane
- Analyzed Data: Francis Hane, Simon Attwood
- Wrote the Manuscript: Francis Hane, Simon Attwood, Zoya Leonenko

5.1. Introduction

Single molecule force spectroscopy (SMFS) is a nanoscale biophysical technique used to probe the unbinding of individual molecules or the unfolding of a polymer such as a protein (Florin, Moy, & Gaub, 1994) or nucleic acids (Liphardt, Dumont, Smith, Tinoco, & Bustamante, 2002). A number of competing analytical models have been developed to extract the parameters such as the dissociation rate at zero force (also called the off rate), k_0, and the thermodynamic parameters, x_β and ΔG, which are the width and height of the energy barrier, respectively (Bizzarri & Cannistraro, 2010). These parameters are fundamental to the understanding of the kinetics and thermodynamics of the interaction of a pair of molecules and allow the comparison of kinetics between different systems and factors which may affect the affinity of two molecules. k_0 is a rate constant which is the inverse of the bond lifetime, τ_0, and measures the rate at which two molecules dissociate at zero force. The kinetic association rate (also referred to as the on rate), k_{on}, is the rate at which two molecules associate. By relating these two rates, the dissociation constant k_D, can be defined as $k_D=k_{off}/k_{on}$ (Bizzarri & Cannistraro, 2010).

In this work we use atomic force spectroscopy to extract unbinding force data for amyloid-β (1-42). We present a comparative analysis of the three models described (Bell-Evans, Dudko-Hummer-Szabo, Friddle-De Yoreo) in a variety of iterations to our AFS data to extract kinetic and thermodynamic data about the rupture of the amyloid-β dimer in an attempt to provide some standardization to the analysis of force spectroscopy experiments.

5.2. Experimental Procedures

We used the protocol as described previously (Hane, Tran, Attwood, & Leonenko, 2013). For a single experiment approximately 1000 force curves were recorded, out of which approximately 5-10% of these showed specific unbinding events. 5 data sets were collected each

using a different cantilever chip. 3 data sets were collected with the same cantilever and 2 others were collected with a softer cantilever.

5.2.1. Force Curve Analysis

JPK data analysis software was used to analyze force curves. Software functions were used to smooth the force curves, level the x-axis, set both axis to 0 and obtaining the tip sample separation, z, to correct for cantilever deflection. A worm-like-chain (WLC) fit was obtained for each force curve and rupture forces were obtained. Data was truncated using Poisson statistics to eliminate force curves that were likely the result of simultaneous multiple unbind events as described in (Karacsony & Akhrimitchev, 2011). These rupture forces were plotted as histograms at the different collected loading rates and fitted with a Gaussian distribution to determine the most probable rupture force. Errors quoted for the most probable rupture force are evaluated as the standard deviation of each distribution, divided by the square root of the effective number of counts for each distribution (estimate of standard error).

Kinetic and thermodynamic parameters k_0, ΔG and x_β were extracted using a number of different dynamic force spectroscopy models.

5.2.2. Extraction of Kinetic Data – Bell-Evans Model

Kinetic parameters for the uncorrected Bell-Evans model were calculated by plotting the most probable rupture force (obtained from histograms) against the natural logarithm of the loading rate calculated by multiplying the cantilever spring constant k_c, by the retraction velocity, v. A straight line was fit to the data using a least squares regression model using Origin v. 9.0 software. The software returned values of R^2 and χ^2 for linear and non-linear fits, respectively, to indicate the quality of the fit to the experimental data. The calculated slope and the y-intercept of this line were used to extract k_0, ΔG and x_β using the Bell-Evans. In another

iteration of the application of this model, we corrected the loading rate for the effect of the PEG linkers by applying equation 5 as described in (Dudko, Hummer, & Szabo, 2008) to calculate the corrected loading rate and reapplied the above described procedure to obtain k_0, ΔG and x_β. In the third iteration, we aggregated the results of all our force curves and equally divided the data into 8 bins according to their corrected loading rates. The most probable rupture force and mean corrected loading rate were calculated for each bin and plotted (fig 23C&D). Once again, we applied the Bell-Evans model to determine k_0, ΔG and x_β. In the last iteration of the application of this model (referred to as aggregate data), the results of all force curves were plotted (about 500 force data points) and the Bell-Evans model applied to the all force plot data points.

5.2.3. Extraction of Kinetic Data – Dudko-Hummer-Szabo Model

All force curves were collected and binned into 8 bins according to their corrected loading rate as described above. We plotted the natural logarithm of the corrected loading rate of each bin vs. the rupture force of each bin, to obtain the bond lifetime versus rupture force relationship as show in figure 23B. The Dudko-Hummer-Szabo model was fit to the data using a Levenberg-Marquardt fitting algorithm using the software's user defined non-linear fitting function. The bond lifetime, τ_0, ΔG and x_β, were returned by the software. k_0 was determined by the inverse relationship $k_0=1/\tau_0$.

5.2.4. Extraction of Kinetic Data – Friddle-DeYoreo Model

Rupture force, F(r) versus corrected loading rate, r, data points were binned and plotted as described above (fig 23C&D). We fit the Friddle-De Yoreo reversible binding equation to these data points and extracted parameters equilibrium force, f_{eq}, thermal scaling factor, f_β, and dissociation rate, $k_{off}(f_{eq})$ at the equilibrium force. These parameters were then used to calculate parameters ΔG, x_β, and k_0 using the equations used in (Friddle, Noy, & De Yoreo, 2012). In the

last iteration of the application of this model, we plotted all force curve data points (approximately 500 data points) and fit the Friddle-De Yoreo model to the entirety of our data to obtain the parameters from the fitting of the Friddle-De Yoreo equation to this data set.

5.3. Results

Force curves were collected at a variety of retraction velocities and plotted as histograms with respect to the average loading rate, $r(F) = v\, k_c$, here k_c is the cantilever spring constant and v the retraction velocity (figure 22). The most probable rupture force as a function of loading rate is consistent with our previous reports (Hane, Tran, Attwood, & Leonenko, 2013). We noted that the distribution of our unbinding forces contained within our histograms broaden with increasing loading rate which is consistent with theoretical models and experimental models (Dudko, Hummer, & Szabo, 2008).

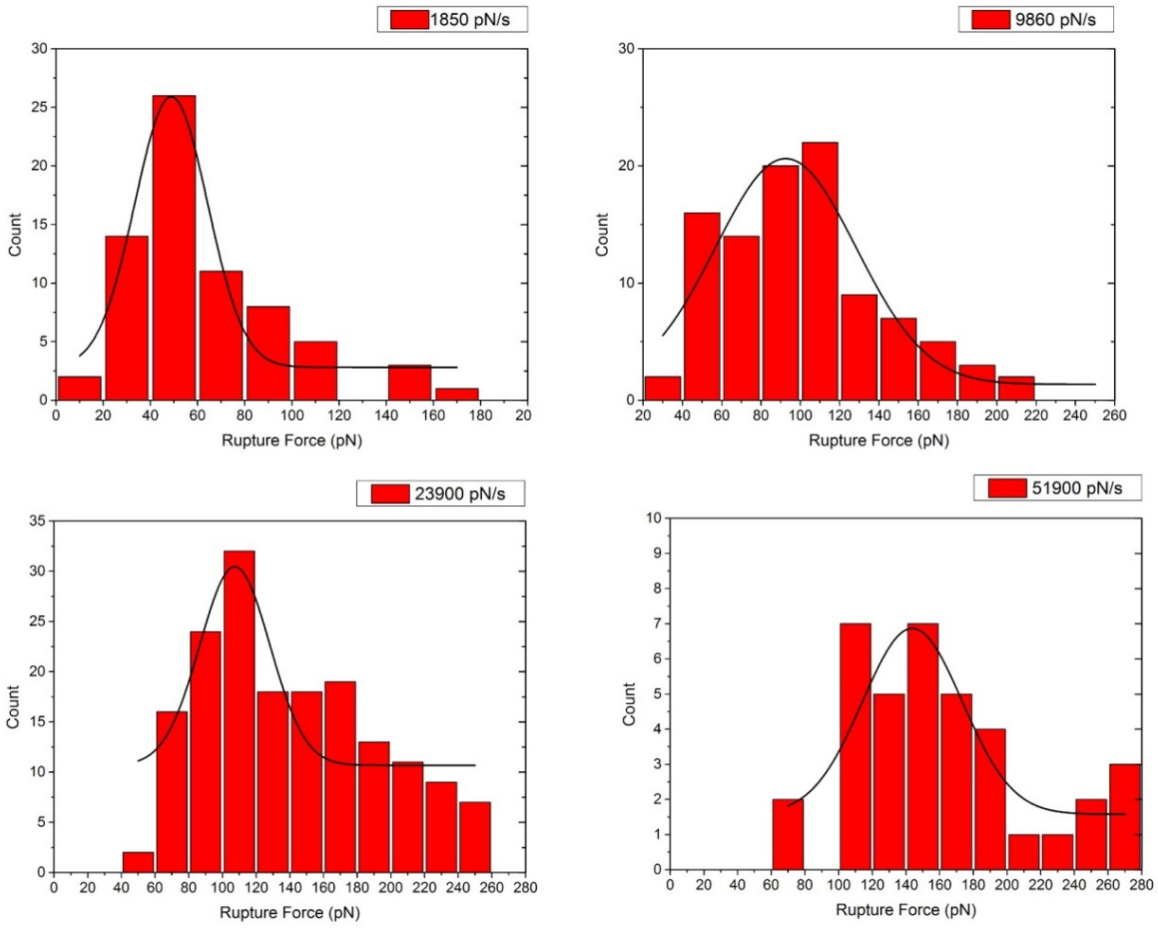

Figure 22- Rupture force histograms and Gaussian fit at corrected loading rates of 1950 pN/s, 9860 pN/s, 23900 pN/s and 51900 pN/s.

5.3.1. Bell-Evans Model

We plotted the most probable rupture forces against the uncorrected loading rate (retraction velocity (nm/s) multiplied by cantilever spring constant (nN/m) (figure 23A). A least-squares linear fit was calculated to best approximate a straight line through the data points (figure 23A). This line through the data when placed on a natural logarithm scale is consistent with what is predicted by Evans (Evans E. , 2001). Parameters of the line were calculated by the graphing software and calculated as a slope of 2.84×10^{-11} and an intercept of 5.34×10^{-10}. We

applied the Bell-Evans model to these line parameters to calculate the following parameters: x_β=143 pm, k_0=240.3 s^{-1}, and ΔG=24.0 k_BT (figure 23A).

5.3.2. Dudko-Hummer-Szabo Model

Using the equation 6, we calculated the bond lifetime, $\tau(F)$ for each bin with mean force, F. We calculated the natural logarithm of $\tau(F)$ and plotted this against the rupture force, F, as shown in figure 23B. We applied the Dudko-Hummer-Szabo model (equation 4) and fit this equation to our data (Dudko, Hummer, & Szabo, 2008). Applying the Dudko-Hummer-Szabo cusp model to our data of the rupture of two Aβ42 peptides, we extracted parameters of x_β=205 pm, k_0=0.68 s^{-1}, and ΔG=7.7 k_BT.

5.3.3. Friddle-De Yoreo Model

To obtain kinetic parameters using the Friddle-De Yoreo model (Friddle, Noy, & De Yoreo, 2012), we plotted the mean unbinding force $\langle F(r) \rangle$ as a function of the loading rate for each set of loading rates as shown in figures 23C&D. The Friddle-De Yoreo reversible binding equation was fit to the data and parameters k_{off}, f_{eq} and f_β were calculated (figure 23C&D). The equilibrium force, f_{eq}, was calculated to be 38.4 pN. Thermodynamic parameters x_β and ΔG were obtained by rearranging equations 7-9. Using the Friddle-De Yoreo model, we obtained values of k_0 = 11.1 s^{-1}, x_β = 104 pm and ΔG = 7.5 k_BT.

A summary of kinetic parameters extracted using different models is given in table 1.

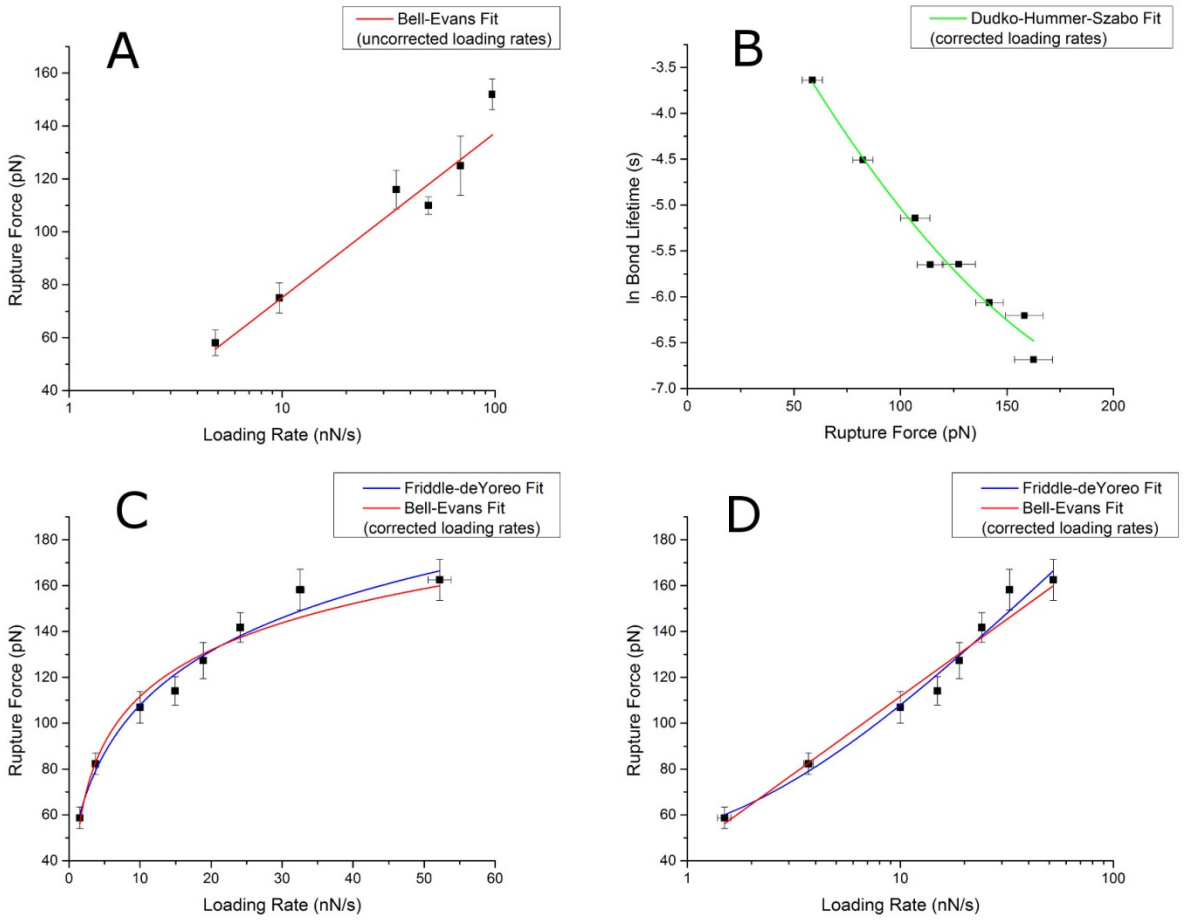

Figure 23- A - Rupture force vs. loading rate using the Bell-Evans model. Most probable rupture forces are plotted against the uncorrected loading rate. Each data point corresponds to the mean rupture force for an experiment conducted at a given retraction velocity. Retraction velocity is converted to loading rate by multiplying by the cantilever spring constant. A straight line Bell-Evans model is fit to the data and the y-intercept and slope is calculated. The adjusted R^2 value was calculated as $R^2 = 0.911$. B - Bond lifetime vs. rupture force fit with the Dudko-Hummer-Szabo model (green) applied to all force curves binned into 8 bins in accordance with corrected loading rate. $\chi 2 = 0.031$. C & D - Aβ unbinding experimental data fitted with the Friddle-De Yoreo reversible binding model (blue) and the Bell-Evans model (red). Data and analysis are identical, but C is on a linear scale and D is on a log10 scale. All data points are binned linker-corrected loading rates. The data used in this graph are identical to that shown in figure 23A, however all force curves were sorted in order of corrected loading rate and binned into 1 of 8 bins according to the corrected loading rate. $R^2 = 0.973$ for the Bell-Evans (red) model and $R^2 = 0.979$ for the Friddle-De Yoreo (blue) model.

DFS Model	x_β (pm)	ΔG (k_BT)	k_0 (s^{-1})	τ_0 (s)
Bell-Evans (uncorrected for PEG linkers)	143±16.9	24.0±3.6	240.3±36.5	0.00416±0.0006
Bell-Evans (loading rates corrected for PEG linker)	143±16.4	27.3±4.1	8.44±1.2	0.112±0.02
Bell-Evans (binned - loading rates corrected)	138±9.7	27.5±2.5	7.14±0.6	0.14±0.01
Bell-Evans (aggregate data)	136±9.4	27.4±2.5	7.55±0.7	0.132±0.01
Dudko-Hummer-Szabo (cusp model)	205±51.7	7.7±0.2	0.68±0.4	1.47±0.9
Friddle-De Yoreo (binned data)	104.2±19.3	7.50±2.7	11.1±7.4	0.090±0.06
Friddle-De Yoreo (aggregate data)	98.9±19.6	7.83±3.0	12.5±8.5	0.080±0.05

Table 2- Comparison of kinetic and thermodynamic parameters using different force spectroscopy models. Different iterations of each model are described in the experimental procedures section.

5.4. Discussion

Comparing the results of these different models and their various iterations, a few important observations stand out. Firstly, a large variation in the dissociation rates between those models which do not correct for the effect of the PEG linker and those that do shows that correcting the loading rate for the effect of the PEG linker is very important for determining accurate dissociation rates although it is minimally important for determining thermodynamic parameters. Secondly, the Friddle-De Yoreo and Dudko-Hummer-Szabo model show similar energy barrier heights, ΔG. Lastly, the width of the energy barrier, x_β, is similar for all models.

It appears that no two models provide near sufficiently similar results to definitively rule out the third model. So which model provides the most rigorous results? Clearly any model that does not account for the effect of the linker molecule is bound to calculate dissociation rates

which are erroneous by several orders of magnitude. We also believe that a model which relies on fewer assumptions is superior to a model which relies on the assumption of the absence of rebinding during pulling.

Given the variance between SMFS experiments conducted under identical conditions, we suggest that the scientific value of SMFS is not to obtain absolute kinetic and thermodynamic parameters of a given system, but rather serves as a tool to compare two or more different experiments or how a variable affects these parameters.

Early force spectroscopy experiments were conducted on the avidin-biotin system, a system known to have complex (ie more than one) binding conformation (Merkel, Nassoy, Leung, Ritchie, & Evans, 1999) (Livnah, Bayer, Wilchek, & Sussman, 1993). When force spectra were collected for this system, multiple lines of best fit were found which were plausibly interpreted as multiple energy barriers with each barrier corresponding to a different method of unbinding. However this interpretation remained popular even though some systems are much simpler than the avidin-biotin complex such as peptides on steel (Landouksi & Dupres, 2011). It is highly unlikely that these systems contain the complex kinetics of the avidin-biotin receptor-ligand pair. Much of this force spectroscopy data have been interpreted as a complex energy landscape containing multiple barriers even when the system involves very simple binding such as peptide to steel (Landouksi & Dupres, 2011) or when the energy barrier is shown to be sub-angstrom by multiple orders of magnitude (Berquand, et al., 2005). Friddle and colleagues provided an alternate interpretation to account for the exponential shape of the rupture force plot which does not require multiple fits to straight lines as the Bell-Evans model does.

While we do not claim that the Bell-Evans model lacks accuracy or rigour for a simple system, we share the concerns noted by Friddle and believe that many reports have “over-

interpreted" the Bell-Evans model and calculated multiple energy barriers where none can plausibly exist, such as at sub-Angsrom length scales.

In summary, we report that three models we used (corrected for the linker effect) give comparable results for x_β and $k_{0,}$ while ΔG parameter correlates well between Dudko-Hummer-Szabo and Friddle-De Yoreo models but differs for the Bell-Evans model. Despite some variation in results due to applying different models, SMFS experiments are very useful to measure the binding forces, as well as to extract kinetic and thermodynamic parameters of the system. These studies are especially useful to evaluate the effect of various factors on binding events. Although a careful consideration of the analytical model applied to fit experimental data should be made to make a correct comparison. We share the opinion of De Yoreo in that multiple slopes in the force-loading rate plots are likely the result of rebinding events and not a multiple energy barrier, especially in simple systems, such as the one we have studied.

5.5. Conclusions

Our data demonstrate that correcting the loading rate for the effect of the linker molecule is imperative for accurately determining dissociation rates. Furthermore, our data show that SMFS experiments are best suited in comparing two different experiments as opposed to obtaining absolutely values. Following the comparison of these DFS models, we share the concerns raised by De Yoreo and colleagues that multi-sloped plots are the result of rebinding events as opposed to multiple energy barriers in most simple systems.

5.6. Supplementary Information

5.6.1. Bell-Evans Calculations

The Bell-Evans equation (Evans E. , 2001) is expanded to obtain a similar form to the straight line equation y=mx+c,

$$F(r) = \left(\frac{k_B T}{x_\beta}\right) \ln r + \left(\frac{k_B T}{x_\beta}\right) \ln \frac{x_\beta}{k_{off}\, k_B T}$$

Therefore when F(r) is plotted against ln r, the slope of the best fit line equals $\left(\frac{k_B T}{x_\beta}\right)$ and the y-intercept equals

$$\left(\frac{k_B T}{x_\beta}\right) \ln \frac{x_\beta}{k_{off}\, k_B T}.$$

All values are converted to standard units, N and N/s. The location of the energy barrier, x_β is determined by the equation,

$$x_\beta = \frac{k_B T}{m}$$

Where m is the slope of the line. k_{off} was determined by rearranging the equation.

$$k_{off} = \frac{x_\beta}{k_B T\, e^{c x_{\beta / k_B T}}}$$

Where c is the y-intercept.

Once k_{off} is determined, we applied the following equation to determine the height of the energy barrier, ΔG (Evans, Halvorsen, Kinoshito, & Wong, 2009).

$$k_{off}\,(F) = \left(\frac{k_B T}{h}\right) e^{-\frac{\Delta G - x_\beta F}{k_B T}}$$

Rearranged, ΔG can be determined as

$$-\Delta G = k_B T \ln \frac{k_0 h}{k_B T}$$

Where h is Plank's constant. For our purposes, we used k_BT as units for ΔG.

5.6.2. Error Analysis

For the Bell-Evans model, errors were determined by the square root of the sum of the squares of the standard error (Taylor, 1997). For example, the standard error of x_β was calculated as follows:

Since x_β is a function of the slope, m,

$$x_\beta = \frac{k_B T}{m}$$

With m being the slope of the line using a least squares fit of the data points, the standard error of x_β is given by the equation,

$$\frac{\delta x_\beta}{x_\beta} = \sqrt{\left(\frac{\delta m}{m}\right)^2 + \left(\frac{\delta T}{T}\right)^2}$$

The standard error of the slope, m, was calculated using the graphing software. The standard error of the temperature was negligible, but still used and estimated as 1 K.

The standard error for all parameters using the Dudko-Hummer-Szabo model (Dudko, Hummer, & Szabo, 2008) were calculated using Origin v 9.0.

Hutter's thermal noise method (Hutter & Bechhoefer, 1993) of cantilever spring constant calculation typically results in a standard error of 10-20% (JPK Instruments AG, 2009). To calculate the standard errors for the Friddle-De Yoreo model (Friddle, Noy, & De Yoreo, 2012), a 15% error was estimated for the cantilever spring constant. Since ΔG is a function of the cantilever spring constant and f_{eq}, the standard error in ΔG was estimated as

$$\delta \Delta G = \Delta G \sqrt{\left(\frac{\delta f_{eq}}{f_{eq}}\right)^2 + 0.15^2}$$

The remainder of standard errors were calculated in a manner similar to the Bell-Evans model.

Chapter 6
Conclusion

6.1. Overview of Results

In this work, I used a combination of atomic force microscopy and atomic force spectroscopy to study the single-molecule interactions of two amyloid-β peptides, the very initial step in the aggregation of amyloid-β leading to amyloid oligomers, fibrils, and eventually, symptomatic Alzheimer's disease. I demonstrated that copper increases the unbinding force of amyloid-β and makes it more difficult for the brain to naturally clear amyloid oligomers. This phenomenon is attributed to the different conformation an amyloid-β takes when copper is involved in the system creating and mediating a stronger bond between the two amyloid-β peptides resulting in the observation that the presence of copper increases the unbinding force between the two peptides.

For the first time, I used AFS to test the use of an inhibitor on a peptide binding complex. I tested the use of an amyloid aggregation inhibitor named SG1 as a potential candidate for preventing the aggregation of amyloid oligomers. By showing that the experimental yield of atomic force spectroscopy (AFS) experiments drops drastically with SG1 as part of the system, SG1 prevents amyloid-β peptides from self-dimerizing and forming dimers, the initial step is Alzheimer's pathogenesis. This method of testing potential pharmaceutical compounds can be used as a high throughput screening device for testing inhibitors and promoters of any receptor-ligand system.

Lastly, I compared the free energy parameters of amyloid-β dimerization using a variety of different models: the Bell-Evans, Dudko-Hummer-Szabo, and Friddle-deYoreo. The field of single molecule force spectroscopy has suffered from a lack of standardization and an "over-

interpretation" of many data resulting in absurd conclusions. My data showed that a model which excludes the effect of the linker molecules produces results which are erroneous by several orders of magnitude. Furthermore, our data supported the observations made by Friddle in that at lower loading rates, the force-loading rate plot is considerably shallower than at higher loading rates and connected by a curved region. Our data leads us to conclude that the Friddle-De Yoreo model provides a superior interpretation to that commonly provided by groups using the Bell-Evans model. Lastly, I propose that rather than using these DFS models to determine absolute quantitative values, these models are best used to determine a difference in kinetic parameters when an experimental variable, such as the presence of metal ions, is altered.

6.2. Future Research

Often, good research yields more questions than answers. The results of these experiments are no different. This project was the first involving single-molecule force spectroscopy in the Leonenko lab. Thankfully, a considerable portion of the experiments conducted were successful and yielded statistically valid results. This project has further possibilities - a considerable number of additional experiments can be conducted relating to the results of this thesis. I proposed additional experiments:

1) What is the effect on the kinetic and thermodynamic parameters when an amyloid fibril promoter or inhibitor is added to the system? Molecules such as Methylene Blue have been demonstrated to inhibit amyloid aggregation. I hypothesize that since the dimer conformation is different between OC+ and A11+ oligomers, there would be a difference in the free energy landscape.

2)What is the effect of metal ions, Cu, Zn, and Fe on the affinity of two amyloid-β peptides? Since Cu increases the unbinding force between two peptides, I hypothesize that the binding affinity of these two peptides also increases.

3) Are there binding sites within a neuron that have a higher affinity for amyloid-β? By growing neuron cells *in vitro* and placing these cells on the combined AFM/fluorescence stage and a peptide on the cantilever tip, force mapping could be conducted to find if there are areas with higher affinity for AB.

4) Are aggregates formed in an SG1 environment OC+ or A11+? Are they neurotoxic? We could further characterize the aggregates formed with SG1 and determine their neurotoxic properties.

Given the expertise gained in the lab of Prof. Leonenko in the field of SMFS, these questions could very well be answered in a continuation of this research program by another PhD student. I encourage my supervisor to continue this research program.

Letters of Copyright Permissions

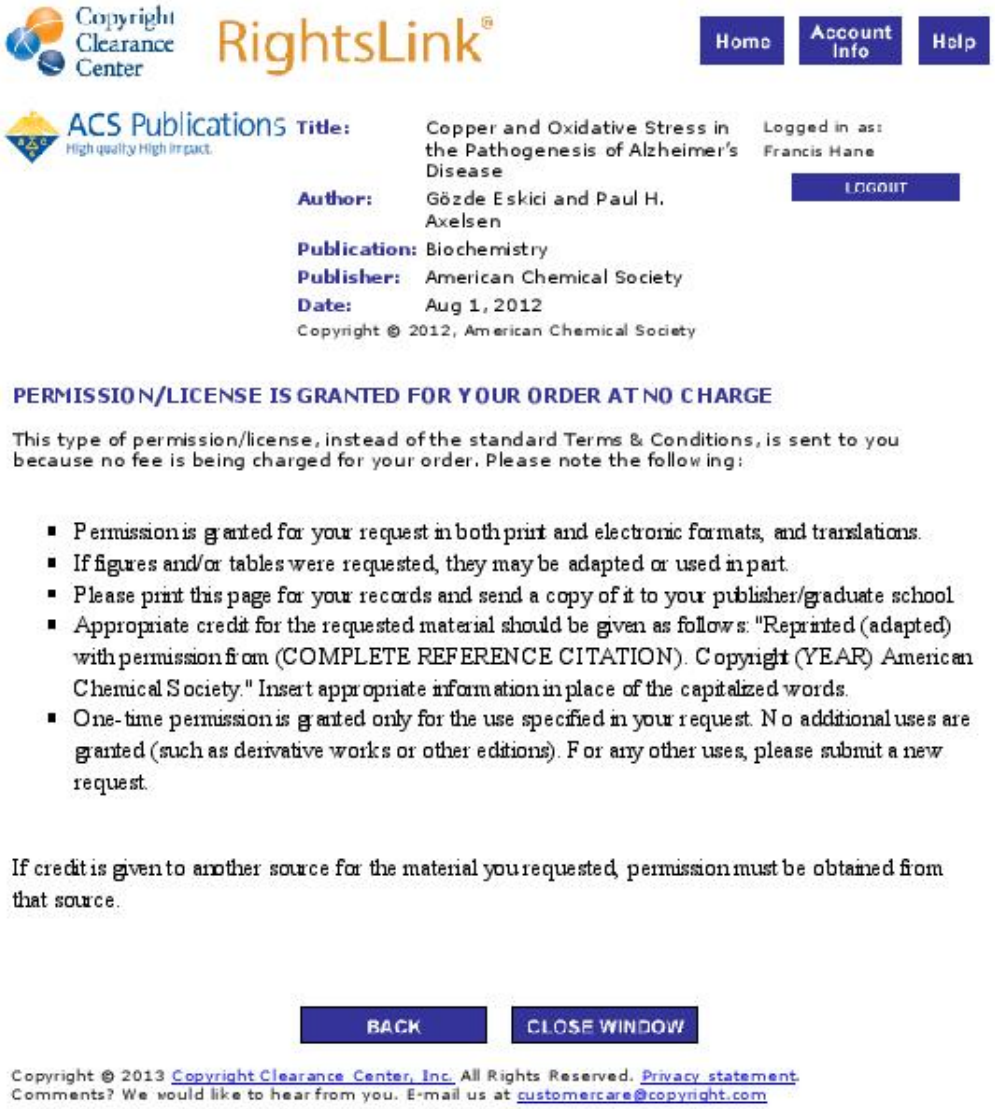

Copyright Clearance Center RightsLink®

Home | Account Info | Help

ACS Publications High quality High impact

Title: Copper and Oxidative Stress in the Pathogenesis of Alzheimer's Disease

Author: Gözde Eskici and Paul H. Axelsen

Publication: Biochemistry

Publisher: American Chemical Society

Date: Aug 1, 2012

Copyright © 2012, American Chemical Society

Logged in as: Francis Hane

LOGOUT

PERMISSION/LICENSE IS GRANTED FOR YOUR ORDER AT NO CHARGE

This type of permission/license, instead of the standard Terms & Conditions, is sent to you because no fee is being charged for your order. Please note the following:

- Permission is granted for your request in both print and electronic formats, and translations.
- If figures and/or tables were requested, they may be adapted or used in part.
- Please print this page for your records and send a copy of it to your publisher/graduate school.
- Appropriate credit for the requested material should be given as follows: "Reprinted (adapted) with permission from (COMPLETE REFERENCE CITATION). Copyright (YEAR) American Chemical Society." Insert appropriate information in place of the capitalized words.
- One-time permission is granted only for the use specified in your request. No additional uses are granted (such as derivative works or other editions). For any other uses, please submit a new request.

If credit is given to another source for the material you requested, permission must be obtained from that source.

BACK | CLOSE WINDOW

Copyright © 2013 Copyright Clearance Center, Inc. All Rights Reserved. Privacy statement.
Comments? We would like to hear from you. E-mail us at customercare@copyright.com

Open-Access License

No Permission Required

PLOS applies the Creative Commons Attribution License (CCAL) to all works we publish (read the human-readable summary or the full license legal code). Under the CCAL, authors retain ownership of the copyright for their article, but authors allow anyone to download, reuse, reprint, modify, distribute, and/or copy articles in PLOS journals, so long as the original authors and source are cited. No permission is required from the authors or the publishers.

In most cases, appropriate attribution can be provided by simply citing the original article (e.g., Kaltenbach LS et al. (2007) Huntingtin Interacting Proteins Are Genetic Modifiers of Neurodegeneration. *PLOS Genet* 3(6): e82. doi:10.1371/journal.pgen.0030082). If the item you plan to reuse is not part of a published article (e.g., a featured issue image), then please indicate the originator of the work, and the volume, issue, and date of the journal in which the item appeared. For any reuse or redistribution of a work, you must also make clear the license terms under which the work was published.

This broad license was developed to facilitate open access to, and free use of, original works of all types. Applying this standard license to your own work will ensure your right to make your work freely and openly available. Learn more about open access. For queries about the license, please contact us.

Copyright Permission Policy

These guidelines apply to the reuse of articles, figures, charts and photos in the Journal of Biological Chemistry, Molecular & Cellular Proteomics and the Journal of Lipid Research.

For authors reusing their own material:

Authors need NOT contact the journal to obtain rights to reuse their own material. They are automatically granted permission to do the following:

- Reuse the article in print collections of their own writing.
- Present a work orally in its entirety.
- Use an article in a thesis and/or dissertation.
- Reproduce an article for use in the author/s courses. (If the author is employed by an academic institution, that institution also may reproduce the article for teaching purposes.)
- Reuse a figure, photo and/or table in future commercial and noncommercial works.
- Post a copy of the paper in PDF that you submitted via BenchPress.
- Link to the journal site containing the final edited PDFs created by the publisher.

EXCEPTION: If authors select the Author's Choice publishing option:

- The final version of the manuscript will be covered under the Creative Commons Attribution license (CC BY), the most accommodating of licenses offered. Click here for details.
- The final version of the manuscript will be released immediately on the publisher's website and PubMed Central.

Please note that authors must include the following citation when using material that appeared in an ASBMB journal:

"This research was originally published in Journal Name. Author(s). Title. Journal Name. Year; Vol:pp-pp. © the American Society for Biochemistry and Molecular Biology."

For other parties using material for noncommercial use:

Other parties are welcome to copy, distribute, transmit and adapt the work — at no cost and without permission — for noncommercial use as long as they attribute the work to the original source using the citation above.

Examples of noncommercial use include:

- Reproducing a figure for educational purposes, such as school work or lecture presentations, with attribution.
- Appending a reprinted article to a Ph.D. dissertation, with attribution.

For other parties using material for commercial use:

Navigate to the article of interest and click the "Request Permissions" button on the middle navigation bar. (See diagram at right.) It will walk you through the steps for obtaining permission for reuse.

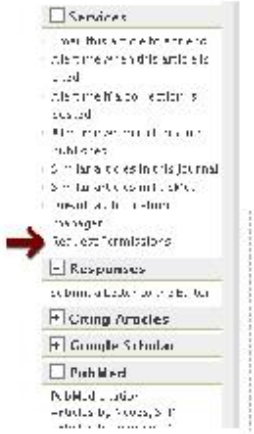

Examples of commercial use by parties other than authors include:

- Reproducing a figure in a book published by a commercial publisher.
- Reproducing a figure in a journal article published by a commercial publisher.

Updated March 20, 2013

NATURE PUBLISHING GROUP LICENSE TERMS AND CONDITIONS

Jun 28, 2013

This is a License Agreement between Francis Hane ("You") and Nature Publishing Group ("Nature Publishing Group") provided by Copyright Clearance Center ("CCC"). The license consists of your order details, the terms and conditions provided by Nature Publishing Group, and the payment terms and conditions.

All payments must be made in full to CCC. For payment instructions, please see information listed at the bottom of this form.

License Number	3177711406915
License date	Jun 28, 2013
Licensed content publisher	Nature Publishing Group
Licensed content publication	Nature Chemistry
Licensed content title	Amyloid-β protein oligomerization and the importance of tetramers and dodecamers in the aetiology of Alzheimer's disease
Licensed content author	Summer L. Bernstein, Nicholas F. Dupuis, Noel D. Lazo, Thomas Wyttenbach, Margaret M. Condron et al.
Licensed content date	Jun 14, 2009
Volume number	1
Issue number	4
Type of Use	reuse in a thesis/dissertation
Requestor type	academic/educational
Format	print and electronic
Portion	figures/tables/illustrations
Number of figures/tables/illustrations	1
High-res required	no
Figures	Figure 5 - Mechanism of oligomerization and eventual fibril formation for Ab42 and for Ab40
Author of this NPG article	no
Your reference number	
Title of your thesis / dissertation	Single Molecule Force Investigations of Amyloid-β Aggregation
Expected completion date	Sep 2013
Estimated size (number of pages)	200
Total	0.00 USD
Terms and Conditions	

Terms and Conditions for Permissions

Nature Publishing Group hereby grants you a non-exclusive license to reproduce this material for this purpose, and for no other use, subject to the conditions below:

1. NPG warrants that it has, to the best of its knowledge, the rights to license reuse of this material. However, you should ensure that the material you are requesting is original to Nature Publishing Group and does not carry the copyright of another entity (as credited in the published version). If the credit line on any part of the material you have requested indicates that it was reprinted or adapted by NPG with permission from another source, then you should also seek permission from that source to reuse the material.

2. Permission granted free of charge for material in print is also usually granted for any electronic version of that work, provided that the material is incidental to the work as a whole and that the electronic version is essentially equivalent to, or substitutes for, the print version. Where print permission has been granted for a fee, separate permission must be obtained for any additional, electronic re-use (unless, as in the case of a full paper, this has already been accounted for during your initial request in the calculation of a print run). NB: In all cases, web-based use of full-text articles must be authorized separately through the 'Use on a Web Site' option when requesting permission.

3. Permission granted for a first edition does not apply to second and subsequent editions and for editions in other languages (except for signatories to the STM Permissions Guidelines, or where the first edition permission was granted for free).

4. Nature Publishing Group's permission must be acknowledged next to the figure, table or abstract in print. In electronic form, this acknowledgement must be visible at the same time as the figure/table/abstract, and must be hyperlinked to the journal's homepage.

5. The credit line should read:
   Reprinted by permission from Macmillan Publishers Ltd: [JOURNAL NAME] (reference citation), copyright (year of publication)
   For AOP papers, the credit line should read:
   Reprinted by permission from Macmillan Publishers Ltd: [JOURNAL NAME], advance online publication, day month year (doi: 10.1038/sj.[JOURNAL ACRONYM].XXXXX)

   Note: For republication from the *British Journal of Cancer*, the following credit lines apply.
   Reprinted by permission from Macmillan Publishers Ltd on behalf of Cancer Research UK: [JOURNAL NAME] (reference citation), copyright (year of publication)For AOP papers, the credit line should read:
   Reprinted by permission from Macmillan Publishers Ltd on behalf of Cancer Research UK: [JOURNAL NAME], advance online publication, day month year (doi: 10.1038/sj.[JOURNAL ACRONYM].XXXXX)

6. Adaptations of single figures do not require NPG approval. However, the adaptation should be credited as follows:

   Adapted by permission from Macmillan Publishers Ltd: [JOURNAL NAME] (reference

citation), copyright (year of publication)

Note: For adaptation from the *British Journal of Cancer*, the following credit line applies.
Adapted by permission from Macmillan Publishers Ltd on behalf of Cancer Research UK: [JOURNAL NAME] (reference citation), copyright (year of publication)

7. Translations of 401 words up to a whole article require NPG approval. Please visit http://www.macmillanmedicalcommunications.com for more information. Translations of up to a 400 words do not require NPG approval. The translation should be credited as follows:

   Translated by permission from Macmillan Publishers Ltd: [JOURNAL NAME] (reference citation), copyright (year of publication).

   Note: For translation from the *British Journal of Cancer*, the following credit line applies.
   Translated by permission from Macmillan Publishers Ltd on behalf of Cancer Research UK: [JOURNAL NAME] (reference citation), copyright (year of publication)

We are certain that all parties will benefit from this agreement and wish you the best in the use of this material. Thank you.

Special Terms:

v1.1

If you would like to pay for this license now, please remit this license along with your payment made payable to "COPYRIGHT CLEARANCE CENTER" otherwise you will be invoiced within 48 hours of the license date. Payment should be in the form of a check or money order referencing your account number and this invoice number RLNK501054114. Once you receive your invoice for this order, you may pay your invoice by credit card. Please follow instructions provided at that time.

Make Payment To:
Copyright Clearance Center
Dept 001
P.O. Box 843006
Boston, MA 02284-3006

For suggestions or comments regarding this order, contact RightsLink Customer Support: customercare@copyright.com or +1-877-622-5543 (toll free in the US) or +1-978-646-2777.

Gratis licenses (referencing $0 in the Total field) are free. Please retain this printable license for your reference. No payment is required.

References

Abdul, H., & Butterfield, D. (2007). . Involvement of PI3K/PKG/ERK1/2 signaling pathways in cortical neurons to trigger protection by cotreatment of acetyl-l-carnitine and alpha-lipoic acid against HNE-mediated oxidative stress and neurotoxicity: Implications for Alzheimer's disease. *Free Radical Biology Medicine 42*, 371-384.

Ahmed, M. e. (2010). Structural conversion of neurotoxic amyloid-beta (1-42) oligomers to fibrils. *Nature Structural Molecular Biology 17*, 561-567.

Akiyama, H., Barger, S., Barnum, S., Bradt, B., & Bauer, J. (2000). Inflammation and alzheimer's disease. Neurobiol Aging 21: 383-421. . *Neurobiology of Aging 21*, 383-421.

Allison, D., Hinterdorfer, P., & Han, W. (2002). Biomolecular force measurements and the atomic force microscope. *Current Opinion in Biotechnology 13*, 47-51.

Allsop, D., Landon, M., & Kidd, M. (1983). The isolation and amino composition of senile plaque core protein. *Brain Research 259*, 348-352.

Alzheimer, A. (1907). Uber eine eigematige Erkrankung der Hirnrinde. *Allg. Z. Psychiatr.Psychisch-Gericht. Med. 64*, 146-148.

Alzheimer's Association. (2011). 2011 Alzheimer's Disease Facts and Figures. *Alzheimers and Dementia 7*, 1-63.

Andreu, J., & Timasheff, S. (1986). The measurement of cooperative protein self-assembly by turbidity and other techniques. *Methods in Enzymology 130*, 47-59.

Antzutkin, O., Balbach, J., Leapman, R., Rizzo, N., Reed, J., & Tycko, R. (2000). Multiple quantum olid-state NMR indicates a parallel, not antiparallel, organization of beta-sheets in Alzheimer's beta-amyloid fibrils. *Proceedings of the National Academy of Sciences 97*, 13045-13050.

Arispe, N., Pollard, H., & Rojas, E. (1993). Giant multilevel cation channels formed by Alzheimer disease amyloid β-protein [Aβ-(1-40)] in bilayer membrane. *Proceedings of the National Academy of Science USA 90*, 10573-10577.

Atwood, C., Obrenovich, M., Liu, T., Chan, H., Perrya, G., Smith, M., et al. (2012). Amyloid-beta: a chameleon walking in two worlds: a review of the trophic and toxic properties of amyloid-beta. *Brain Research Reviews 43*, 1-16.

Atwood, C., Perry, G., Zeng, H., Kato, Y., Jones, W., Ling, K., et al. (2004). Copper mediates dityrosine cross-linking of Alzheimer's amyloid-beta. *Biochemistry 43*, 560-568.

Atwood, C., Scarpa, R., Huang, Z., Moir, R., Jones, W., Fairlie, D., et al. (2000). Characterization of copper interactions with alzheimer amyloid beta peptides: identification of an attomolar-affinity copper binding site on amyloid beta1-42. *Journal of Neurochemistry 75*, 1219-1233.

Auer, S., Ricchiuto, P., & Kashchiev, D. (2012). Two-Step Nucleation of Amyloid Fibrils: Omnipresent or not? *Journal of Molecular Biology 422*, 723-730.

Azimi, S., & Rauk, A. (2011). On the Involvement of Copper Binding to the N-Terminus of the Amyloid Beta Peptide of Alzheimer's Disease: A Computational Study on Model Systems. *International Journal of Alzheimer's Disease 2011*, 1-15.

Balbach, J., Petkva, A., Oyler, N., Antzutkin, O., Gordon, D., Meredith, S., et al. (2002). Supramolecular Structure in Full-Length Alzheimer's beta-Amyloid Fibrils: Evidence for a Parallel beta-sheet organization from solid-state Nuclear Magentic Resonance. *Biophysical Journal 83*, 1205-1216.

Bard, F., Barbour, R., Cannon, C., Caretto, R., Fox, M., & Games, D. (2003). Epitope and isotype specificities of antibodies to β-amyloid peptide for protection against Alzheimer's disease like neuropathology. *Proceedings of the National Academy of Sciences USA 100*, 2023-2028.

Bard, F., Cannon, C., Barbour, R., Burke, R., Games, D., Grajeda, H., et al. (2000). Peripherally administered antibodies against amyloid β-peptide enter the central nervous system and reduce pathology in a mouse model of Alzheimer disease. *Nature Medicine 6*, 916-919.

Barnham, K., Haeffner, F., & Ciccotosto, G. (2004). Tyrosine gated electron transfer is key to the toxic mechanism of Alzheimer's disease beta-amyloid. *FASEB Journal 18*, 1427-1429.

Barrett, P., Song, Y., Van Horn, W., Hustedt, E., Schafer, J., Hadziselimovic, A., et al. (2012). The Amyloid Precursor Protein Has a Flexible Transmembrane Domain and Binds cholesterol. *Science 336*, 1168-1171.

Barrow, C., & Zagorski, M. (1992). Solution structures of beta peptide and its constituent fragments: relation to amyloid deposition. *Science 253*, 179-182.

Barz, B., & Urbanc, B. (2012). Dimer Formation Enhances Structural Differences between Amyloid b-Protein (1–40) and (1–42): Explicit-Solvent Molecular Dynamics Study. *PLoS ONE 7*, e34345.

Bauer, H., Aebi, U., Hanner, M., Herman, R., Muller, M., Arvinte, T., et al. (1995). Architecture and Polymorphism of Fibrillar Supramolecular Assemblies Produced by in Vitro Aggregation of Human Calcitonin. *Journal Of Stuctural Biology 115*, 1-15.

Behi, C., Davis, J., Lesley, R., & Schubert, D. (1994). Hydrogen peroxide mediates amyloid beta protein toxicity. *Cell 77*, 817-827.

Bell, G. (1978). Models for the Specific Adhesion of Cells to Cells. *Science 200*, 618-627.

Bellesia, G., & Shea, J.-E. (2009). Diversity of kinetic pathways in amyloid fibril formation. *The Journal of Chemical Physics 131*, 111102.

Bellesia, G., & Shea, J.-E. (2009). Effect of beta-sheet propensity on peptide aggregation. *The Journal of Chemical Physics 130*, 145103.

Berendsen, H., van der Spoel, D., & van Drunen, R. (1995). GROMACS: A message-passing parallel molecular dynamics implementation. *Computer Physics Communications 91*, 43-56.

Bernstein, S., Dupuis, N., Lazo, N., Wyteenbach, T., Condron, M., Bitan, G., et al. (2009). Amyloid-b protein oligomerization and the importance of tetramers and dodecamers in the aetiology of Alzheimer's disease. *Nature Chemistry 1*, 326-332.

Berquand, A., Xia, N., Castner, D., Clare, B., Abbott, N. D., Adriaensen, Y., et al. (2005). Antigen binding forces of single antilysozyme Fv fragments explored by atomic force microscopy. *Langmuir 21*, 5517-5523.

Bertram, L., & Tanzi, R. (2005). The genetic epidemiology of neurodegenerative disease. *The Journal of Clinical Investigation 115*, 1449-1458.

Bieschke, J., Herbst, M., Wiglenda, T., Friedrich, R., Boeddrich, A., Schiele, F., et al. (2012). Small molecule conversion of toxic oligomers to non-toxic beta-sheet-rich amyloid fibrils. *Nature Chemical Biology 8*, 93-101.

Bin, Y., Chen, S., & Xiang, J. (2013). pH-dependent kinetics of copper ions binding to amyloid-β peptide. *Journal of Inorganic Biochemistry 119*, 21-27.

Bitan, G., Kirkitadze, M., Lomakin, A., Vollers, S., Benedek, G., & Teplow, D. (2003). Amyloid beta-protein (Abeta) assembly: Abeta40 and Abeta42 through distinct patheays. *Proceedings of the National Academy of Sciences 100*, 330-335.

Bizzarri, A., & Cannistraro, S. (2010). The application of atomic force spectroscopy to the study of biological complexes undergoing a biorecognition process. *Chemical Society Reviews 39*, 734-749.

Bogden, J., Troiano, R., & Joselow, M. (1977). Copper, Zinc, Magnesium, and Calcium in Plasma and Cerebrospinal Fluid of Patients with Neurological Diseases. *Clinical Chemistry 23*, 485-489.

Bonda, D., Lee, H.-G., Blair, J., Zhu, X., Perry, G., & Smith, M. (2011). Role of metal dyshomeostasis in Alzheimer's disease. *Metallomics 3*, 267-270.

Bonda, D., Wang, X., Perry, G., Numomura, A., Tabaton, M., Zhu, X., et al. (2010). Oxidative stress in Alzheimer disease: a possibility for prevention. *Neuropharmicology 59*, 290-294.

Booth, D., Sunde, M., Bellotti, V., Robinson, C., Hutchinson, W., Fraser, P., et al. (1997). Instability, unfolding and aggregation of human lysozyme variants underlying amyloid fibrillogenesis. *Nature 385*, 787-793.

Broersen, K., Rousseau, F., & Schymkowitz, J. (2010). The culprit behind amyloid-beta peptide related neurotoxicity in Alzheimer's disease: oligomer size or conformation? *Alzheimer's Research Therapy 2*, 12.

Brookmeyer, R., Corrada, M., Curriero, F., & Kawas, C. (2002). Survival following a diagnosis of Alzheimer's disease. *Archives of Neurology 59*, 1764-1767.

Bucciantini, M., Giannoni, E., Chiti, F., Baroni, F., Formigli, L., Zurdo, J., et al. (2002). Inherent toxicity of aggregates implies a common mechanism for protein misfolding diseases. *Nature 416*, 507-511.

Buchete, N.-V., Tycko, R., & Hummer, G. (2005). Molecular Dynamics Simulations of Alzheimer's beta-amyloid Protofilaments. *Journal of Molecular Biology 353*, 804-821.

Bush, A., & Tanzi, R. (2008). Therapeutics for Alzheimer's Disease Based on the Metals Hypothesis. *Neurotherapeutics: The Journal of the American Society for Experimental NeuroTherapeutics 5*, 421–432.

Bush, A., Pettingell, W., & Multhaup, G. (1994). Rapid induction of Alzheimer's amyloid-beta formation by zinc. *Science 265*, 1464-1467.

Bustamante, C., Marko, J. S., & Smith, S. (1994). Entropic elasticity of lambda-phage DNA. *Science 265*, 1599-1600.

Butterfield, A. Y., Varadarajan, S., & Koppal, T. (1999). Amyloid β-peptide-associated free radical oxidative stress, neurotoxicity, and Alzheimer's disease . *Methods in Enzymology 309*, 746-768.

Butterfield, S., & Lashuel, H. (2010). Amyloidogenic Protein–Membrane Interactions: Mechanistic Insights from Model Systems. *Angewandte Chemie 49*, 5628 – 5654.

Cadenas, E., & Davies, K. (2000). Mitochondrial free radical generation, oxidative stress, and aging. *Free Radical Biological Medicine 29*, 222-230.

Campioni, S., Mannini, B., Zampagni, M., Pensalfini, A., Parrini, C., Evangelisti, E., et al. (2010). A causative link between the the structure of aberrant protein oligomers and their toxicity. *Nature Chemical Biology 6*, 140-147.

Canadian Study of HeaIth and And Working Group. (1994). Canadian study of heaith and aging: study methods and prevalence of dementia. *Canadian Medical Association Journal 150*, 899-913.

Carrell, R., & Gootu, B. (1998). Conformational changes and disease — serpins, prions and Alzheimer's. *Current Opinions in Structural Biology 8*, 799-809.

Chen, R.-Y., & Glabe, C. (2006). Distinct Early Folding and Aggregation Properties of Alzheimer Amyloid-beta Peptides AB40 and AB42. *The Journal of Biological Chemistry 281*, 24414–24422.

Chen, W., Liuo, Y., Yu, H., Cheng, I., & Cen, Y. (2011). Distinct Effects of Zn2+, Cu2+, Fe3+, and Al3+ on Amyloid-β Stability, Oligomerization, and Aggregation. *The Journal of Biological Chemistry 286*, 9646-9656.

Cheng, Y., Feng, Z., Zhang, Q., & Zhang, J. (2006). Beneficial effects of melatonin in experimental models of Alzheimer disease. *Acta Pharamcology Sin 27*, 129-139.

Chimon, S., Shaibat, M., & Ishii, Y. (2007). Evidence of fibril-like beta-sheet structures in neurotoxic amyloid-intermediate of Alzheimer's beta-amyloid. *Nature Structural Molecular Biology 14*, 1157-1164.

Chiti, F., & Dobson, C. (2006). Protein misfolding, functional amyloid, and human disease. *Annual Review of Biochemistry 75*, 333-366.

Chiti, F., & Dobson, C. (2009). Amyloid formation by globular proteins under native conditions. *Nature Chemical Biology 5*, 15-22.

Choi, B., & Zheng, W. (2009). Copper transport to the brain by the blood-brain barrier and blood-CSF barrier. *Brain Research 1248*, 14-21.

Cirrito, J., May, P., O'Dell, M., Taylor, J., Parsadanian, M., Cramer, K., et al. (2003). In Vivo Assessment of Brain Interstitial Fluid with Microdialysis reveals Plaque-Associated Changes in Amyloid-β Metabolism and Half-Life. *Neuroscience 23*, 8844-8853.

Citron, M. (2004). Strategies for disease modification in Alzheimer's disease. *Nature Reviews Neuroscience 5*, 677-685.

Citron, M. (2010). Alzheimer’s disease: Strategies for disease modification. *Nature Reviews Drug Discovery 9*, 387-398.

Connelly, L., Jang, H., Teran Arce, F., Capone, R., Kotler, S., Ramachandran, S., et al. (2012). Atomic Force Microscopy and MD Simulations Reveal Pore-Like Structures of All-D-Enantiomer of Alzheimer’s β-Amyloid Peptide: Relevance to the Ion Channel Mechanism of AD Pathology. *Journal of Physical Chemistry B 116*, 1728−1735.

Côté, S., Laghaei, R., Derreumaux, P., & Mousseau, N. (2012). Distinct Dimerization for Various Alloforms of the Amyloid-Beta Protein: Aβ1−40, Aβ1−42, and Aβ1−40(D23N). *The Journal of Physical Chemistry B 116*, 4043-4055.

Cotman, C., & Berchtold, N. (2002). Exercise: a behavioural intervention to enhance brain health and plascticity. *Trends in Neuroscience 25*, 295-301.

Cramer, P., Cirrito, J., Wesson, D., Lee, D., Karlo, C., Zinn, A., et al. (2012). ApoE-Directed Therapeutics Rapidly Clear beta-Amyloid and Reverse Deficiets in AD Mouse Models. *Science 335*, 1503-1506.

Crespo, R., Rocha, F., Damas, A., & Martins, P. (2012). A Generic Crystallization-like Model That Describes the Kinetics of Amyloid Fibril Formation. *The Journal of Biological Chemistry 287*, 30585-30594.

Cuajunco, M., Goldstein, L., Numomura, A., Smith, M., Lim, J., Atwood, C., et al. (2000). Evidence that the beta-amyloid plaques of Alzheimer's disease represent the redox silencing and entombment of abeta by zinc. *The Journal of Biological Chemistry 275*, 19439-19442.

Curtain, C., Ali, F., & Volitakis, I. (2001). Alzheimer's disease amyloid binds Cu and Zn to generate an allosterically-ordered membrane penetrating structure containing SOD-like subunits. *The Journal of Biological Chemistry 276*, 20466-20473.

Curtain, C., Ali, F., Smith, D., Bush, A., Masters, C., & Barnham, K. (2003). Metal Ions, pH, and Cholesterol Regulate the Interactions of Alzheimer's Disease Amyloid-beta Peptide with Membrane Lipid. *The Journal of Biological Chemistry 272*, 2977-2289.

Dahlgren, K., Manelli, A., Stine, W., Baker, L., Krafft, G., & LaDu, M. (2002). Oligomeric and Fibrillar Species of Amyloid-b Peptides Differentially Affect Neuronal Viability. *The Journal of Biological Chemistry 277*, 32046–32053.

Dekosky, S., Williamson, J., & Fitzpatrick, A. (2008). Ginkgo biloba for prevention of dementia: a randomized controlled trial. *Journal of the American Medical Association 300*, 2253-2262.

DeMeyer, G., Shapiro, F., Vanderstichele, H., Vanmechelen, E., & Engelborghs, S. (2010). Diagnosis independent Alzheimer's disease biomarker signature in cognitiveily normal elderly people. *Archieves of Neurology 67*, 949-956.

Dikalov, S., Vitek, M., & Mason, R. (2004). Cupric-amyloid beta peptide complex stimulates oxidation of ascorbate and generation of hydroxyl radical. *Free Radical Biological Medicine 36*, 340-347.

DiPaolo, G., & Kim, T. (2011). Linking lipids to Alzheimer's disease: cholesterol and beyond. *Nature 12*, 284-296.

Dobson, C., & Karplus, M. (1999). The fundamentals of protein folding: bringing together theory and experiment. *Current Opinion in Structural Bioilogy 9*, 2-101.

Doraiswamy, P., & Finefrock, A. (2004). Metals in our minds: therapeutic implications for neurodegenerative disorders. *Lancet Neurology 3*, 431-434.

Dudko, O., Hummer, G., & Szabo, A. (2006). Intrinsic Rates and Activation Free Energies from Single-Molecule Pulling Experiments. *Physical Review Letters 96*, 108101.

Dudko, O., Hummer, G., & Szabo, A. (2008). Theory, analysis, and interpretation of single-molecule force spectroscopy experiments. *Proceedings of the National Academy of Sciences USA 105*, 15755-15760.

Erdmann, R., & Swartz, U. (2004). Adhesion clusters under shared linear loading: A stochastic analysis. *Europhysics Letters 66*, 603-609.

Eskici, G., & Axelsen, P. (2012). Copper and Oxidative Stress in the Pathogenesis of Alzheimer's Disease. *Biochemistry 51*, 6289-6311.

Esler, W., Felix, A., Stimson, E., Ghiraldi, J., Lu, Y., Vinters, H., et al. (2000). Alzheimer's disease amyloid propogation by a template-dependant dock-lock mechanism. *Biochemistry 39*, 6288-6295.

Evans, E. (2001). Probing the Relation Between Force-Lifetime-and Chemistry of Single Molecular Bonds. *Annual Review of Biophysics Biomolecular Structure 30*, 105-128.

Evans, E., & Richie, K. (1997). Strength of a weak bond connected by flexible polymer chains. *Biophysical Journal 76*, 2439-2447.

Evans, E., Halvorsen, K., Kinoshito, K., & Wong, W. (2009). A New Approach to Analysis of Single Molecule Force Measurements. In P. Hinterdorfer, & A. van Oijen, *Handbook of Single Molecule Biophysics* (pp. 571-588). New York: Springer.

Evans, K., Berger, E., Cho, C., Weisgraber, K., & Lansbury, P. (1995). Apolipoprotein E is a kinetic but not a thermodynamic inhibitor of amyloid formation: implications for the pathogenesis and treatment of Alzheimer disease. *Proceedings of the National Academy of Sciences USA 92*, 763-767.

Faller, P., & Hureau, C. (2009). Bioinorganic chemistry of copper and zinc ions coordinated to amyloid-beta peptide. *Dalton Transactions 7*, 1080-1094.

Fandrich, M. (2012). Oligomeric Intermediates in Amyloid Formation: Structural Determination and Mechanisms of Toxicity. *Journal of Molecular Biology 421*, 427-440.

Feaga, H., Maduka, R., Foster, M., & Szalai, V. (2011). Affinity of Cu+ for the copper-binding domain of the amyloid-β peptide of Alzheimer's disease. *Inorganic Chemistry 50*, 1614-1618.

Fezoui, Y., Hartley, D., Harper, J., Khurana, R., & Walsh, D. (2000). An improved method of preparing the amyloid beta-protein for fibrillogenesis and neurotoxicity experiments. *Amyloid-internation Journal of Experimental and Clinical Investigation 7*, 166-178.

Florin, E., Moy, V., & Gaub, H. (1994). Adhesion forces between individual ligand-receptor pairs. *Science 264*, 415-417.

Freund-Levi, Y., Eriksdotter-Jonhagen, M., & Cederholm, T. (2006). Omega-3 fatty acid treatment in 174 patients with mild to moderate Alzheimer's disease: OmegAD study: a randomized double-blind trial. *Acheives of Neurology 63*, 1402-1408.

Friddle, R., Noy, A., & De Yoreo, J. (2012). Interpreting the widespread nonlinear force spectra of intermolecular bonds. *Proceedings of the National Academy of Sciences USA 109*, 13573–13578.

Ganguli, M., Chandra, V., Kamboh, M., Johnston, J., Dodge, H., Thelma, B., et al. (2000). Apolipoprotein E polymorphism and Alzheimer's disease: The Indo-US Cross-national Demential Study. *Achieves of Neurology 57*, 824-830.

Garai, K., Sahoo, & Maiti, S. e. (2007). Zinc lowers amyloid-beta toxicity by selectively precipitating aggregation intermediates. *Biochemistry 46*, 10655-10663.

Garg, A. (1995). Escape-field distribution for escape from a metastable potential well subject to a steadily increasing bias field. *Physical Review B 51*, 15592-15595.

Garzon-Rodriguez, W., Yatsimirsky, A., & Glabe, C. (1999). *Biorganic Medical Chemistry Letters 9*, 2243-2248.

Geng, J., Zhao, C., Ren, J., & Qu, X. (2010). Alzheimer's disease Amyloid beta converting left-handed Z-DNAs back to right-handed B-form. *Chemical Communications 46*, 7187-7189.

Gestwicki, J., Crabtree, G., & Graef, I. (2004). Harnessing chaperones to generate small-molecule inhibitors of amyloid ß aggregation. *Science 306*, 865-869.

Glabe, C. (2008). Structural Classification of Toxic Amyloid Oligomers. *The Journal of Biological Chemistry 283*, 29639-29645.

Glenner, G., & Wong, C. (1984). Alzheimer's disease: initial report of the purification and characterization of a novel cerebrovascuiar amyloid protein. *Biochemical and Biophyisical Research Communications 120*, 885-890.

Goldsbury, C., Copper, G., Goldie, K., Muller, S. S., Misur, M., Engel, A., et al. (1997). Polymorphic Fibrillar Assembly of Human Amylin. *Journal of Structural Biology 119*, 17-27.

Gorevic, P., Castaiio, E., Sarnia, R., & Fmgione, B. (1987). Ten to fourteen residue peptides of Alzheimer's disease protein are sufncient for amyloid fibd formation and its characteristic X-ray ciBiaction pattern. *Biochemical and Biophysical Research Communications 147*, 854-872.

Grenough, J., Camarakis, M., & Bush, A. (2012). Metal dyshomeostasis and oxidative stress in Alzheimer's disease. *Neurochemistry International 62*, 540-555.

Guo, S., Lad, N., Ray, C., & Akhremitchev, B. (2009). Association Kinetics from Single Molecule Force Spectroscopy Measurements. *Biophysical Journal 96*, 3412-3422.

Gurland, B., Wilder, D., Lantigua, R., Stern, Y., & Chen, J. (1999). Rates of dementia in three ethnoracial groups. *International Journal of Geriatric Psychiatry 14*, 481-493.

Ha, C., Ryu, J., & Park, C. B. (2007). Metal Ions Differentially Influence the Aggregation and Deposition of Alzheimer's beta-Amyloid on a Solid Template. *Biochemistry 46*, 6118-6125.

Han, D., Wang, H., & Yang, P. (2008). Molecular modeling of zinc and copper binding with Alzheimer's Amyloid-beta Peptide. *Biometals 21*, 189-196.

Han, D., Wang, H., & Yang, P. (2008). Molecular Modelling of Zinc and Copper binding to Alzheimer's Amyloid-beta Peptide. *Biometals 21*, 189-196.

Hane, F. (2009). *The Structure and Function of Pulmonary Surfactant: The Effect of Amyloid Fibril Formation.* Waterloo, Canada: University of Waterloo.

Hane, F., Drolle, E., Gaikwad, R., Faught, Z., & Leonenko, Z. (2011). Amyloid-beta Aggregation on Model Lipid Membranes: an Atomic Force Microscopy Study. *Journal of Alzheimer's Disease 26*, 485–494.

Hane, F., Tran, G., Attwood, S., & Leonenko, Z. (2013). Cu2+ Affects Amyloid-beta (1–42) Aggregation by Increasing Peptide-Peptide Binding Force. *PLoS ONE 8*, e59005.

Härd, T., & Lendel, C. (2012). Inhibition of Amyloid Formation. *Journal of Molecular Biology 421*, 441-465.

Hardy, J. (2006). Alzheimer's Disease: The amyloid cascade hypothesis: An update and reappraisal. *Journal of Alzheimer's Disease 9*, 151-153.

Hardy, J., & Allsop, D. (1991). Amyloid deposition as the central event in Alzheimer's disease. *Transactions in Pharmaceutical Science 12*, 383-388.

Hardy, J., & Higgins, G. (1992). Alzheimer's Disease: The amyloid cascade hypothesis. *Science 256*, 184-185.

Harper, J., & Lansbury, P. (1999). Models of Amyloid Seeding in Alzheimer's Disease and Scrapie: Mechanistics Truths and Physiological Consequences of Time Dependant Solubility of Amyloid Proteins. *Annual Reviews of Biochemistry 66*, 385-407.

Harper, J., Liber, C., & Lansbury, P. (1997). Atomic force microscopic imaging of seeded fibril formation and fibril branching by the Alzheimer's disease amyloid-beta protein. *Chemical Biology 4*, 951-959.

Harris, N., Song, Y., & Kiang, C.-H. (2007). Experimental Free Energy Surface Reconstruction from Single-Molecule Force Spectroscopy using Jarzynski's Equality. *PNAS 99*, 0681011-0681014.

Hartter, D., & Barnea, A. (1988). Brain tissue accumulates copper-67 by 2 ligand-dependnat saturable processes: a high affinity, low capacit and a low affinity, high capacity process. *Journal of Biological Chemistry 263*, 799-805.

He, X., Giurleo, J., & Talaga, D. (2010). Role of Small Oligomers on the Amyloidogenic Aggregation Free Energy Landscape. *Journal of Molecular Biology 395*, 134-154.

Health, U. N. (2012, 09 18). *Effect of LY2062430 on the Progression of Alzheimer's Disease (EXPEDITION).* Retrieved 12 18, 2012, from ClincicalTrials.gov: http://www.clinicaltrials.gov/show/NCT00905372

Hebert, L., Scherr, P., Bienas, J., Bennett, D., & Evans, D. (2003). Alzheimer's Disease in the US population: Prevalence estimates using the 2000 census. *Achieves of Neurology 60*, 1119-1122.

Hebert, L., Scherr, P., McCann, K., & Beckett, L. E. (2001). Is the risk of developing Alzheimer's disease greater for women than for men? *American Jounral of Epidemiology 153*, 132-136.

Hernendez, F., Gomex de Barreda, E., Fuster-Matanzo, A., Lucas, J., & Avila, J. (2010). GSK3: a possible link between beta amyloid peptide and tau protein. *Experimental Neurology 223*, 322-325.

Hesse, L., Beher, C., Masters, G., & Multhaup, G. (1994). The beta A4 amyloid precursor protein binding to copper. *FEBS Letters 349*, 109-116.

Hewitt, N., & Rauk, A. (2009). Mechanism of hydrogen peroxide production by copper-bound amyloid beta peptide: A theoretical study. *Journal of Physical Chemistry B 113*, 1202-1209.

Hinterdorfer, P., & Dufrêne, Y. (2006). Detection and localization of single molecular recognition events using atomic force microscopy. *Nature Methods 3*, 347-355.

Hou, L., & Zagorski, M. (2006). NMR Reveals Anomalous Copper(II) Binding to the Amyloid Aβ Peptide of Alzheimer's Disease. *Journal of the American Chemical Society 128*, 9260–9261.

Huang, T.-H. J. (2001). *Alzheimer Amyloid-beta Peptide Aggregation: Altemate Products of Fibril Formation.* Toronto, ON: University of Toronto.

Huang, X., Atwood, C., Moir, R., Hartorn, M., & Tanzi, R. (2004). Trace metal contamination initiates the apparent auto-aggregation, amyloidosis, and oligomerization of alzheimer's a beta peptides. *Journal of Biological Inorganic Chemistry 9*, 954-960.

Huang, X., Cuajungco, M., & Atwood, C. e. (1999). Cu(II) potentiation of Alzheimer A-beta neurotoxicity: correlation with cell-free hydrogen. *The Journal of Biological Chemistry 274*, 37111-37116.

Hummer, G., & Szabo, A. (2003). Kinetics from non-equilibrium pulling experiments. *Biophysical Journal 85*, 5-15.

Hurshman, A., White, J., Powers, E., & Kelly, J. (2004). Transthyretin aggregation under partially denaturing conditions is a downhill polymerization. *Biochemistry 43*, 7365-7381.

Hutter, J., & Bechhoefer, J. (1993). Calibration of atomic-force microscope tips. *Review of Scientific Instruments 64*, 1868-1873.

Innocenti, M., Salvietti, E., Guidotti, M., Casini, A., Bellandi, S., Forest, M., et al. (2010). Trace copper(ii) or zinc(ii) ions drastically modify the aggregation behavior of amyloid-beta(1-42): An afm study. *Journal of Alzheimer's Disease 19*, 1323-1329.

Ionescu-Zanetti, C., Khurana, R., Gillespie, J., Petrick, J., Trabachino, L., Minert, L., et al. (1999). Monitoring the assembly of Ig light-chain amyloid fibrils by atomic force microscopy. *Proceedings of the National Academy of Sciences 96*, 13175-13179.

Jang, J., & Surh, Y. (2003). Protective effect of resveratrol on beta-amyloid-induced oxidative PC12 cell death. *Free Radical Biological Medicine 34*, 1100.

Jimenez, J., Nettleton, E., Bouchard, M., Robinson, C., Dobson, C., & Saibil, H. (2002). The protofilament structure of insulin amyloid fibrils. *Proceedings of the National Academy of Sciences USA 99*, 9196–9201.

Johannson, J. (2005). Amyloid Fibrils: Mini-review series. *FEBS Letters 272*, 5241.

Jomova, K., Vondrakova, D., Lawson, M., & Valko, M. (2010). Metals, oxidative stress and neurodegenerative disorders. *Molecular Cellular Biochemistry 345*, 91-104.

Jonsson, T., Atwal, J., Steinberg, S., Snaedal, J., Jonsson, P., Bjornsson, S., et al. (2012). Amutation in APP protects against Alzheimer's disease and age related cognative decline. *Nature 488*, 96-99.

JPK Instruments AG. (2007). *JPK Nanowizard II User Handbook.* Berlin, Germany: JPK Instruments AG.

JPK Instruments AG. (2009). *Technical Summary: Calibration of atomic-force microscope tips.* Berlin: JPK Instruments AG.

Jun, S., & Saxena, S. (2007). The aggregated state of amyloid-beta peptide in vitro depends on Cu(II) concentration. *Angewandte Chemie (International Edition) 46*, 3959-3961.

Kakiya, N., Saito, T., Nilsson, P., Matsuba, Y., Tsubuki, S., Takei, N., et al. (2012). Cell Surface Expression of the Major Amyloid-β Peptide (Aβ)-degrading Enzyme, Neprilysin, Depends on Phosphorylation by Mitogen- ctivated Protein Kinase/Extracellular Signal-regulated Kinase Kinase (MEK) and Dephosphorylation by Protein Phosphatase 1a. *The Journal of Biological Chemistry 287*, 29362–29372.

Kambhampaty, A. (2012, 09 04). *Eli Lilly's solanezumab faces grim prospects of attaining conditional FDA approval in mild Alzheimer's.* Retrieved 12 18, 2012, from Financial Times: http://www.ft.com/intl/cms/s/2/cbc228be-f6d3-11e1-827f-00144feabdc0.html#axzz297a59RYv

Karacsony, O., & Akhrimitchev, B. (2011). On the Detection of Single Bond Ruptures in Dynamic Force Spectorscopy by AFM. *Langmuir 27*, 11287-11291.

Kardos, J., Kovacs, I., Hajos, F., Kalman, M., & Simonyi, M. (1989). Nerve-Endings from Rat-Brain Tissue Release Copper Upon Depolarization: A Possible Role in Regulating Neuronal Excitability. *Neuroscience Letters 103*, 139-144.

Karr, W., & Szalai, V. (2008). Cu(II) binding to monomeric, oligomeric, and fibrillar forms of the Alzheimer's disease amyloid-beta peptide. *Biochemistry 47*, 5006–5016.

Karran, E., Mercken, M., & Stooper, B. (2011). The amyloid cascade hypothesis for Alzheimer's disease: an appraisal for the development of therapeutics. *Nature Reviews Drug Discovery 10*, 698-712.

Karuppagounder, S., Pinto, J., Zu, H., & al, e. (2009). Dietary supplementation with resveratrol reduces plaque pathology in a transgenic model of Alzheimer's disease. *Neurochemistry International 54*, 111-118.

Kayed, R. H. (2003). Common structure of soluble amyloid oligomers implies common mechanisms of pathogenesis. *Science 300*, 486-489.

Kayed, R., Pensalfini, A., Margol, L., Sokolov, Y., Sarsoza, F., Hed, E., et al. (2009). Annular Protofibrils Are a Structurally and Functionally Distinct Type of Amyloid Oligomer. *The Journal of Biological Chemistry 284*, 4230-4237.

Kim, B.-H., Palermo, N., Lovas, S., Zaikova, T., Keana, J., & Lyubchenko, Y. (2011). Single-Molecule Atomic Force Microscopy Force Spectroscopy Study of AB1-40 Interactions. *Biochemistry 50*, 5154-5162.

Kirchner, D., Abraham, C., & Selkoe, D. (1986). X-ray diffraction from intraneuronal paired helical filaments and extraneuronal amyloid fibers in Alzheimer disease indicates cross-beta conformation. *Proceedings of the National Academy of Sciences USA 83*, 503-507.

Klug, G., Losic, D., Subasinghe, S., Aguilar, M.-I., Martin, L., & Small, D. (2003). Beta-Amyloid protein oligomers induced by metal ions and acid pH are distinct from those generated by slow spontaneous ageing at neutral pH. *European Journal of Biochemistry 270*, 4282-4293.

Knopman, D., S, D., J, C., Chui, H., & Corey-Bloom, J. (2001). Practise parameter: Diagnosis of dementia. *Neurology 56*, 1143-1153.

Koudinov, A., Berezov, T., & Koudinova, N. (1998). Alzheimer's amyloid beta and lipid metabolism: a missing link? . *FASEB Journal 12*, 1097-1099.

Kovacs, H., Mark, A., Johansson, J., & van Gunsteren, W. (1995). The effect of environment on the stability of an integral membrane helix: Molecular dynamics simulations of surfactant protein C in chloroform, methanol and water. *Journal of Molecular Biology 247*, 808-822.

Kramers, H. (1940). Brownian motion in a field of force and the diffusion model of chemical reactions. *Physica (Utrecht) 7*, 284-304.

Kremer, J., Pallitto, M., Sklansky, D., & Murphy, R. (2000). Correlation of β-Amyloid Aggregate Size and Hydrophobicity with Decreased Bilayer Fluidity of Model Membranes. *Biochemistry 39*, 10309-10318.

Krishnan, R., Goodman, J., Mukhopadhyay, S., Pacheco, C., Lemke, E., Deniz, A., et al. (2012). Conserved features of intermediates in amyloid assembly determine their benign or toxic states. *Proceedings of the National Academy of Science USA 109*, 11172–11177.

Ladiwala, A., Litt, J., Kane, R., Aucoin, D., Smith, S., Ranjan, S., et al. (2012). Conformational Differences between Two Amyloid beta Oligomers of Similar Size and Dissimilar Toxicity. *The Journal of Biological Chemistry 287*, 24765–24773.

Lambert, M., Barlow, A., Chromy, B., Edwards, C., Freed, R., Liosatos, M., et al. (1998). Diffusible, nonfibrillar ligands derived from Abeta1-42 are potent central nervous system neurotoxins. *Proceedings of the National Academy of Science 26*, 6448-6453.

Landouksi, J., & Dupres, V. (2011). Probing peptide-inorganic surface interaction at the single molecule level using force spectroscopy. *Chemphyschem 12*, 1310-1316.

Lannfelt, L., Blennow, K., Zetterberg, H., Batsman, S., Ames, D., Harrison, J., et al. (2008). Safety, Efficacy, and Biomarker Findings of PBT2 in Targeting Aβ as a Modifying Therapy for Alzheimer's Disease: A Phase IIa, Double-Blind, Randomised, Placebo-Controlled Trial. *Lancet Neurology 7*, 779-786.

Lansbury, P., Costa, P., Griffiths, J., Simon, E., & Auger, M. (1995). Structural model for the beta-amyloid fibril based on interstrand alignment of an antiparallel-sheet comprising a C-terminal peptide. *Nature Structural Biology 2*, 990-998.

Lee, V. (2002). Amyloid binding ligands as Alzheimer's disease therapies. *Neurobiological Aging 23*, 1039-1042.

Lee, Y. S., Kim, H. Y., Kim, Y., Seo, J. H., Roh, E. J., Han, H., et al. (2012). Small molecules that protect against b-amyloid-induced cytotoxicity by inhibiting aggregation of beta-amyloid. *Bioorganic and Medicinal Chemistry 20*, 4921–4935.

Li, J., Zhu, M., Ranjamani, S., & Uversky, V. F. (2004). Rifampicin inhibits α-synuclein fibrillation and disaggregates fibrils. *Chemical Biology 11*, 1513-1521.

Lin, H., Bhatia, R., & Lal, R. (2001). Amyloid-beta protein forms ion channels: implications form Alzeimer's diease pathophysiology. *The FASEB Journal 15*, 2433-2445.

Liochev, S. (1999). The mechanism of "Fenton-like" reactions and their importance for biological systems. A biologist's view. *Metal Ions Biological Systems 36*, 1-39.

Liphardt, J., Dumont, S., Smith, S., Tinoco, I., & Bustamante, C. (2002). Equilibrium information from nonequilibrium measurements in an experimental test of Jarzynski's equality. *Science 296*, 1832-1835.

Liu, C., Sawaya, M., Cheng, P., Zheng, J., Nowick, J., & Eisenberg. (2011). Characteristics of amyloid-related oligomers revealed by crystal structures of macrocyclic beta-sheet mimics. *Journal of the American Chemical Society 133*, 6736-6744.

Liu, G., Men, P., Perry, G., & Smith, M. (2010). Nanoparticle and iron chelators as a potential novel Alzheimer therapy. *Methods of Molecular Biology 610*, 123-144.

Livnah, O., Bayer, E., Wilchek, M., & Sussman, S. (1993). Three-dimensional structures of avidin and the avidin-biotin complex. *Proceedings of the National Academy of Sciences USA 90*, 5076-5080.

Lomakin, A., Chung, D. S., Benedek, G., Kirschner, D., & Teplow, D. (1996). On the nucleation and growth of amyloid- beta protein fibrils: Detection of nuclei and quantitation of rate constants. *Proceedings of the National Academy of Sciences USA 93*, 1125-1129.

Loo, D., Copani, A., Pike, C., Whittemore, E., Walencewicz, A., & Cotman, C. (1993). Apoptosis is induced by fbamyloid in cultured central nervow system neurons. *Proceedings of the National Academy of Sciences 90*, 7950-7955.

Lord, A., Gumucio, A., Englund, H., Sehlin, D., Sunquist, V., & Soderberg, L. (2009). An amyloid-beta protofibril-selective antibody prevents amyloid formation in a mouse model of Alzheimer's disease. *Neurobiological Disease 36*, 425-434.

Lovell, H., Xie, C., & Markesbury, W. (1999). Protection against amyloid beta peptide toxicity by zinc. *Brain Research 823*, 88-95.

Lovestone, S., & Reynolds, C. (1997). The phosphorylation of tau: a critical stage in neurodevelopment and neurodegenerative processes. *Neuroscience 78*, 309-324.

Luheshi, L., Hoyer, W., Barros, T., Härd, I., Brorsson, A., & Macao, B. (2010). Sequestration of the Aβ peptide prevents toxicity and promotes degradation in vivo. *PLoS Biology 8*, e1000334.

Luhrs, T., Rotter, C., Adrian, M., Riek-Loher, D., Bohrmann, B., Dobeli, H., et al. (2005). 3D structure of Alzheimer's amyloid-beta(1– 42) fibrils. *Proceedings of the National Academy of Sciences USA 102*, 17342–17347.

Lutsenko, S., Bhattacharjee, A., & Hubbard, A. (2010). Copper handling machinery of the brain. *Mettallomics 2*, 596-608.

Lyubchenko, Y., Kim, B.-H., Krasnoslobodtsev, A., & Yu, J. (2010). Nano Imaging and Protein Misfolding Diseases. *WIREs Nanomedicine and Nanobiotechnology*, pp. 526-544.

Ma, B., & Nossinov, R. (2002). Stabilities and conformations of Alzheimer's Beta-amyloid peptide oligomers (AB16-22,AB16–35, and AB10-35): Sequence effects. *Proceedings of the National Academy of Science 99*, 14126-14131.

Ma, B., & Nussinov, R. (2012). Selective Molecular Recognition in Amyloid Growth and Trasmission and Cross-Barrier Species. *Journal of Molecular Biology 421*, 172-184.

Mahley, R. (1988). Apolipoprotein E: Cholesterol transport protein with expanding role in cell biology. *Science 240*, 622-630.

Makin, S., Atkins, E., Sikorski, P., Johanssen, J., & Serpell, L. (2005). Molecular basis for amyloid fibril formation and stability. *Proceedings of the National Academy of Sciences USA 102*, 315-320.

Markesbury, W. (1997). Oxidative stress hypothesis in Alzheimer's disease. *Free Radical Biological Medicine 23*, 134-147.

Markesbury, W., & Lovell, M. (2007). Damage to lipids, proteins, DNA and RNA in mild cognative impairment. *Archieves in Neurology 64*, 954-956.

Massi, F., & Staub, J. (2001). Energy Landscape Theory for Alzheimer's Amyloid beta peptide Fibril Elongation. *PROTEINS: Structure, Function, and Genetics 42*, 217–229.

Masters, C., Simms, G., Weinman, N., Multlraup, G., McDonaid, B., & Beyreuther, K. (1985). Amyloid plaque core protein in Alzheimer disease and Down syndrome. *Proceedings of the National Academy of Sciences USA 82*, 4245-4249.

Masuda, Y., Uemura, S., & Irie, K. (2008). Verification of the C-terminal intramolecular beta-sheet in the AB42 aggregates using solid state NMR: implications for the potent neurotoxicity through the formation of radicals. *Bioorganic Medical Chemistry Letters 18*, 3206-3210.

Mathaiyah, B., Essa, M., Chauhan, V., & Chauhan, A. (2011). Protective effects of walnut extract against amyloid beta peptide-induced cell death and oxidative stress in PC12 cells. *Biomedical Life Science 36*, 2096-2103.

Matsumura, S., Shinoda, K., Yamada, M., Yokojima, S., Inoue, M., Ohnishi, T., et al. (2012). Two Distinct Amyloid-beta Protein (AB) Assembly Pathways Leading to Oligomers and Fibrils Identified by Combined Fluorescence Correlation Spectroscopy, Morphology, andToxicity Analyses. *The Journal of Biological Chemistry 286*, 11555–11562.

Mattson, M. (2003). Gene-diet interactions in brain aging and neurodegenerative disorders. *Annual Internal Medicine 139*, 441-444.

Mattson, M. (2004). Pathways towards and away from Alzheimer's disease. *Nature 430*, 631-629.

Mattson, M., Cheng, B., Culwell, A., Esch, F., Lieberburg, I., & Rydel, R. (1993). Evidence for excitoprotective and intraneuronal calcium-regulation roles for secreted forms of the beta-amyloid precursor protein. *Neuron 10*, 243-254.

Mawuenyega, K., Sigurdson, W., Ovod, V., Munsell, L., Kasten, T., Morris, J., et al. (2010). Decreased clearance of CNS beta-amyloid in Alzheimer's disease. *Science 330*, 6012.

Mayeux, R. (2003). Epidemiology of neurodegeneration. *Annual Review of Neuroscience 26*, 81-104.

Mayeux, R., Tang, M., & Mehta, P. (1999). Plasma amyloid beta-peptide 1–42 and incipient Alzheimer's disease. *Annals of Neurology 46*, 412-416.

McAllister, C., Karymov, M., Kawano, Y., Lushnikov, A., Mikeikin, A., Uversky, V., et al. (2005). Protein INteractions and misfolding analyzed by AFM force Spectrocopy. *Journal of Molecular Biology 354*, 1028-1042.

Merkel, R., Nassoy, P., Leung, A., Ritchie, K., & Evans, E. (1999). Energy landscapes of receptor-ligand bonds explored with dynamic force spectroscopy. *Nature 397*, 50-53.

Minicozzi, V., Stellato, F., Comai, M., Serra, M., Potrich, C., Meyer-Klaucke, W., et al. (2008). *Journal of Biological Chemistry 283*, 10784-10792.

Minino, A., Xu, J., & Kochanek, K. (2010). *Deaths: Preliminary Data for 2008.* Hyattsville MD: National Center for Health Statistics.

Mithu, V. S., Sarkar, B., Bhowmik, D., Chandrakesan, M., Maiti, S., & Madhu, P. (2011). Zn+ Binding Disrupts the Asp23-Lys28 Salt Bridge without Altering the Hairpin-Shaped Cross-b Structure of Ab42 Amyloid Aggregates. *Biophysical Journal 101*, 2025-2032.

Miura, T., Suzuki, N., Kohata, N., & Takeuchi, H. (2000). T . Miura, K. Suzuki, N. Kohata, H. Takeuchi, Metal binding modes directly produces hydrogen peroxide through metal ion reduction,of Alzheimer's amyloid beta-peptide in insoluble aggregates. *Biochemistry 38*, 7024-7031.

Moores, B., Drolle, E., Attwood, S., Simons, J., & Leonenko, Z. (2011). Effect of Surfaces on Amyloid Fibril Formation. *PLoS ONE 6*, e25954.

Morgado, I., Wieligmann, K., Bereza, M., Rönickec, R., Meinhardt, K., Annamalai, K., et al. (2012). Molecular basis of β-amyloid oligomer recognition with a comformational antibody fragment. *Proceedings of the National Academy of Sciences USA 109*, 12503–12508.

Mothana, B., Roy, S., & Rauk, A. (2009). Molecular dynamics study of the interaction of a beta(13-23) with beta-sheet inhibitors. *ARKIVOC*, 116-134.

Mousseau, N. (2012). Distinct dimerization for various alloforms of the amyloid-beta protein: A beta(1-40), a beta(1-42), and a beta(1-40)(d23n). *Journal of Physical Chemistry B 116*, 4043-4055.

Muller, W., Eckert, G., S. K., Cairns, N. M., & Gattz, W. (1998). Effects of β-amyloid peptides on the fluidity of membranes from frontal and parietal lobes of human brain. High potencies of Aβ1-42 and Aβ1-43. *Amyloid 5*, 10-15.

Murray, I., Sindoni, M., & Axelsen, P. (2005). Promotion of oxidative lipid membrane damage by amyloid beta proteins. *Biochemistry 44*, 12606-12613.

Mutisya, E., Bowling, A., & Beal, M. (1994). Cortical cytochrome oxidase activity is reduced in Alzhemier's disease. *Journal of Neurochemistry 63*, 2179-2184.

Nair, N., Perry, G., Smith, M., & Reddya, P. (2010). NMR Studies of Zinc, Copper, and Iron Binding to Histidine, the Pricipal Metal Ion Complexing Site of Amyloid-beta peptide. *Journal of Alzheimer's Disease 20*, 57-66.

Narayan, P., Orte, A., Clarke, R., Bolognesi, B., Hook, S., Ganzinger, K., et al. (2012). The extracellular chaprone clusterin sequesters oligomeric forms of the amyloid beta 1-40 peptide. *Nature Structural and Molecular Biology 19*, 79-84.

Necula, M., Kayed, R., Milton, S., & Glabe, C. (2007). Small molecule inhibitors of aggregation indicate that amyloid β oligomerization and fibrillization. *Journal of Biological Chemistry 282*, 10311–10324.

Nelson, R., & Eisenberg, D. (2006). Recent atomic models of amyloid fibril structure. *Current Opinion in Structural Biology 16*, 260–265.

Nelson, R., Sawaya, M., Balbirnie, M., Madsen, A., Riekel, C., & Eisenberg, D. (2005). Structure of the cross-beta spine of Amyloid-like Fibrils. *Nature 435*, 773-778.

Neugroschl, J., & Sano, M. (2010). Current Treatment and Recent Clinical Research in Alzheimer's Disease. *Mount Sinai Journal of Medicine 77*, 3-16.

Nussbaum, J., Schilling, S., Cynis, H., Silva, A., Swanson, E., Wangsanut, T., et al. (2012). Prion-like behaviour and tau-dependent cytotoxicity of pyroglutamylated amyloid-beta. *Nature 485*, 651-655.

Oe, T., Ackermann, B., Inoue, K., Berna, M., Garner, C., Gelfanova, V., et al. (2006). Quantitative Analysis of Amyloid β Peptides in Cerebrospinal Fluid of Alzheimer's disease patients by Immunoaffinity Purification and Stable Isotope Dilution Liquid Chromatography/Negative Electrospray Ionization Tandem Mass. *Rapid Communcations in Mass Spectrometry 20*, 3723-3735.

Ono, K., & Yamada, M. (2011). Low-n oligomers as therapeutic targets of Alzheimer's disease. *Journal of Neurochemistry 117*, 19-28.

Ono, K., Condron, M., & Teplow, D. (2009). Structure–neurotoxicity relationships of amyloid-beta protein oligomers. *Proceedings of the National Academy of Sciences 106*, 14745-14750.

Ono, K., Hirohata, M., & Yamada, M. (2005). Ferulic acid destabilizes preformed β-amyloid fibrils in vitro. *Biochemistry and Biophysics Research Communications 336*, 444-449.

Ono, K., Li, L., Takamura, Y., Yoshiike, Y., Zhu, L., Han, F., et al. (2012). Phenolic Compounds Prevent Amyloid beta Protein Oligomerization and Synaptic Dysfunction by Site-specific Binding. *The Journal of Biological Chemistry 287*, 14631–14643.

O'Nuallain, B., Hrncic, R., Wall, R., Weiss, D., & Solomon, A. (2006). Diagnostic and therapeutic potential of amyloid-reactive IgG antibodies contained in human sera. *Journal of Immunology 176*, 7071-7078.

Opazo, C., Hunag, X., Chernu, R., Moir, R., Roher, A., White, A., et al. (2002). Metalloenzyme-like activity of Alzheimer's disease beta-amyloid Cu-dependent catalytic conversion of dopamine, cholesterol, and biological reducing agents to neurotoxic H(2)O(2). *Journal of Biological Chemistry 277*, 40302-40308.

Paravastu, A., Leapman, R., & Tycko, R. (2008). Molecular structural basis for polymorphism in Alzheimer's beta-amyloid fibrils. *Proceedings of the National Academy of Science USA 105*, 18349-18354.

Pearl, R. (1928). *The Rate of Living: Being an Account of Some experimental Studies on the Biology of Life Duration.* New York: AA Knopf.

Pedersen, J., Østergaard, J., Rozlosnik, N., Gammelgaard, B., & Heegaard, N. (2012). Cu(II) Mediates Kinetically Distinct, Non-amyloidogenic Aggregation of Amyloid-beta Peptides. *The Journal of Biological Chemistry 286*, 26952–26963.

Percel, A., Hudaky, P., & Palfi, V. (2007). Dead-End Street of Protein Folding: Thermodynamic Rationale of Amyloid Fibril Formation. *Journal of the American Chemical Society 129*, 14959-14965.

Perczel, A., Hudaky, P., & Palfi, V. (2007). Dead-End Street of Protein Folding: Thermodynamic Rationale of Amyloid Fibril Formation. *Journal of the American Chemical Society 129*, 14959-14965.

Petkova, A., Ishii, Y., Balbach, J., Antzutkin, O., Leapman, R., Delaglio, F., et al. (2002). A structural model for Alzheimer's β-amyloid fibrils based on experimental constraints

from solid state NMR. *Proceedings of the National Academy of Sciences USA 99*, 16742-16747.

Petkova, A., Leapman, R., Guo, Z., Yau, W.-M., Mattson, M., & Tycko, R. (2005). Self Propogating molecular level polymorphism in Alzheimers beta-amyloid fibrils. *Science 307*, 262-265.

Petkova, A., Yau, W., & Tycko, R. (2006). Experimental constraints on quaternary structure in Alzheimer's beta-amyloid fibrils. *Biochemistry 45*, 498-512.

Pimplikar, S. (2009).) Reassessing the amyloid cascade hypothesis of Alzheimer0s disease. *International Journal of Biochemical Cell Biology 41*, 1261-1268.

Potter, G., Plassman, B., Burke, J., Kabeto, M., & Langa, K. (2009). Cognative performance and informant reports in the diagnosis of cognative impairment and dementia in African-Americans and whites. *Alzhiemers & Dementia 5*, 445-453.

Puglielli, L., Freidlich, A., & Setchell, K. (2005). Cholesterol oxidase mimetic activity of Alzheimer's Disease beta-amyloid. *Journal of Clinical Investigation 115*, 2556-2563.

Pul, R., Dodel, R., & Stangel, M. (2011). Antibody based therapy in Alzheimer's disease. *Expert Opinion in Biological Therapy 11*, 343-357.

Qiang, W., Yau, W.-M., Luo, Y., Mattson, M., & Tycko, R. (2012). Antiparallel β-sheet architecture in Iowa-mutant beta-amyloid fibrils. *The Proceedings of the National Academy of Sciences USA 109*, 4443–4448.

Quist, A., Doudevski, I., Lin, H., Azimova, R., Ng, D., Frangione, B., et al. (2005). Amyloid ion channels: a common structural ling for protein-misfolding diseases. *Proceedings of the National Academy of Sciences USA 102*, 10427-10432.

Raffa, D., & Rauk, A. (2007). Molecular dynamics study of the beta amyloid peptide of alzheimer's disease and its divalent copper complexes. *Journal of Physical Chemistry B 111*, 3789-3799.

Rauk, A. (2009). The chemistry of Alzheimer's disease. *Chemical Society Reviews 38*, 2698–2715.

Riceevans, C., Miller, N., Bolwell, G., Bramley, P., & Pridham, J. (1995). *Free Radical Research 22*, 375.

Rico, F., Oshima, A., Hinterdorfer, P., Fujiyoshi, Y., & Scheuring, S. (2011). Two-Dimensional Kinetics of Inter-Connexin Interactions from Single-Molecule Force Spectroscopy. *Journal of Molecular Biology 412*, 72-79.

Riener, C., Stroh, C., Ebner, A., Klampfl, C., Gall, A., Romanin, C., et al. (2003). Simple Test system for single molecule recognition force spectroscopy. *Analytica Chimica Acta 479*, 59-75.

Roberson, E., & Mucke, L. (2006). 100 Years and Counting: Prospects for Defeating Alzheimer's Disease. *Science 314*, 781-784.

Roy, S. (2010). *Designing Novel Peptidic Inhibitors of Beta Amyloid Oligomerization.* Calgary, AB: University of Calgary.

Roy, S., & Rauk, A. (2005). Alzheimer's disease and the 'ABSENT' hypothesis: mechanism for amyloid beta endothelial and neuronal toxicity. *Medical Hypotheses 65*, 123-137.

Ryan, T., Friedhube, A., Lind, M., Howlett, G., Masters, C., & Roberts, B. (2012). Small Amphipathic Molecules Modulate Secondary Structure and Amyloid Fibril-forming Kinetics of Alzheimer Disease Peptide A-beta 1–42. *The Journal of Biological chemistry 287*, 16947–16954.

Saitoh, T., Sundsmo, M., Roch, -M., Kimma, N., Cole, G., Schubert, D., et al. (1989). Secreted form of amyloid B protein precursor is involved in the growth regulation of fibroblasts. *Cell 58*, 615-622.

Sandberg, A., Luheshi, L., Söllvander, S., Pereira de Barros, T., Macao, B., Knowles, T., et al. (2010). Stabilization of neurotoxic Alzheimer amyloid-β oligomers by protein engineering. *Proceedings of the National Academy of Science 107*, 15595-15600.

Sarell, C., Wilkinson, S., & Viles, J. (2010). Substoichiometric Levels of Cu2+ Ions Accelerate the Kinetics of Fiber Formation and Promote Cell Toxicity of Amyloid-beta from Alzheimer Disease. *The Journal of Biological Chemistry 285*, 41533–41540.

Sayre, L., Perry, G., & Smith, M. (1999). Redox metals and neurodegenerative disease. *Current Opinion in Chemical Biology 3*, 220-225.

Scheidt, H., Morgado, I., & Huster, D. (2012). Solid-state NMR Reveals a Close Structural Relationship between Amyloid-beta Protofibrils and Oligomers. *The Journal of Biological Chemistry 287*, 22822–22826.

Scheidt, H., Morgado, I., Rothemund, S., Huster, D., & Fandrich, M. (2011). Solid state NMR spectroscopic investigation of amyloid beta protofibrils: implication of a beta-sheet remodelling upon maturation into terminal amyloid fibrils. *Agnewandte Chemie International Edition (English) 50*, 2837-2840.

Scheuner, D., Eckman, C., Jensen, M., Song, X., Citron, M., Suzuki, N., et al. (1996). Secreted amyloid beta-protein similar to that in the sede plaques of Alzheimer's disease is increased in vivo by the presenilin 1 and 2 and APP mutations Linked to fdial Alzheimer's disease. *Nature Medicine 2*, 864-870.

Schlierf, M., & Rief, M. (2006). Single-molecule unfolding force distributions reveal a funnel-shaped energy landscape. *Biophysics Journal 90*, L33.

Schmechel, D. S.-V. (1993). Increased amyloid beta-peptide deposition in cerebrai cortex as a consequence of apolipoprotein E genotype in late-onset Alzheimer disease. *Proceedings of the National Academy of Science USA 90*, 9649-9653.

Schwaiger, I., Kardinal, A., Schleicher, M., Noegel, A., & Rief, M. (2004). A mechanical unfolding intermediate in an actin-crosslinking protein. *Nature Structural and Molecular Biology 11*, 81-85.

Sciarretta, K., Gordon, D., Petkova, A., Tycko, R., & Meredith, S. (2005). Abeta40-Lactam(D23/K28) models a conformation highly favorable for nucleation of amyloid. *Biochemistry 44*, 6003-6014.

Sehgal, N., Gupta, A., Khader Valli, R., Datt Joshi, S., Mills, J., Hamel, E., et al. (2012). Withania somnifera reverses Alzheimer’s disease pathology by enhancing low-density lipoprotein receptor related protein in the liver. *The Proceedings of the National Academy of Science USA 109*, 3510-3515.

Seifert, U. (2000). Rupture of multiple parallel molecular bonds under dynamic loading. *Physical Review Letters 84*, 2750-2753.

Seifert, U. (2002). Dynamic strength of adhesion molecules: Role of rebinding and self-consistent rates. *Europhysics Letters 58*, 792-798.

Selkoe, D. (1991). The molecular pathology of Alzheimer's disease. *Neuron 6*, 487-498.

Selkoe, D. (2000). Toward a comprehensive theory for Alzheimer’s disease. Hypothesis: Alzheimer’s disease is caused by the cerebral accumulation and cytotoxicity of amyloid beta-protein. *Annals of the New York Academy of Science 924*, 17-25.

Selkoe, D. (n.d.). *Amyloid hypothesis - beta oligomers and plaques.* Retrieved 10 21, 2013, from DNA Learning Center: http://www.dnalc.org/view/2134-Amyloid-hypothesis-beta-oligomers-and-plaques.html

Serpell, L. (2000). Alzheimer's amyloid fibrils: structure and assembly. *Biochemie et Biophysica Acta 1502*, 16-30.

Seshadri, S., Wolf, P. B., Au, R., & McNulty, K. (1997). Lifetime risk of dementia and Alzheimer's disease: The impact of mortality on risk estimates in the Framingham Study. *Neurology 49*, 1498-1504.

Shimmyo, Y., Kihara, T., Akaike, A., Niidome, T., & Sugimoto, H. (2008). Flavonols and flavones as BACE-1 inhibitors: Structure-activity relationship in cell-free, cell-based, and in silico studies reveal novel pharmacophore features. *Biochemie et Biophysica Acta 1780*, 819-825.

Shin, B., & Saxena, S. (2008). Direct evidence that all three histidine residues coordinate to Cu(II) in amyloid beta 1-16. *Biochemistry 47*, 9117-9123.

Shlyakhtenko, L., Gill, A., Filonov, A., Cerovac, Z., Lushnikov, A., & Lyubchenko, Y. (2003). Silatrane-based surface chemistry for immobilization of DNA, protein-DNA complexes and other biological materials. *Ultramicroscopy 97*, 279-287.

Skaat, H., Chen, R., Grinberg, I., & Margel, S. (2012). Engineered Polymer Nanoparticles Containing Hydrophobic Dipeptide for Inhibition of Amyloid-β Fibrillation. *Biomacromolecules 2012*, 2662−2670.

Smith, D., Cappai, D., & Barnham, K. (2007). The redox chemistry of the Alzheimer's disease amyloid β peptide. *Biochimica et Biophysica Acta 1768*, 1976–1990.

Smith, M., Numomura, A., Zhu, X., Takeda, A., & Perry, G. (2000). Metabolic, metallic, and mitotic sources of oxidative stress in Alzheimer disease. *Antioxident Redox Signal 2*, 413-420.

Sokolov, Y., Kozak, A., Kayed, R., Chanturiya, A., Glabe, C., & Hall, J. (2006). Soluble Amyloid Oligomers Increase Bilayer Conductance by Altering Dialectric Structure. *The Journal of General Physiology 128*, 637-647.

Soreghan, B., Kosmoski, J., & and Glabe, C. (1994). Surfactant properties of Alzheimer's A beta peptides and the mechanism of amyloid aggregation. *Journal of Biological Chemistry 18*, 28551-28554.

Stanyon, H., & Viles, J. (2012). Human Serum Albumin Can Regulate Amyloid-beta Peptide Fiber Growth in the Brain Interstitium. *The Journal of Alzheimers Disease 287*, 28163–28168.

Stefani, M. (2012). Structural features and cytotoxicity of amyloid oligomers: Implications in Alzheimer's disease and other diseases with amyloid deposits. *Progress in Neurobiology 99*, 226-245.

Stöhr, J., Watts, J., Mensinger, Z., Oehler, A., Grillo, S., DeArmonda, S., et al. (2012). Purified and synthetic Alzheimer's amyloid beta (AB) prions. *The Proceedings of the National Academy of Sciences 109*, 11025–11030.

Stroud, J., Liu, C., Teng, P., & Eisenberg, D. (2012). Toxic fibrillar oligomers of amyloid-β have cross-beta structure. *Proceedings of the National Academy of Sciences USA 109*, 7717–7722.

Strunz, T., Oroszlan, K., Schafer, & Guntherodt, H. J. (1999). Dynamic force spectroscopy of single DNA molecules. *Proceedings of the National Academy of Sciences USA 96*, 11277–11282.

Suetherman, A., & Belfort, G. (2005). Protein structureal pertubations and aggregation on homogenous surfaces. *Biophysical Journal 88*, 1322-1333.

Suwalsky, M., Bolognin, S., & Zatta, P. (2009). Interaction between alzheimer's amyloid-beta and amyloid-beta-metal complexes with cell membranes. *Journal Of Alzheimers Disease 17*, 81-90.

Suzuki, N., Cheung, T., Cai, T., Cai, X., Odaka, A., Otvos, L., et al. (1994). An increased percentage of long amyloid beta protein secreted by familial amyloid protein precursor (BPP717) mutants. *Science 264*, 1336-1340.

Suzuko, K., Miura, T., & Takeuchi, H. (2001). Inhibitory effect of copper(II) on zinc(II)-induced aggregation of amyloid beta-peptide. *Biochemcal Biophysical Research Communications 285*, 991-996.

Syme, C., Nadal, R., Rigby, S., & Viiles, J. (2004). Copper Binding to the Amyloid-beta (AB) Peptide Associated with Alzheimer's Disease. *The Journal of Biological Chemistry 279*, 18169–18177.

Szyperski, T., Vandenbussche, G., Curstedt, T., Ruysschaert, J., Wuthrich, K., & Jan, J. (1998). Pulmonary surfactant-associated polypeptide C in a mixed organic solvent transforms from a monomeric alpha-helical state into insoluble beta-sheet aggregates. *Protein Science 7*, 2533-2540.

Tabner, B., Turnbull, S., & El-Agnaf, O. e. (2002). Formation of hydrogen peroxide and hydroxyl radicals from A(beta) and alpha-synuclein as a possible mechanism of cell death in Alzheimer's disease and Parkinson's disease. *Free Radical Biological Medicine 32*, 1076-1083.

Tanzi, R., McClatchey, A., Lampereti, E., Villa-Komaroff, L., Gusella, J., & Neve, R. (1988). Protease inhibitor domain encoded by an amyloid protein precursor mRNA associated with AIzheimer's disease. *Nature 331*, 528-530.

Taylor, J. (1997). *An Introduction to Error Analysis.* Sausalito: University Science Books.

Tees, D., Waugh, R., & Hammer, D. (2001). A microcantilever device to assess the effect of force on the lifetime of selectin-carbohydrate bonds. *Biophysical Journal 80*, 668-682.

Thinakaran, G., & Koo, E. (2008). Amyloid Precursor Protein Trafficking, Processing, and Function. *Journal of Biological Chemistry 283*, 29615-29619.

Tjernberg, L., Naslund, J., Lindquist, F., Johannsson, J., Karlstrom, A., & al, e. (1996). Arrest of beta-amyloid fibril formation by a pentapeptide ligand. *Journal of Biological Chemistry 271*, 8545-8548.

Tougu, V., Karafin, A., & Palumaa. (2008). Binding of zinc(II) and copper(II) to the full length Alzheimer's amyloid-beta peptide. *Journal of Neurochemistry 104*, 1249-1259.

Tougu, V., Karafin, A., Zovo, K., Chung, R., Howells, C., West, A., et al. (2009). *Journal of Neurochemistry 110*, 1784-1795.

Tougu, V., Tiiman, A., & Palumaa, P. (2011). Interactions of Zn(II) and Cu(II) ions with Alzheimer's amyloid-beta peptide. Metal ion binding, contribution to fibrillization and toxicity. *Metallomics 3*, 250–261.

Townsend, K., & Pratico, D. (2005). Novel therapeutic opportunities for Alzheimer's disease: focus on nonsteroidal anti-inflammatory drugs. *FASEB Journal 19*, 1592.

Ueda, K., Fukui, Y., & Kageyama, H. (1994). Amyloid beta protein-induced neuronal cell death: neurotoxic properties of aggregated amyloid beta protein. *Brain Research 639*, 240-244.
Verdier, Y., & Penke, B. (2004). Binding sites of amyloid beta peptide in cell plasma membrane and implications in Alzheimer's disease. *Current Protein Peptide Science 5*, 19-31.
Walsh, D., & Selkoe, D. (2004). Oligomers in the brain: the emerging role of soluble protein aggregates in neurodegeneration. *Protein Peptide Letters 11*, 213-228.
Walsh, D., Hartley, D., Kusumoto, Y., Fezoui, Y., Condron, M., Lomakin, A., et al. (1999). Amyloid-beta protein fibrillogenesis. *Journal of Biological Chemistry 274*, 25945-25952.
Walsh, D., Klyubin, I., Fadeeva, J., Cullen, W., Anwyl, R., Wolfe, M., et al. (2004). Naturally secreted oligomers of amyloid-beta protein potently inhibit hippocampal long-term potentiation in vivo. *Nature 416*, 535-539.
Wang, J., Ho, L., & Zhao, Z. (2006). Moderate consumption of Cabernet Sauvignon attenuates Abeta neuropathology in a mouse model of Alzheimer's disease. *FASEB Journal 20*, 2313-2320.
Wang, Q., Walsh, D., Rowan, M., Selkoe, D., & Anwyl, R. (2004). Block of long-term potentiation by naturally secreted and synthetic amyloid beta-peptide in hippocampal slices is mediated via activation of the kinases c-Jun N-terminal kinase, cyclin-dependent kinase 5, and p38 mitogen-activated protein kinase as well a. *Journal of Neuroscience 24*, 3370-3378.
Whitehouse, P., Martino, A., Antuono, P., Lowenstein, P., Coyle, J., Price, D., et al. (1986). Nicotinic acetylcholine binding sites in Alzheimer's disease. *Brain Research 371*, 146-151.
Whitson, J., Selkoe, D., & Cotman, C. (1989). Amyloid beta protein enhances the survival of hippocampal neurons in vitro. *Science 243*, 1488-1490.
Wischik, C., Edwards, P., Lai, R., Roth, M., & Harrington, C. (1996). Selective inhibition of Alzheimer disease-like tau aggregation by phenothiazines. *Proceedings of the National Academy of Sciences USA 93*, 11213–11218.
Wu, J., Breydo, L., Isas, M., Lee, J., Kuznetsov, Y., Langen, R., et al. (2010). Fibrillar Oligomers Nucleate the Oligomerization of Monomeric Amyloid-beta but Do Not Seed Fibril Formation. *The Journal of Biological Chemistry 285*, 6071–6079.
Yamaguchi, T., Yagi, H., Goto, Y., Matsuzaki, K., & Hoshino, M. (2010). A Disulfide-Linked Amyloid-β Peptide Dimer Forms a Protofibril-like Oligomer through a Distinct Pathway from Amyloid Fibril Formation. *Biochemistry 49*, 7100-7107.
Yang, F., Lim, G., Begum, A., Ubeda, O., Simmons, M., Ambegaokar, S., et al. (2005). Curcumin inhibits formation of amyloid beta oligomers and fibrils, binds plaques, and reduces amyloid in vivo. *Journal of Biological Chemistry 280*, 5892-5901.
Yu, J., Malkova, S., & Lyubchenko, Y. (2008). α-Synuclein Misfolding: Single Molecule AFM Force Spectroscopy Study. *Journal of Molecular Biology 384*, 992–1001.
Yu, L., Edalji, R., Harlan, J. E., Holzman, T. F., Lopez, A. P., Labkovsky, B., et al. (2009). Structural charecterization of a soluble amyloid-beta peptide oligomers. *Biochemistry 48*, 1870-1877.
Yu, X., & Zheng, J. (2011). Polymorphic Structures of Alzheimer's beta-Amyloid Globulamers. *PLoS ONE 6*, e20575.

Zatta, P., Tognon, G., & Carampin, P. (2003). Melatonin prevents free radical formation due to the interaction between beta-amyloid peptides and metal ions [Al(III), Zn(II), Cu(II), Mn(II), Fe(II)]. *Journal of Pineal Research 35*, 98-103.

Zhang, X., Wojcikiewicz, E., & Moy, V. (2002).) Force spectroscopy of the leukocyte function associated antigen-1/intercellular adhesion molecule-1 interaction. *Biophysical Journal 83*, 2270-2279.

Zhao, L. N., Chiu, L. N., Benoit, J., Chew, L. Y., & Mu, Y. (2011). Amyloid ! Peptides Aggregation in a Mixed Membrane Bilayer: A Molecular Dynamics Study. *Journal of Physical Chemistry B 115*, 12247–12256.

Zhao, L. N., Long, H., Mu, Y., & Yue Chew, L. (2012). The Toxicity of Amyloid-beta Oligomers. *International Journal of Molecular Science 13*, 7303-7327.

Zhou, B., Teramukai, S., & Fukushima, M. (2007). Prevention and treatment of dementia or Alzheimer's disease by statins: a meta-analysis. *Dementia Geratrics and Cognative Disorders 23*, 194-201.

Zhu, X., Lee, H., Perry, G., & Smith, M. (2007). Alzheimer disease, the two-hit hypothesis: an update. *Biochemie et Biophysica Acta 1772*, 494-502.

Zidar, J., & Merzel, F. (2011). Probing Amyloid-Beta Fibril Stability by Increasing Ionic Strengths. *The Journal of Physical Chemistry B 115*, 2075–2081.

Appendix A
Atomic Force Spectroscopy Protocols

Molecular Weights of Reagents (g/mol)

aminopropylsilatrane (APS)	232.4
aminopropyl-triethoxysilane (APTES)	221.4
triethanolamine	149.2
NHS-PEG-maleimide	3400
Cys-Aβ42	4617.3
HEPES	238.3
tris(2-carboxyethyl)phosphine (TCEP)	286.7
SG1 (note-30% of weight is retained H_2O)	991.2
Sodium Chloride (NaCl)	58.4

All reagents can be purchased from Sigma-Aldrich except APS which must be synthesized. Peptides are purchased from Anaspec. SG1 is synthesized by the Rauk group and stored in -20C.

Cleaning Surfaces

Reagents and Supplies:

Bruker MLCT cantilevers
Mica (SPI Supplies)
Ethanol (lab grade)
MilliQ Water
1 mL microcentrifuge tubes or similar
Tweezers (curved, blunt nose work best)
Scotch Tape

Protocol

1. Wash MLCT cantilever tips in ethanol and water, dry with dryed argon or nitrogen
    - Cut off the cap for a 1 mL microcentrifuge tube. These caps will be used for all chemical modifications of the cantilever tips.
    - Fill 1 cap with ethanol and another with MilliQ water.
    - Using curved blunt nose tweezers, gently remove a cantilever from the case and dip in and out of the ethanol bath 3 times. Remove the cantilever and dip in and out of the water bath 3 times.
    - Place a piece of mica in a petri dish. Place the cleaned cantilever on the mica inside the petri dish. Place a nitrogen hose under the petri dish cover and apply a low pressure stream of nitrogen into the petri dish until all liquid has evaporated from around the cantilever. This will take approximately 10 minutes depending on ambient humidity.
    - Remove the mica sheet with the cantilever on tip and place the mica and cantilever into a UV cleaner. The mica serves as a suitable platform for handling the cantilever.
2. Cleave Mica
    - Use scotch tape and press to attach to mica.

- Remove the scotch tape from mica. You should see a very thin layer of mica stuck to the tape.
- Place cleaved mica into a petri dish for dust free storage.

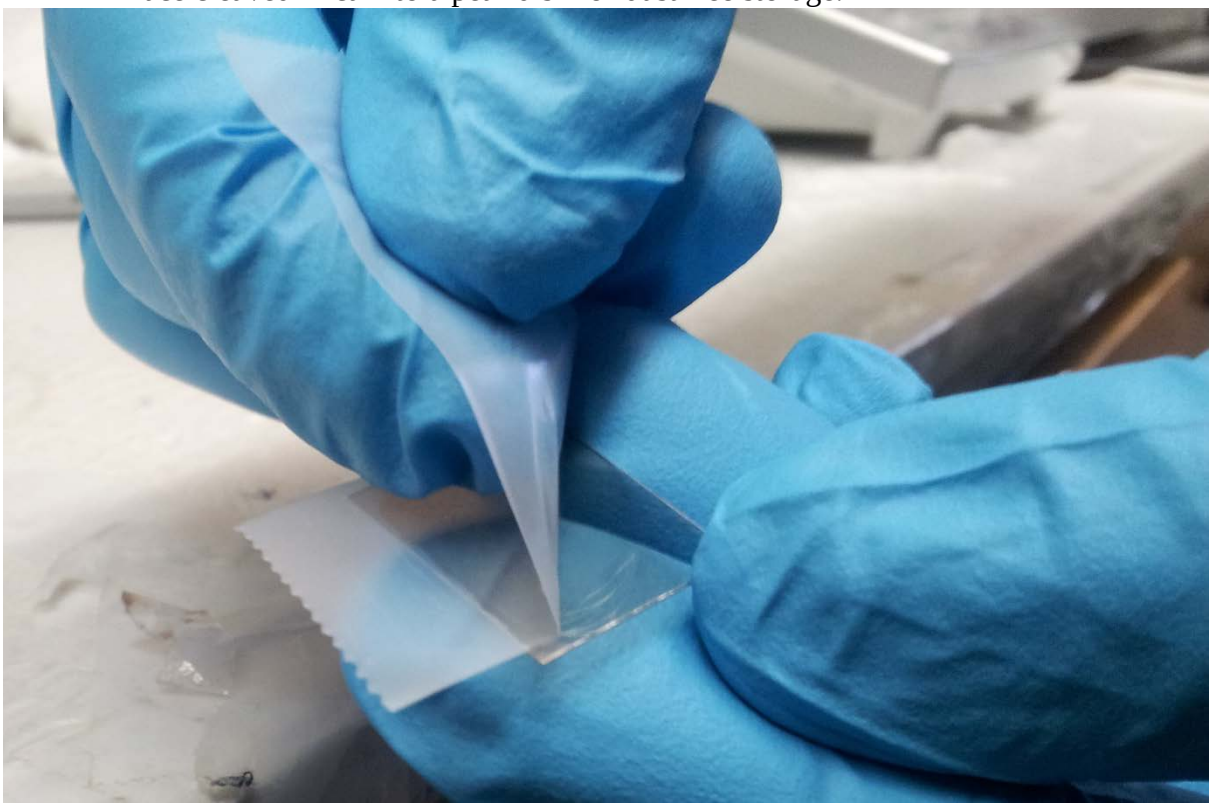

Synthesize Aminopropyl Silatrane (APS)

Reagents and Supplies

Vacuum evaporation apparatus
Triethanolamine
Sodium
Aminopropyl-triethoxy-silane (APTES)
Round bottom flask
Magnetic stirrer and stir bar
Pistle and Mortar
Syringe

Protocol

1. Heat silicon oil bath to 60C.
2. Remove 4.13g (3.67mL) of triethanolamine with a syringe from the container (note triathenaolamine has very low viscosity and will take a while to get drawn into the syringe) and place in round bottom flask.
3. Add 1mg sodium and add to round bottom flask.
    - Na acts as a catalyst and is removed from the reaction during evaporation.
    - Na is not included in the reaction, so you can just cut off a “speck”. An exact amount is not necessary

4. Add 6.12g of APTES to round bottom flask.
4. Add magnetic stir bar to flask and set up vacuum evaporator to top of flask to apply a vacuum.
5. Stir mixture until the reaction is complete. This is indicated by the precipitation of the product into a solid white crystalline product. This may take upto 1 hour. The product will be hard and encase the stir bar. You will need to use a mortar and pestle to make the product into a powder.
6. Make a 50 mM stock solution of APS in deionized water. The molecular weight of APS is 232.4. Add 5.81g of APS to 500mL of deionized water.
7. Take a sample of the product to the NMR lab and obtain a 1D NMR spectra. The spectra should look similar to the one shown below.

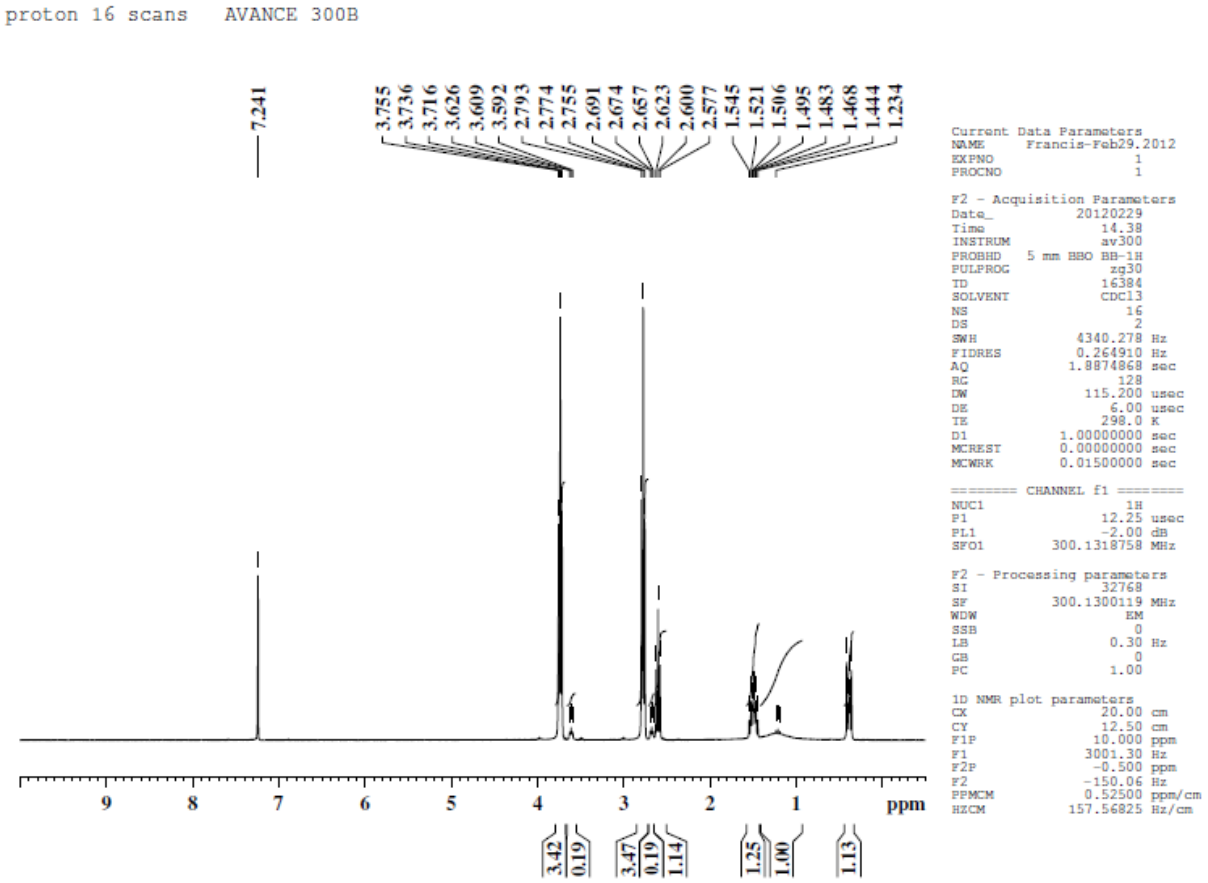

Preparing Stock Solutions

Reagents and Supplies

Aminopropylsilatrane (APS)
N-hydroxyl succinamide-polyethelene glycol-maleimide (NHS-PEG-mal) (also called mal-PEG-SVA)
tris(2-carboxyethyl)phosphine (TCEP)
Dimethylsulfoxide (DMSO)
HEPES buffer
Sodium Chloride (NaCl)
Hydrochloric Acid (HCl)
Sodium hydroxide (NaOH)
Pipettes
Beakers
Balance
Bottles

HEPES Buffer

1. Prepare HEPES buffer with a concentration of 50mM and 150mM of NaCl, pH 7.4.
2. Fill a 1L bottle with approximately 750mL of MilliQ water. Add 11.9g of HEPES buffer and 8.76g NaCl. Stir until dissolved completely using magnetic stir bar.

3. Add water until level reaches the 1L mark.
4. Test pH. Adjust pH using HCl or NaOH.
5. Store in fridge.

Aminopropylsilatrane (APS) - 167μM
1. To make 167μM solution of APS, add 334μL of 50mM stock solution of APS to 100mL of MilliQ water.
    - It is not absolutely necessary that APS is prepared at this solution but probably should be within an order of magnitude to work best.
2. Store in fridge.

tris(2-carboxyethyl)phosphine (TCEP) – 200nM
1. To make 200nM solution of TCEP, serial dilutions must be made.
2. Add 57.3mg TCEP to 1L of water. This will yield a 200μM solution. Mix well.
3. Add 1mL of the 200μM solution to 1L of water. Mix well. This solution is 200nM.
4. Store in -20C freezer.

NHS-PEG-mal - 167μM
1. Add 56.8mg of NHS-PEG-mal to 100mL of DMSO. Mix well.
2. Store in aliquots for further use in -20C freezer.

Cys-Amyloid-β (1-42) – 20nM
1. Add 0.5mL of DMSO to 0.5mg bottle of cys-Aβ (Anaspec-Freemont, CA) and shake to dissolve. There are 1.08e-7 moles of Aβ in this solution.
2. Add Aβ to 50mL HEPES in a beaker or centrigufe tube to make a stock solution of 2.2μM. Mix well.
3. Add 1mL of the 2.2μM stock solution to 100mL of HEPES to make a 22nM solution of cys-Aβ. Store Aβ for 15 minutes at room temperature.
4. Aliquot the Aβ in 1mL centrifuge tubes by taking 0.5mL of Aβ and 0.5mL of TCEP.
5. Store Aβ aliquots in -20C freezer.
6. When ready for use, thaw Aβ and centrifuge at 14000RPM for 15 minutes. Remove the top half of the aliquot and place in another centrifuge tube. This will ensure primarily monomeric forms of the peptide are used.

Surface Modification of AFM tips and Mica
Reagents and Supplies
167μM APS solution
167μM NHS-PEG-Maleimide solution
22nM cys-Aβ42 solution
Mica (freshly cleaved)
Bruker MLCT cantilevers (cleaned)
Pipettes
Petri dishes

Protocol - Cantilevers

1. Remove the caps of a number of centrifuge tubes.
    - These will serve as a bath for the reagents when modifying the surface of the cantilever tips. Place these caps in a petri dish to keep dust free.
2. Using a pipette, fill tube caps with APS solution. Using blunt nose curved tweezers, place 1 cantilever chip in each tube cap. Soak 30 minutes.
    - This silanates the surface preparing it for linker attachment.
4. Fill other tube caps with MilliQ water. After 30 minutes, remove cantilever chips and immerse in water 3 times, placing the cantilevers in and out of the water. Place cantilevers on mica and place in a petri dish and dry with nitrogen.
5. Fill different tube caps with NHS-PEG-mal solution. Place cantilevers in NHS-PEG-mal solution for 3 hours.
6. After 3 hours, rinse cantilevers with DMSO by immersing them 3 times in a DMSO filled tube cap. Store in HEPES solution.

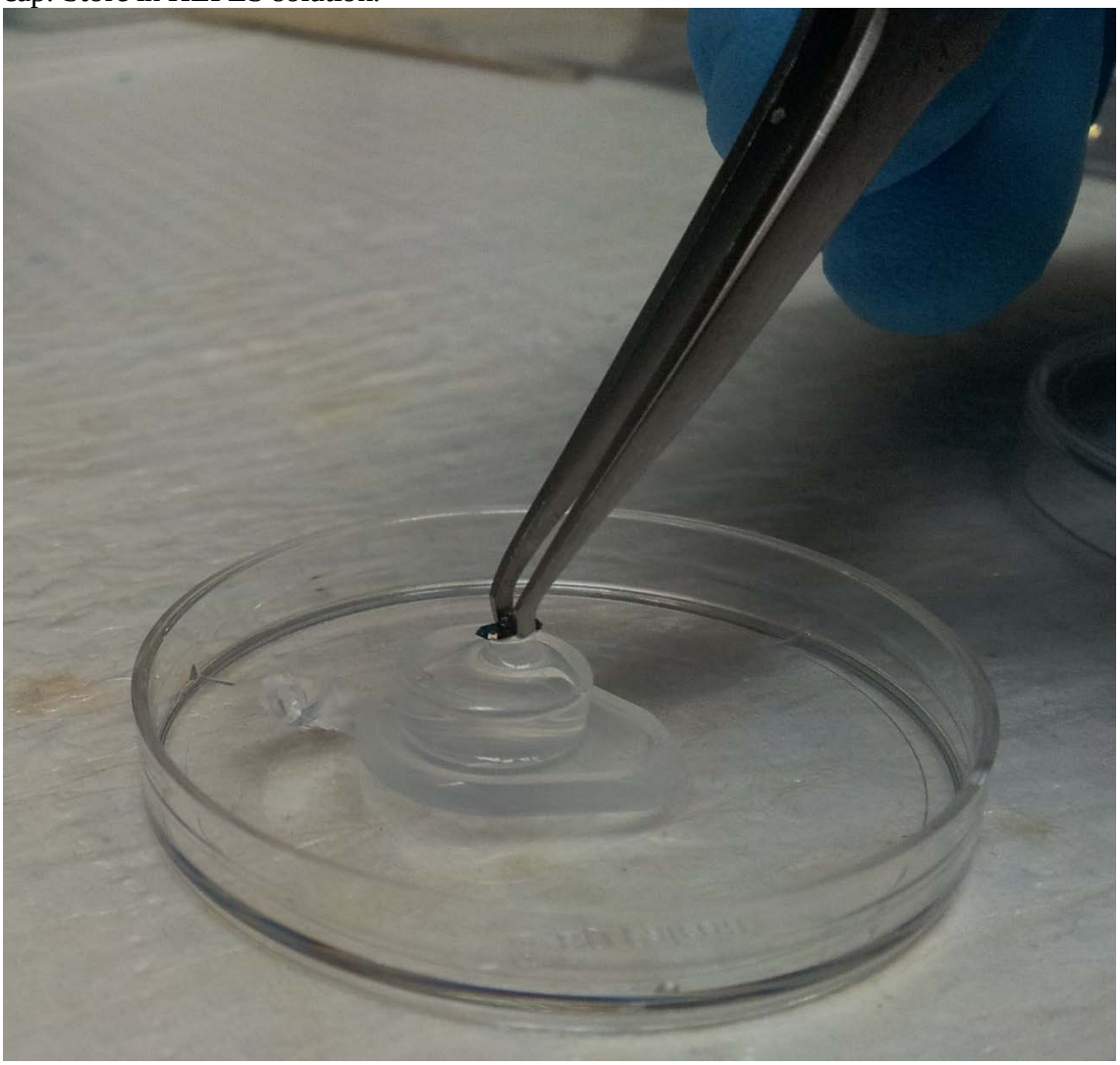

Protocol - Mica

1. Place freshly cleaved mica in petri dish. Soak mica in APS solution for 30 minutes by applying 100µL of APS to the surface of the mica.
2. After 30 minutes, rinse mica 3 times with 100µL of water from pipette. Dry in petri dish with nitrogen.
3. Apply 100µL of NHS-PEG-mal to each mica surface and allow to soak for 3 hours.
4. After 3 hours use pipette to rinse mica 3 times with 100µL of DMSO. Store mica in petri dish soaked with HEPES buffer.

Protocol – cys-Aβ42 Attachement

1. Using the above techniques, soaking cantilever tips in tube caps and using 100µL to soak mica, prepare to attach the Aβ.
2. Centrifuge Aβ solution at 14000RPM for 15 minutes as described above.
3. Using the top of the solution (it doesn't separate in phases) and the above techniques immerse tips and cantilevers in Aβ solution for 30 minutes.
4. After 30 minutes rinse tips and mica with HEPES buffer.
5. Immerse mica and tips in beta-mercaptoethanol to quench unreacted maleimide groups.
    - This ensures that there are no binding events between Aβ on the tip and maleimide on the surface or vice versa.
    - Maleimide is very toxic and this step must be done under a fume hood. Everything must be disposed of (gloves, etc) in a garbage can located outside or cleaned well with DMSO.
    - If you open a bottle of DMSO this will likely result in the lab being uninhabitable for at least 2 days.
6. Wash mica and tip with HEPES buffer 3 times and store in HEPES until ready for use.
    - Do not store for greater than 24 hours.

Preparation of Inhibitors and Metal Ions

Reagents and Supplies

Inhibitor powder (eg SG1)
Metal ion powder
Pipettes
Microcentrifuge tubes

Protocol – Inhibitors

1. Prepare 7µM stock solution of SG1 (MW 991.2) by adding 1mg of SG1 to 100mL HEPES.
    - Inhibitors come in different amounts. Use entire amount to make solution.
    - 30% of the mass of inhibitors is retained water.
2. Dilute stock solution to desired concentrations – typically 20, 40 and 200nM.

Protocol

1. Prepare stock solution of metal solutions such as Cu, Zn or Fe.
2. Dilute stock solutions to desired concentrations – typically 20nM.

Atomic Force Spectroscopy – JPK Nanowizard II[4]

Calibration of Cantilever[5]

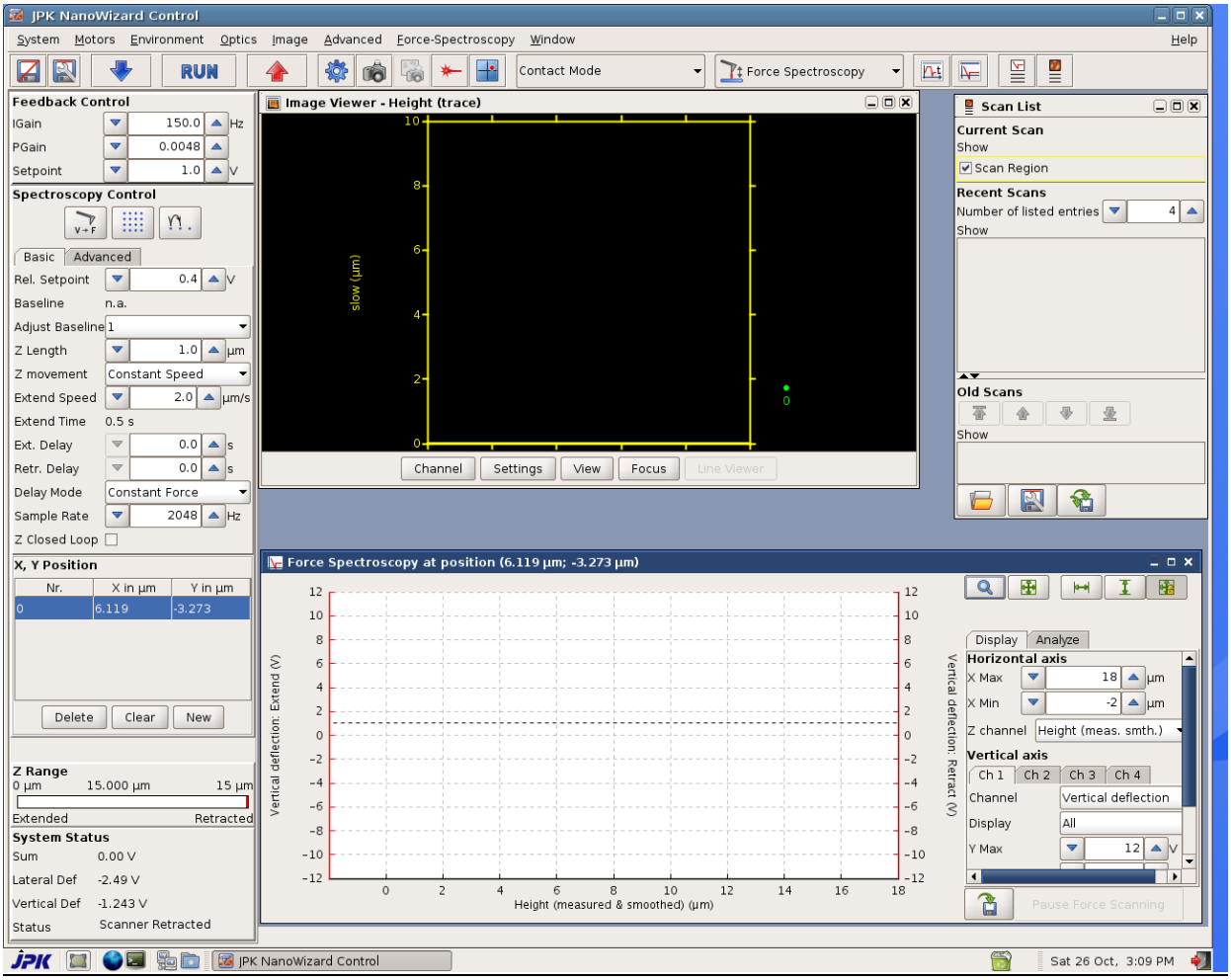

1. Load Bruker MLCT cantilever chip into glass cantilever holder. Secure with retaining spring and install in AFM head.

[4] All images from JPK User Manual. © JPK Instruments AG 2009.
[5] Adapted from a protocol written by Youngjik (Vince) Choi

2. Open JPK Desktop and select Contact Mode and Force Spectroscopy mode
3. Adjust the laser and mirror to achieve laser alignment with a good sum signal

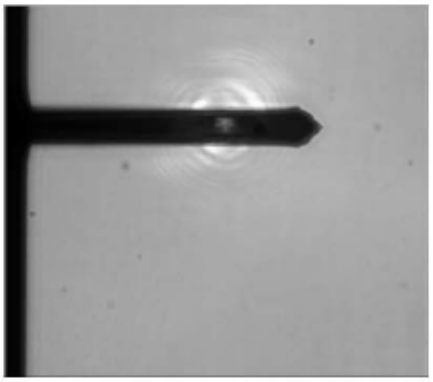

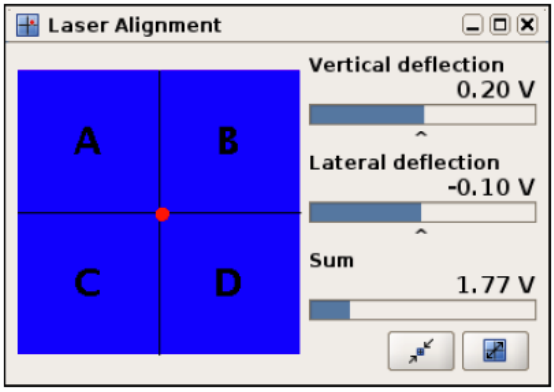

4. Select run and collect one force curve. Stop scanning and save this force curve as a calibration curve.
3. SelectV→F, click “Relative” tab.
    - This is in the “spectroscopy control” in the left.
    - This will open the calibration window.

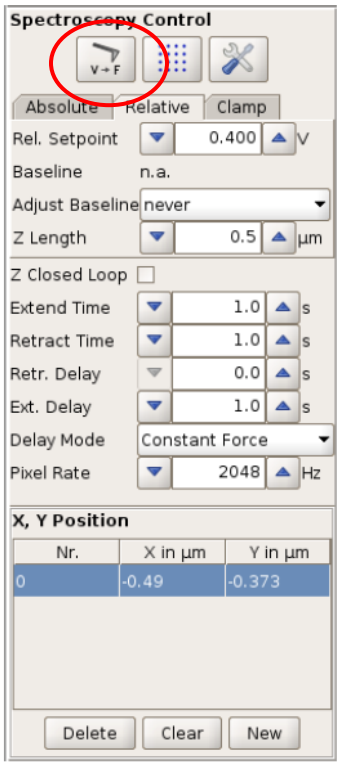

4. Calibrate sensitivity
    - This converts mV to nm.
    - Select magnifying glass and szoom in to the deflection part (steep part) of the force curve.
    - Click “manual sensitivity selection”.
    - Click and drag a line that matchs the deflection of the force curve.
    - Click “accept value” and “use it”

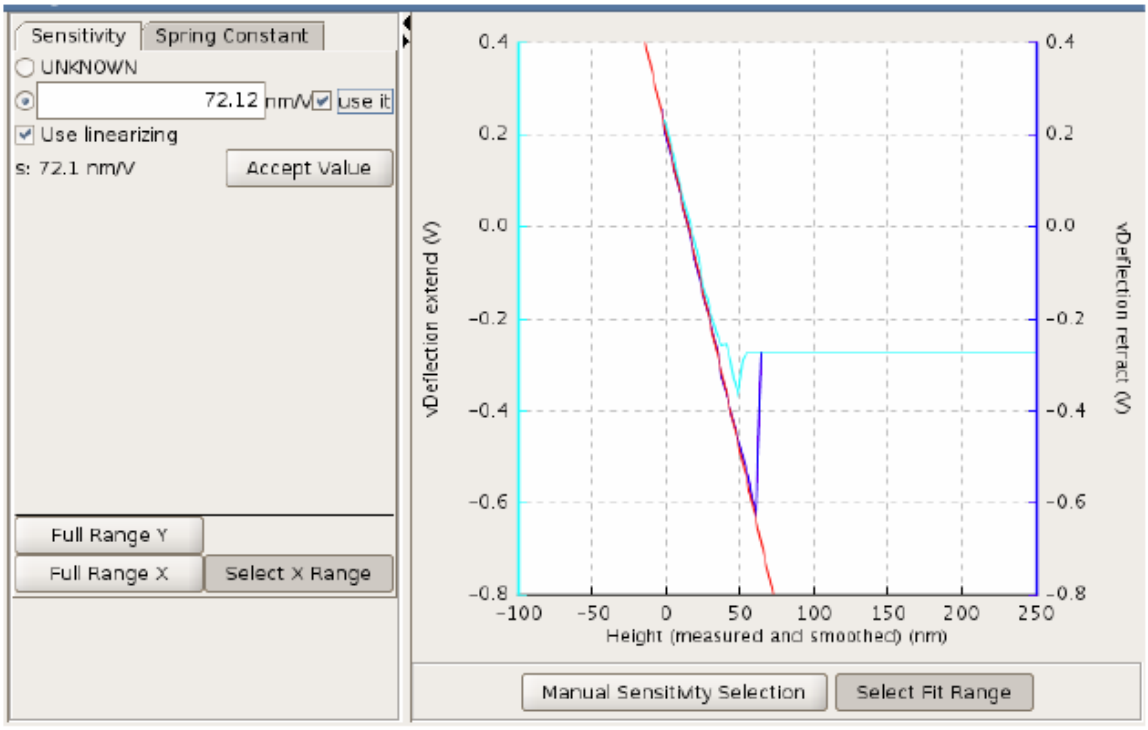

5. Calibrate spring constant
    - Click on “Spring Constant” tab
    - Raise the motors 500µm up
    - Click the infinity symbol at the bottom. You should see a Bell curve appear.
    - Click the infinity symbol again.
    - Select “Select Fit Range” drag and select the Bell curve from left to right.
    - Click “Accept Value” and “Use it”

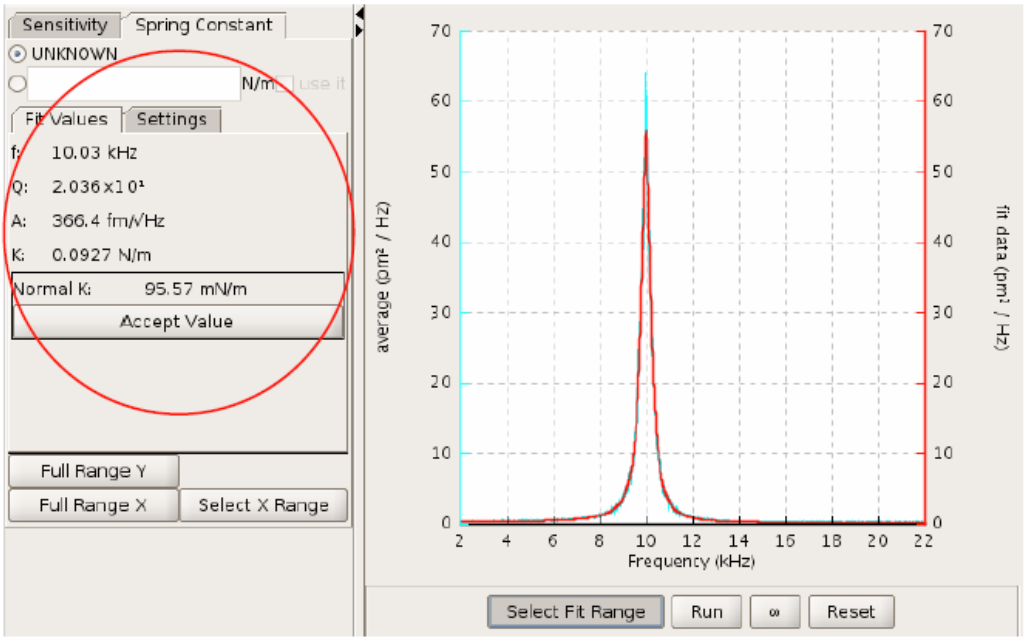

Atomic Force Spectroscopy Data Collection

1. Select a grid of 30x30 data points over 100μm (or whatever you want).
2. Select a z-length of 0.1μm.
3. Select "Constant Velocity" and select a suitable retraction velocity.
4. Select a dwell time of 0.5 sec.
    - This will allow adequate time for the peptides to bind. The time for bond formation is about 0.1 sec.
5. Ensure you are saving force curves in a suitable folder.
6. Click "Run". Ensure that force curves are being saved and that suitable curves are being collected.
7. Typical force spectroscopy settings are Igain 40, pgain 0.0048, set point 10 nN, relative set point 0.9.

Dynamic Force Spectroscopy (DFS)

1. DFS is done by using different loading rates. Loading rate, $r=vk_c$. where v is the retraction velocity and k_c is the cantilever spring constant.
2. Loading rates should be collected across 4 orders of magnitude. Suggested loading rates are 300, 1000, 3000, 10000, 30000, 100000 pN/s. Assuming a spring constant of 100 mN/m, retraction velocities should be set as follows for the corresponding mean loading rate:

Loading Rate (pN/s)	**Retraction Velocity (nm/s)**
300	3
1000	10
3000	30
10000	100
30000	300
100000	1000

3. Each set of loading rates should be saved in a different folder with a descriptive name.

Force Spectroscopy Analysis – Selecting Successful Binding Events

1. Open JPKSPM Data Porcessing Software.
2. Open the folder where files are located.
3. Click on each curve file name and look at the curve. If there is a successful binding event go to the next curve. If there is no successful binding event, click "delete".
    - See images for example
    - Notice large non-specific interaction in the first image, but a successful WLC event after.

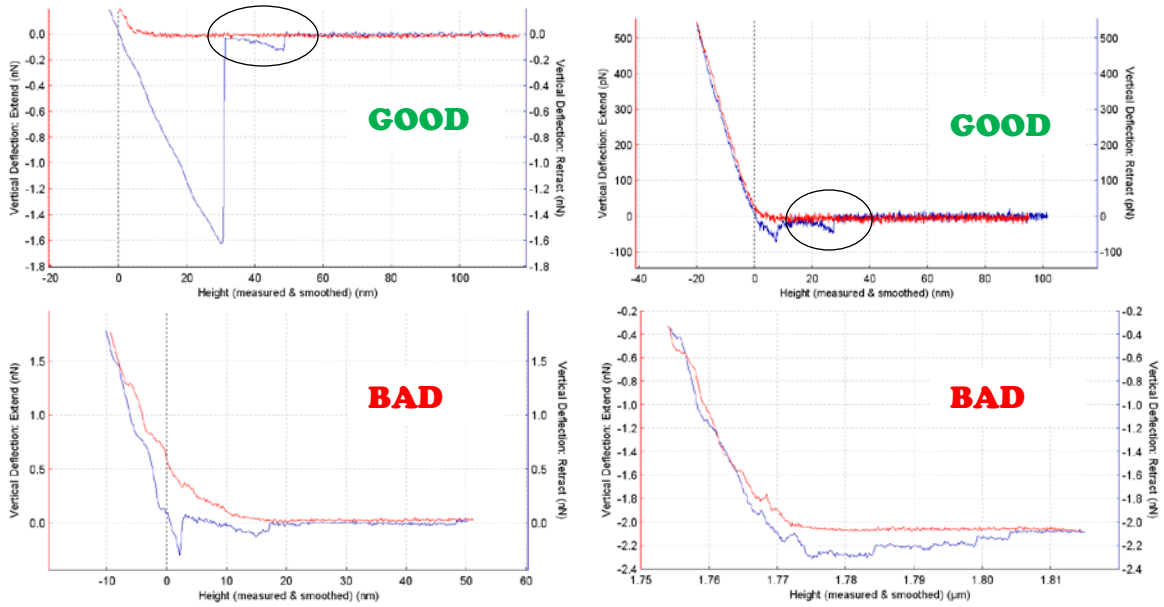

Force Spectroscopy Analysis – Creating Batch Processing File

1. Open the JPKSPM Data Processing software
2. File – Open
   - Open a selected force curve
3. Smooth Force Data
4. Subtract baseline
   - This makes the approach and retract equal to zero
   - You may need to select a region with a constant approach height (ie flat section)
5. Calibrate for sensitivity and spring constant.
   - Ensure these values are equal to the calibrated values of the cantilever
6. Correct height for cantilever bending.
   - Because the cantilever bends, this height must be corrected.
   - This process will make the steep tip-surface contact section vertical.
7. Shift origin of force curve.
   - Ensure that the point at which the retraction passes through the base line is equal to 0 on the x-axis.
8. Apply a worm like chain (WLC) fit.
   - It is best to do this manually by clicking on the WLC icon and selecting “new”
   - Manually select the fit by finding the WLC region of the force curve
9. Save the batch process.

* Numbers in boxes below correspond to steps in above protocol

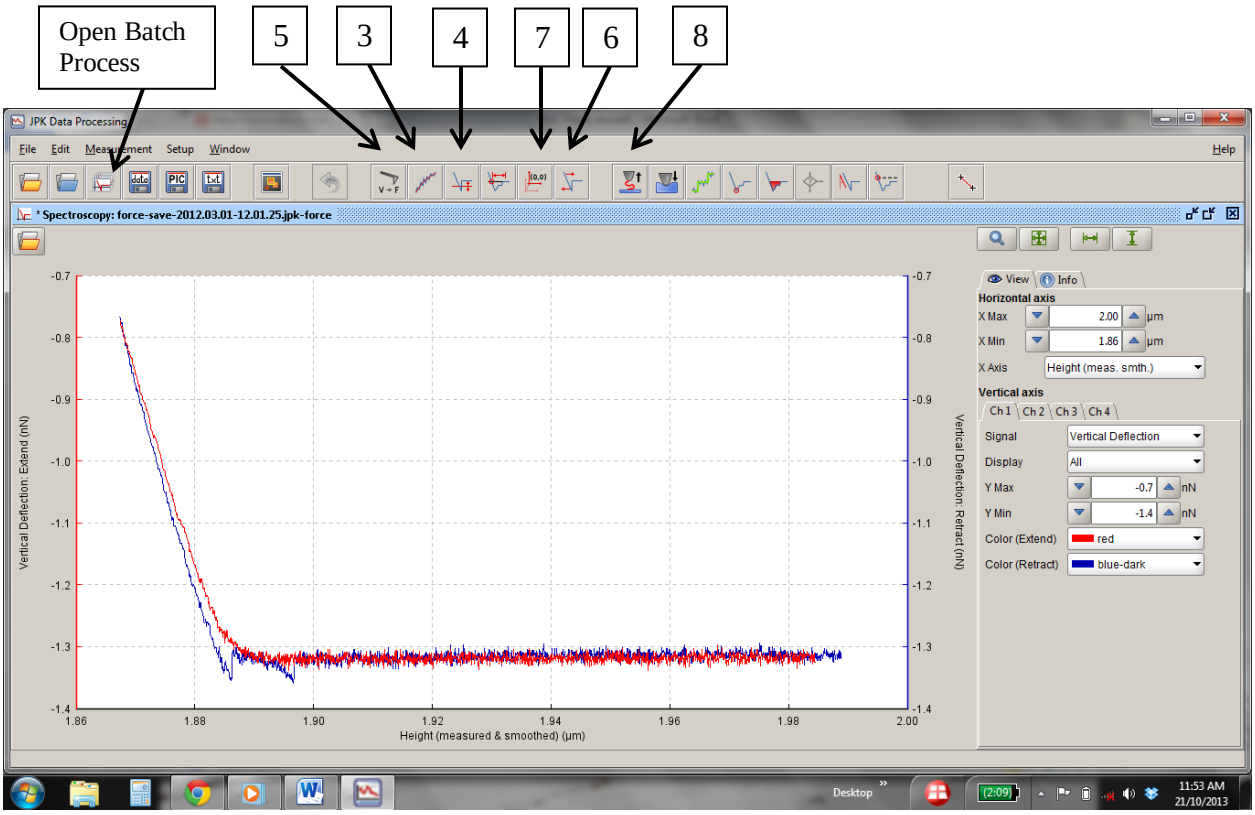

Force Spectroscopy Analysis – Batch Processing

1. Click open batch of force curves.
2. Select folder where curves are located.
3. Select batch process.
    - Click browse
    - Select “Save curve position in file”
4. Select “Export as .txt?”. Click finish.
5. Select all batch processes (ie smooth, level curve, etc).
6. Manually level baseline, shift origin and select WLC region if needed.
7. Click “keep” or “discard” if the curve is not good.
8. When all curves have been analyzed, select “save”.

Force Spectroscopy Analysis – Data Analysis

1. Open the text file containing the results of the data. This file will be called something similar to “results-#date-chainfits. Select and copy all text.
2. Copy data into MS Excel.
3. Keep columns for rupture force, contour length, loading rate and persistence length.
4. Put all relevant information into this spreadsheet (date, spring constant, concentrations, etc.). This will save you from referencing your lab notbook constantly.
5. Calculate means and standard errors for all data.

6. This data can be exported into Origin for presenting histograms and rupture force vs. loading rate plots.

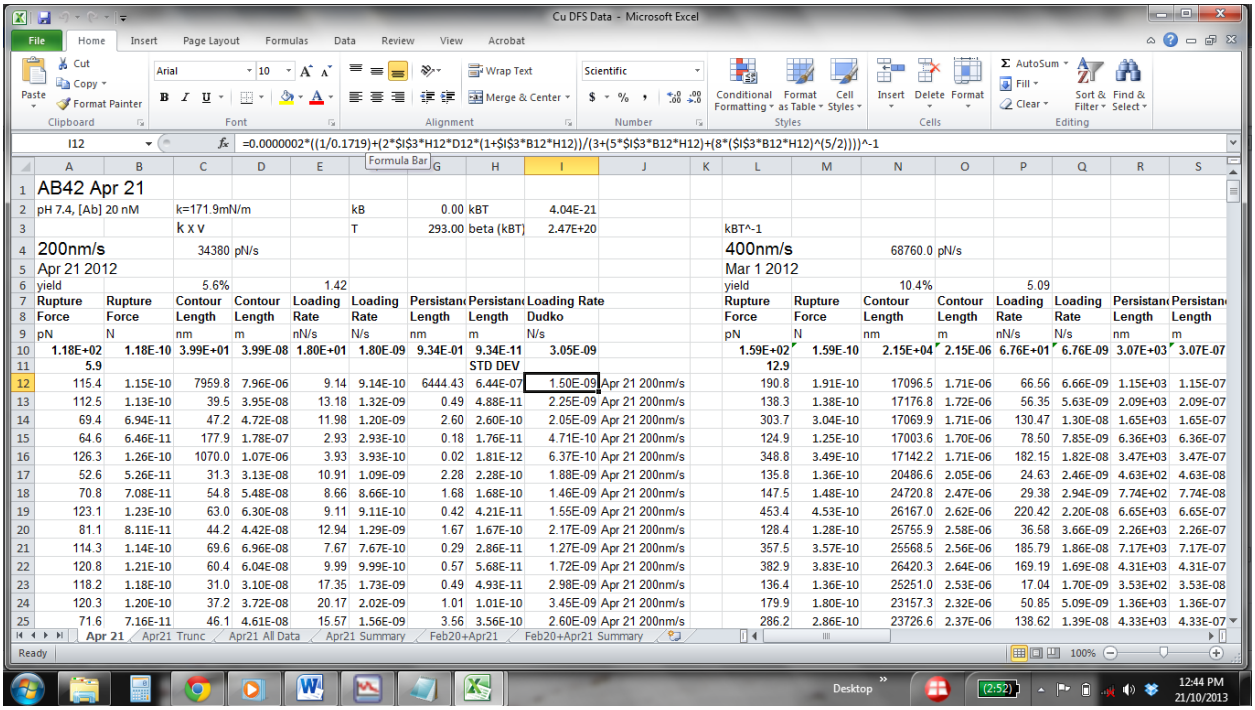

Cu DFS Data - Microsoft Excel

=0.0000002*((1/0.1719)+(2*I3*H12*D12*(1+I3*B12*H12))/(3+(5*I3*B12*H12)+(8*(I3*B12*H12)^(5/2))))^-1

	A	B	C	D	E	F	G	H	I	J	K	L	M	N	O	P	Q	R	S
1	AB42 Apr 21																		
2	pH 7.4, [Ab] 20 nM		k=171.9mN/m			kB	0.00	kBT	4.04E-21										
3			k x v			T	293.00	beta (kBT)	2.47E+20			kBT^-1							
4	200nm/s		34380	pN/s								400nm/s		68760.0	pN/s				
5	Apr 21 2012											Mar 1 2012							
6	yield		5.6%		1.42							yield		10.4%		5.09			
7	Rupture	Rupture	Contour	Contour	Loading	Loading	Persistan	Persistan	Loading Rate			Rupture	Rupture	Contour	Contour	Loading	Loading	Persistan	Persistan
8	Force	Force	Length	Length	Rate	Rate	Length	Length	Dudko			Force	Force	Length	Length	Rate	Rate	Length	Length
9	pN	N	nm	m	nN/s	N/s	nm	m	N/s			pN	N	nm	m	nN/s	N/s	nm	m
10	**1.18E+02**	**1.18E-10**	**3.99E+01**	**3.99E-08**	**1.80E+01**	**1.80E-09**	**9.34E-01**	**9.34E-11**	**3.05E-09**			**1.59E+02**	**1.59E-10**	**2.15E+04**	**2.15E-06**	**6.76E+01**	**6.76E-09**	**3.07E+03**	**3.07E-07**
11	**5.9**							STD DEV				**12.9**							
12	115.4	1.15E-10	7959.8	7.96E-06	9.14	9.14E-10	6444.43	6.44E-07	1.50E-09	Apr 21 200nm/s		190.8	1.91E-10	17096.5	1.71E-06	66.56	6.66E-09	1.15E+03	1.15E-07
13	112.5	1.13E-10	39.5	3.95E-08	13.18	1.32E-09	0.49	4.88E-11	2.25E-09	Apr 21 200nm/s		138.3	1.38E-10	17176.8	1.72E-06	56.35	5.63E-09	2.09E+03	2.09E-07
14	69.4	6.94E-11	47.2	4.72E-08	11.98	1.20E-09	2.60	2.60E-10	2.05E-09	Apr 21 200nm/s		303.7	3.04E-10	17069.9	1.71E-06	130.47	1.30E-08	1.65E+03	1.65E-07
15	64.6	6.46E-11	177.9	1.78E-07	2.93	2.93E-10	0.18	1.76E-11	4.71E-10	Apr 21 200nm/s		124.9	1.25E-10	17003.6	1.70E-06	78.50	7.85E-09	6.36E+03	6.36E-07
16	126.3	1.26E-10	1070.0	1.07E-06	3.93	3.93E-10	0.02	1.81E-12	6.37E-10	Apr 21 200nm/s		348.8	3.49E-10	17142.2	1.71E-06	182.15	1.82E-08	3.47E+03	3.47E-07
17	52.6	5.26E-11	31.3	3.13E-08	10.91	1.09E-09	2.28	2.28E-10	1.88E-09	Apr 21 200nm/s		135.8	1.36E-10	20486.6	2.05E-06	24.63	2.46E-09	4.63E+02	4.63E-08
18	70.8	7.08E-11	54.8	5.48E-08	8.66	8.66E-10	1.68	1.68E-10	1.46E-09	Apr 21 200nm/s		147.5	1.48E-10	24720.8	2.47E-06	29.38	2.94E-09	7.74E+02	7.74E-08
19	123.1	1.23E-10	63.0	6.30E-08	9.11	9.11E-10	0.42	4.21E-11	1.55E-09	Apr 21 200nm/s		453.4	4.53E-10	26167.0	2.62E-06	220.42	2.20E-08	6.65E+03	6.65E-07
20	81.1	8.11E-11	44.2	4.42E-08	12.94	1.29E-09	1.67	1.67E-10	2.17E-09	Apr 21 200nm/s		128.4	1.28E-10	25755.9	2.58E-06	36.58	3.66E-09	2.26E+03	2.26E-07
21	114.3	1.14E-10	69.6	6.96E-08	7.67	7.67E-10	0.29	2.86E-11	1.27E-09	Apr 21 200nm/s		357.5	3.57E-10	25568.5	2.56E-06	185.79	1.86E-08	7.17E+03	7.17E-07
22	120.8	1.21E-10	60.4	6.04E-08	9.99	9.99E-10	0.57	5.68E-11	1.72E-09	Apr 21 200nm/s		382.9	3.83E-10	26420.3	2.64E-06	169.19	1.69E-08	4.31E+03	4.31E-07
23	118.2	1.18E-10	31.0	3.10E-08	17.35	1.73E-09	0.49	4.93E-11	2.98E-09	Apr 21 200nm/s		136.4	1.36E-10	25251.0	2.53E-06	17.04	1.70E-09	3.53E+02	3.53E-08
24	120.3	1.20E-10	37.2	3.72E-08	20.17	2.02E-09	1.01	1.01E-10	3.45E-09	Apr 21 200nm/s		179.9	1.80E-10	23157.3	2.32E-06	50.85	5.09E-09	1.36E+03	1.36E-07
25	71.6	7.16E-11	46.1	4.61E-08	15.57	1.56E-09	3.56	3.56E-10	2.60E-09	Apr 21 200nm/s		286.2	2.86E-10	23726.6	2.37E-06	138.62	1.39E-08	4.33E+03	4.33E-07

Apr 21 | Apr21 Trunc | Apr21 All Data | Apr21 Summary | Feb20+Apr21 | Feb20+Apr21 Summary

Ready

Appendix B
List of Publications of Francis Hane

Publications related to PhD Research

Hane F, Lee B, Petoyan A, Rauk A, Leonenko Z. Testing a Synthetic Amyloid Aggregation Inhibitor using Atomic Force Spectroscopy. Biosensors and Bioelectronics. Manuscript accepted for publication.

Hane F, Attwood S, Leonenko Z. Comparison of three competing dynamic force spectroscopy models to study binding forces of Amyloid-β 1-42. Soft Matter. Manuscript submitted for publication.

Hane F, Tran G, Atwood S, Leonenko, Z. (2013). Cu(2+) Changes Amyloid-β (1-42) Aggregation by Increasing Peptide-Peptide Binding Forces. PLoS ONE. 8:e59005.

Other Publications

Hane F, Drolle E, Choi Y, Attwood S, Leonenko Z. (2013). Atomic force microscopy and Kelvin probe force microscopy to study Alzheimer's disease. Materials Science & Technology 2013 Collected Proceedings. Manuscript accepted for publication.

Drolle E*, **Hane F*,** Lee B, Leonenko Z. (2013). Atomic force microscopy to study molecular mechanisms of amyloid fibril formation and toxicity in Alzheimer's disease. Drug Metabolism Reviews. Manuscript accepted for publication. *co-first authors

Hane F. (2013). Are amyloid fibrils molecular spandrels? FEBS Letters. Manuscript in press.

Hane F. (2013). Intellectual Property Rights and User Facility Agreements. Nature Biotechnology. 31:116-117.

Finot E, Markey L, **Hane F**, Amrein M, Leonenko, Z. (2012). Combined Atomic Force Microscopy and Spectroscopic Ellipsometry applied to the analysis of lipid-protein thin films. Colloid Surface B. 104:289-293.

Drolle E, **Hane F,** Choi Y, Gaikwad R, Attwood S, Leonenko Z. (2012). Atomic force microscopy and Kelvin probe force microscopy to study the mechanism of amyloid fibril formation and toxicity. Microscopy and Microanalysis. 18:884-885.

Hane F, Gaikwad R, Drolle E, Faught E, Leonenko Z. (2011). Adsorption of Amyloid-β on Model Lipid Membranes. Journal of Alzheimer's Disease. 26(3):484-495.

Hane F. (2011). Aeronautics and Interjurisdictional Immunity in Canada. Annals of Air and Space Law. XXXVI: 571-578

Hane F, Drolle L, Leonenko Z. (2010). Effect of cholesterol and amyloid-beta on multilayer formation of thin lipid films: an atomic force microscopy study. Nanomedicine: Nanotechnology, Biology and Medicine. 6:808-814.

Moores B, **Hane F**, Eng L, Leonenko Z. (2010). Kelvin probe force microscopy in application to biomolecular films: Frequency modulation, amplitude modulation, and lift mode. Ultramicroscopy. 110:708-711.

Hane F, Moores B, Leonenko Z. (2009). Effect of SP-C on Surface Potential Distribution in Pulmonary Surfactant: an AFM and KPFM Study. Ultramicroscopy. 109:268-273.

Hane F, Leonenko Z. Amyloid-β Restores Adhesion Properties of Pulmonary Surfactant Affected by High Levels of Cholesterol. Manuscript submitted for publication.